



UNIVERSITÀ DEGLI STUDI DI NAPOLI
FEDERICO II

Tesi di Dottorato in Fisica Fondamentale ed Applicata
XVII Ciclo

Dipartimento di Scienze Fisiche

Complesso Universitario di Monte S. Angelo

via Cintia - 80126 Napoli Italia

Procolo Lucignano

Coherent manipulation of mesoscopic devices

Candidato

Dr. Procolo Lucignano

Coordinatore

Prof. Arturo Tagliacozzo

Anno accademico 2003-2004

Contents

Ringraziamenti	1
Introduction	3
Bibliography	7
1 Quantum dots with spin orbit coupling	11
Abstract	11
1.1 Introduction	11
1.2 FSP state and dot reconstruction	15
1.3 Inclusion of spin-orbit	18
1.4 Spin and charge density in the multiplet $S = 5/2$, $M = 10$. .	25
1.5 FIR absorption	28
1.5.1 Kohn Theorem	28
1.5.2 Coupling Hamiltonian and FIR spectra	30
1.6 Comparison between the dot and a QHF disk	31
1.6.1 Quantum Hall Ferromagnet	32
1.6.2 Dot with spin-orbit coupling	34
1.7 Discussion	36
Appendix 1A	
QHF Spin Density	39
Bibliography	40
2 Adiabatic control and Berry phase	45
Abstract	45
2.1 Introduction	45
2.2 Berry Phase in QM	46
2.3 Two electron Quantum Dot:	
A Possible $SU(2)$ Berry Phase	50
2.3.1 Solution of the low energy spin Hamiltonian	54
2.3.2 The exact propagator	56
2.3.3 Calculation of the Berry phase	57
2.4 Detection of the Berry phase: a possible transport experiment	58
2.4.1 Model Hamiltonian for the electron on the ring	59
2.4.2 Topology of the ring	60
2.4.3 Path-integral of a spinful particle on the ring	61
2.4.4 Saddle point approximation	62
2.4.5 Conductance oscillations	66
2.5 Discussion	68

Appendix 2A	
Some properties of the operators S and T	71
Appendix 2B	
Mapping of the low energy effective Hamiltonian onto the two spin 1/2 model	71
Appendix 2C	
Mapping of the two spin 1/2 model onto the single spin model	72
Appendix 2D	
Adiabatic and exact propagator	74
Appendix 2E	
Path integral for a spinful particle on a ring	76
Bibliography	79
3 Fast optical control of an out of equilibrium Josephson junction	83
Abstract	83
3.1 Introduction	83
3.2 Characteristic time scales	86
3.3 The non-equilibrium qp distribution	88
3.3.1 Non-equilibrium electron-hole pair excitations induced by optical irradiation	88
3.3.2 Inelastic diffusion of the qp's at initial times	91
3.4 Changes of the superconductive properties on the time scale ω_c^{-1}	93
3.4.1 The correction to the gap parameter	93
3.4.2 Correction to the Josephson current	96
3.5 Classical dynamics of the irradiated junction	98
3.6 Discussion	101
Appendix 3A	
Quasiclassical time dependent Green's function approach	104
Appendix 3B	
Kinetic equation for $n(\omega, r, t)$	107
Appendix 3C	
Equation of motion of G^R	107
Bibliography	108

List of Figures

1.1	Single particle Fock and Darwin states of a parabolically confined two dimensional quantum dot	16
1.2	Energy levels vs magnetic field without SO coupling for the dot with $N = 2$ electrons at $U = 13 meV$ and $\omega_d = 5meV$. . .	17
1.3	Slater determinants quoted in the text are depicted. Quantum numbers are $N = 5$, $S = 1/2$ for the state at $B = 0$ [a] and $S = 5/2$ for the state at $B = B^*$, the magnetic field value at which the maximum absolute value of S is achieved [b]. . .	17
1.4	Energy levels without SO coupling for the dot with $N = 5$ electrons at $U = 13 meV$ and $\omega_d = meV$. Magnetic field values are: (in units of $\hbar\omega_c$): $B = 5 meV$ [top], $B = B^* = 7 meV$ [middle], $B = 11.5 meV$ [bottom]. The total M is on the x axis. The levels are drawn with short, medium or long dashes, depending on the total spin : $S = 1/2, 3/2, 5/2$. . .	18
1.5	Splitting of the lowest lying multiplet for $N = 5, S = 5/2$ and $M = 10$ vs strength α of the SO interaction, at $B = B^* = 7 meV$, $U = 13 meV$ and $\omega_d = 5 meV$. The levels are labeled by J_z	20
1.6	Energy levels with $N = 5$, $B = 7 meV$, $\omega_d = 5 meV$, and $\alpha = 100 meV\text{\AA}$, for different U values. In the upper panel we show the crossings that allow the <i>FSP</i> polarized state to be the ground state when U is large. Ordering of the levels is magnified in the bottom panels for three different U values. . .	21
1.7	N=2 particles dot: energy spectrum vs magnetic field ω_c in the presence of the <i>SO</i> . $\omega_d = 5meV$, $U = 13meV$, $\alpha = 250meV\text{\AA}$. The GS is $J_z = 0$, the FES is $J_z = 1$	21
1.8	N=3 particles dot: energy spectrum vs magnetic field ω_c in the presence of the <i>SO</i> . $\omega_d = 7meV$, $U = 13meV$, $\alpha = 250meV\text{\AA}$. The GS is $J_z = 3/2$, the FES is $J_z = 5/2$	22
1.9	N=4 particles dot: energy spectrum vs magnetic field ω_c in the presence of the <i>SO</i> . The GS is $J_z = 4$, the FES is $J_z = 5$. $\omega_d = 7meV$, $U = 13meV$, $\alpha = 250meV\text{\AA}$	22
1.10	GS-FES spin gap vs α at $\omega_c = 8meV$ for a 3 particles ($N = 3$) dot with $\omega_d = 7meV$, $U = 13meV$, $\alpha = 250meV\text{\AA}$	23
1.11	Spin and charge density of the ground state (black) and the first excited state (red) for the dot with N=2 [top], N=3 [middle], N=4 [bottom]. $\omega_d = 7meV$, $U = 13meV$, $\alpha = 250meV\text{\AA}$	23

- 1.12 Charge density, azimuthal spin density S_z , in plane spin density S_r , in the radial direction, in the GS ($N = 5, J = 15/2$) at various SO couplings: $\alpha = 5, 100, 250 \text{ meV\AA}$. Here $B = 7 \text{ meV}$, $U = 13 \text{ meV}$ and $\omega_d = 5 \text{ meV}$ 24
- 1.13 Occupation numbers $n_{n=m,m,\sigma}$ in the GS with $N = 4(5)$ electrons (left(right)) without SO (top) and with SO ($\alpha = 100 \text{ meV\AA}$) (bottom). Other parameter values are $B = 7 \text{ meV}$, $U = 13 \text{ meV}$, $\omega_d = 5 \text{ meV}$. White bars refers to spin down, grey bars refer to spin up. The FSP GS of the dot with $N = 4(5)$ electrons has total spin $S = 2(5/2)$ and the z -component of the total angular momentum $J_z = (15/2)$ 24
- 1.14 The occupation numbers $n_{n=m,m,\sigma}$ in the state at $J_z = 15/2, 23/2, 25/2$ for small U [*left*], and large U [*right*]. White bars refers to spin down, grey bars refers to spin up. We stress that at $U = 0$ the ordering of the levels, corresponding to the three panels on the left is changed with respect to the ones on the right ($U = 13 \text{ meV}$). (see Fig. 1.6 [bottom panels]). 26
- 1.15 Charge density, azimuthal spin density S_z , in plane spin density S_r , in the radial direction, at various J_z . Parameters are $N = 5, \alpha = 100 \text{ meV\AA}$, $U = 13 \text{ meV}$ and $\omega_d = 5 \text{ meV}$ 26
- 1.16 N=3 particles dot: FES spin density (arb.units) for a) $\alpha = 150 \text{ meV\AA}$, b) $\alpha = 250 \text{ meV\AA}$, c) $\alpha = 350 \text{ meV\AA}$. By increasing the SO there is a squeezing close to the center and some reduction of $\langle \sigma_z \rangle$ 27
- 1.17 Absorption spectrum vs magnetic field for a) N=2 particles, b) N=4 particles 31
- 1.18 Slater determinants quoted in the text with the same labels. Quantum numbers are $N = 5, S = 5/2$ and J_z . Upper/ lower triangle refer to single particle states labeled by j_z and p/q . Other possible quantum numbers do not appear. The dots mark occupied states. 35
- 2.1 N=2 particles dot: (Left box) energy spectrum vs magnetic field ω_c in the absence of the SO. $\omega_d = 5 \text{ meV}$, $U = 13 \text{ meV}$, (Right box) energy spectrum vs magnetic field ω_c in the presence of the SO. Same parameter values and $\alpha = 250 \text{ meV\AA}$ 50
- 2.2 Slater determinant representation of the lowest lying states. We label with a - the orbitals $n = 0, m = 0$ and with a + the orbitals $n = 1, m = 1$ 51
- 2.3 Average value of the spin projection along the z axis using the adiabatic propagator (black curve) and the exact propagator for different values of the product rT . When rT is very large the average value $\langle \tilde{S}_z \rangle$ is very close to the one calculated in the adiabatic approximation 56

2.4	Sketch of a possible transport experiment across a quantum ring	58
2.5	Conductance vs ϕ/ϕ_0 for (left panel) ideal coupling with the contacts $r = 0$ and (right panel) more realistic contacts $r \neq 0$ for different values of the reflection amplitude at the contacts	66
2.6	Conductance vs $k_{SO}R$ for (left panel) ideal coupling with the contacts $r = 0$ and (right panel) more realistic contacts $r \neq 0$ for different values of the reflection amplitude at the contacts	67
2.7	Conductance vs ϕ/ϕ_0 for ideal coupling with the contacts $r = 0$ and corresponding average value of the outgoing spin $\langle S_z \rangle$	68
2.8	Conductance vs ϕ/ϕ_0 for ideal coupling with the contacts $r = 0$ and corresponding average value of the outgoing spin $\langle S_z \rangle$	69
3.1	Sketch of the Josephson junction exposed to a laser radiation pulse.	84
3.2	Pair breaking	88
3.3	Variation of the gap immediately after the pulse vs the inverse of duration of the pulse $\tau_c^{-1} = \omega_c$ in units of Δ . Our approximations break down for very low ratios ω_c/Δ (long pulses). On the other hand, large ω_c/Δ represent very short pulses: this situation is unrealistic with the available optical devices.	96
3.4	Voltage behavior in time for different energy released on the sample and the quality factor $Q = 100$. The voltage is normalized to $V_0 = \omega_{pJ}\varphi_0/c$	99
3.5	Voltage behavior in time with different quality factors Q in the linear conductance model (A,B) and the non-linear conductance model as given by Eq. (3.43) (C). The voltage is normalized to $V_0 = \omega_{pJ}\varphi_0/c$	100
3.6	Switching front in the parameter space a) $(\omega_c/\Delta, q)$ at fixed current bias $\gamma = J_b/J_c^o$ and b) (γ, q) at fixed ω_c/Δ , for $Q = 100$ and $\omega_D/\Delta = 10$. The full curves have been added as a guide for the eye: they mark the border between the zero voltage (Josephson) state and the voltage state. q is the coupling strength due to the laser pulse.	101

Ringraziamenti

Quando, tre anni fa, scrissi, come mio primo lavoro, la tesi di Laurea, qualche stupida forma di rigidità mi spinse ad evitare ringraziamenti e dediche. Alla fine del mio triennio di dottorato, ammetto di essermi ricreduto. La mia tesi di dottorato, frutto del mio lavoro, è figlia anche dei successi, delle fatiche e dei sacrifici di molte persone. Esse hanno contribuito a rendere più facile il mio percorso umano e scientifico di quest'ultimo triennio, aiutandomi nelle forme più disparate e arricchendomi mediante collaborazioni e discussioni. Sento pertanto doveroso ringraziare tutte queste persone e dedicare loro sia questa tesi che i lavori che sono riuscito a pubblicare.

È d'obbligo citare per primo il "prof." (Arturo Tagliacozzo): è lui che mi ha iniziato alla ricerca, che mi ha spinto verso le interessanti tematiche della fisica della materia condensata, che ha talvolta moderato le mie disinvoltate frenesie matematiche, talvolta risvegliato le mie curiosità sopite. Egli mi ha spinto a non accontentarmi mai di una comprensione superficiale della fisica, ma a cercare nei dettagli e nelle sfumature, apparentemente irrilevanti, il comportamento più intimo e vero della materia. Un grazie ancora perché non mi ha mai negato una spiegazione o qualche minuto di discussione anche quando era oberato e per i vari consigli che mi ha dato nei momenti meno facili. Lo ringrazio, insomma, per essere stato il più disponibile dei maestri ed il migliore dei collaboratori sia dal punto di vista umano che scientifico. Ringrazio Mimmo Giuliano per avermi dato tanti stimoli per avvicinarmi a problemi più squisitamente Teorici: è soprattutto grazie a lui ed al "prof" che ho formato il mio piccolo bagaglio Teorico (con la "T" grande). Ringrazio, poi, Benoit Jouault per avermi trasmesso la passione per la fisica numerica, che in passato avevo snobbato, ed avermi svelato tanti trucchi per usare al meglio un calcolatore. Ringrazio Dario Bercioux per essere stato un costante punto di confronto scientifico ed umano, un sicuro punto di riferimento e, soprattutto, un vero amico. Non posso non citare i miei 'compagni di birra' Claudio Cacciapuoti e Carlo Manzo, e tutti i 'coinquilini di studio' che nell'aula dottorandi sono stati sempre disponibili alla conversazione scientifica e ricreativa e poi Francesco Tafuri il cui straripante entusiasmo per la fisica mi ha spesso travolto. Ringrazio Enzo Capozza per aver contribuito a fare chiarezza sulle nostre approssimazioni quasiclassiche. Ringrazio Giacomo Rotoli ed Enrico Santamato per la fruttuosa collaborazione scientifica, Bruno Preziosi per avermi ben accolto, come suo assistente nel corso di Fisica II, senza mai farmi sentire a disagio, Enzo Marigliano per le interessanti discussioni sulla fisica dei quantum ring e Vittorio Cataudella per la lettura critica della tesi e l'interesse mostrato verso il mio lavoro. Un ringraziamento particolare va, poi, a Guido Celen-

tano, persona impagabilmente cortese e disponibile nonchè segretario dalla rara efficienza. Guido ha traghettato noi dottorandi, lungo il nostro iter, in maniera ineccepibile e ci ha aiutato nelle modalità più disparate, risolvendo, in maniera solerte, qualsiasi problema di sua competenza, accollandosi, non di rado, anche pratiche di nostra competenza pur di sgravarci dagli oneri burocratici (cui noi fisici siamo fisiologicamente reietti) e di sottrarci alle lungaggini degli ambienti amministrativi. Ringrazio i miei genitori e la mia famiglia tutta per avermi sempre supportato moralmente ed economicamente, per non avermi mai fatto pesare gli orari 'da albergo' con i quali per lunghi periodi ho frequentato casa, per aver sempre avuto una parola di conforto al momento opportuno e, soprattutto, per aver sempre creduto che una persona "normale", come me, potesse intraprendere la strada della ricerca. Infine ringrazio la persona che più di tutte mi è stata vicina, che ha sacrificato, per questo mio lavoro, serate fuori e diversi fine settimana; con lei ho condiviso momenti belli e brutti, nei momenti "facili" è stata foriera di serenità ed in quelli meno "facili" l'unica reale valvola di sfogo per me. A lei il mio ultimo grazie prima di raccontare un po' di fisica...

Introduction

According to an empirical law introduced by Gordon Moore [1] in 1965 the miniaturization of semiconducting electronic devices allows to double the number of transistors in a chip, and so its computational power, approximately every two years. This law was very well verified until 1980. Since that date, the processors power begun to double even faster: roughly every 18 months. If one, without paying too much attention to the physical limitations of the miniaturization, tries to make predictions about what will be the future of semiconducting chips by simply applying Moore's law, he should obtain the crazy result that in 2020, the continuation of geometrical scaling would mean that there would be less than one electron available for switching each transistor on microchips [2]. Obviously the physical limits to miniaturization will be reached well before and, actually, a reasonable prediction warns that the end of Moore's law will be very close, within 10 years. Therefore, in recent years, the scientific community is devoting an increasing interest in the direction of studying alternative devices. Richard Feynman, first, pointed out the possibility to build computers at the atomic scale, able to realize quantum operations [3]. Such devices have been called *quantum computers* and their building blocks are the so called *quantum bits*. This thesis is not devoted to qubits but discusses some topics strictly related to them. A simple example of the extraordinary computational power of a quantum computer is the very celebrated Shor algorithm. In 1994 Peter Shor [4] discovered an algorithm based on quantum computers capable of factorizing the RSA-129 code [5] (the cryptography code created in 1977 by R. Rivest, A. Shamir and L. Adleman) in 8 seconds by using 2000 qubits¹. That performance appeared absolutely extraordinary compared with the experimental result obtained in the same year by using 1600 net connected computers working together for about 8 months.

This result gave a strong improvement in both the theoretical and experimental research on quantum computers. Theoretical papers have been produced to evaluate the physical limits to computation [7] and to describe both quantum algorithms and candidate devices for quantum computation [8]. Recently, many proposed quantum bits are solid state mesoscopic devices. In particular some of them are based on superconducting materials (mainly Nb) such as the charge qubit [9] or the flux qubits [10], some others are based on semiconductors (mainly based on GaAs-AlGaAs heterostructures) double quantum dots [11] [12], and there are also many other proposals [13].

¹Actually, in his original proposal Shor hypothesized the use of 100000 quantum bits, the reformulation of the problem in terms of 2000 qubits was due to Deutsch, Barenco and Eckert [6] few months later

The big common problem of all of these devices is the decoherence due to their coupling with the environment and between themselves. In general, in actual devices, the coherence time is, today, shorter than the time needed for the computation, so basically at the moment this technology is not available. Once the scientific community will be able to solve this problem, another point will be addressed, which is the way in which these quantum systems will have to be manipulated in a controlled fashion.

The topic of the manipulation of quantum states of the solid state coherent devices is the central goal of this thesis. We have studied different manipulation techniques on different devices. From the theoretical point of view, this has been very stimulating, giving me the opportunity to use different approaches ranging from non equilibrium Green's function theories to numerical physics, to path integrals and many others. The problems studied concerns both the superconductors physics and the semiconductors physics. They are reported in three chapters; each chapter has its own appendixes, a bibliography, and a detailed discussion in the end, so that the reader could read whatever chapter independently of the others. In what follows I briefly summarize the topics developed in this work describing them as they appear in the chapters.

In chapter one we deal with the physics of 2D quantum dots. We first introduce the basics of quantum dots [14] showing some interesting results obtained in the presence of a Rashba spin orbit coupling.

In the presence of a magnetic field orthogonal to the dot plane the dot undergoes a sequence of transitions. When the magnetic field is weak the dot is unpolarized, the spins of the electrons tend to form singlets thus minimizing the total spin and also the orbital angular momentum is minimum. By increasing the magnetic field the dot reaches its Fully Spin Polarized(FSP) state that is, both the orbital and the spin angular momentum is maximum. By further increasing B the dot reconstructs and changes its shape as an effect of the magnetic squeezing. We mainly focus on the FSP state of the dot: in the case of a 2 electrons dot it corresponds to the very celebrated singlet triplet crossing, observed experimentally in 1999 [15]. We have found that, independently of the number of electrons in the dot, its ground state and low lying excitations are similar to a Quantum Hall Ferromagnet (QHF) close to filling 1 [16]. In fact when the dot is FSP the ground state is ferromagnetic like and the first excited state is a spin wave excitation very similar to the skyrmion excitation of the Quantum Hall disk. The shape of this excitation can be squeezed and manipulated by tuning the electric field orthogonal to the dot plane, that is by varying the Rashba spin orbit coupling. The ground state and the first excited state look very appealing: they are two well defined spin states with a tunable spin gap of the order of microwaves between them. So, we have studied the possibility to induce a transition between this two states by mean of a Far Infrared Radiation (FIR). If possible, this could allow for a coherent manipulation of the spin

state of a dot [17]. In fact, in this framework, the quantum manipulation of the dot is intended as the flipping of the dot spin by mean of an external FIR field.

Our numerical results show that such a spin manipulation is possible. So the FIR can be useful for a coherent manipulation of the spin states of the dot. Moreover, as explained in detail in chapter one, the FIR can also allow to monitor the crossover to the FSP state. This crossover, interestingly enough, becomes sharper and sharper by increasing the number of particles on the dot, which means that we are going in the direction of the thermodynamic limit and of a phase transition, when increasing the dot size toward a quantum Hall disk.

In the second chapter we deal with the possibility of performing an adiabatic manipulation of the two electron dot close to the singlet triplet crossing. This idea emerged in view of the fact that some quantum algorithms assume that the system dynamically evolves through a sequence of unitary transformations, or that a set $\vec{\lambda}$ of external control parameters of the Hamiltonian H smoothly changes in time [18]. In particular, if adiabatic evolution is realized across a closed path γ in the parameter space, close enough to an accidental level degeneracy, the nontrivial topology of the space makes the state of the system to take a “geometrical” phase Γ , referred to as “Berry Phase” [19]. The value of Γ may be controlled by properly choosing γ . Following this idea, geometric adiabatic evolution has recently been proposed as a way to operate with superconducting devices without destroying phase coherence [20, 21].

In the two electron quantum dot the single triplet crossing becomes an anti crossing in the presence of a Rashba coupling. In other words by cyclically modulating in time an electric field orthogonal to the dot plane, and as a consequence the Rashba coupling, we can tune the dot close enough to the level degeneracy point. The nontrivial topology of the space allows the many body wavefunction to acquire a “geometrical” phase Γ . This phase is in general an Ahronov Anandan phase [22] and in the adiabatic limit a “Berry Phase” [19]. In order to properly describe this situation we introduce an effective low energy Hamiltonian by projecting the full Hamiltonian onto the singlet and the triplet states involved in the anti-crossing. Such a projection gives us a simple two level Hamiltonian that, in the adiabatic limit recalls the very celebrated two level Berry Hamiltonian. Solving this simple model we show that the many body wavefunction of the dot acquires a geometrical phase [23].

Then we describe a possible transport experiment that should allow for reading out such a geometrical phase. The device studied, in this case, is not a quantum dot but a quantum ring. This choice allows us to simplify the calculations and gives us a very clear physical picture. Moreover such a structure is capable of producing a geometrical phase without any time dependent parameter because, in this case, we can deal with the electrons semiclassically.

The electrons themselves, by moving into the arms of the ring, experience time dependent external fields varying according to semi-classical equations of motions. Some evidences of geometric phases are described; interestingly in the non adiabatic regime, that is when a strong spin orbit and a weak magnetic fields are present, some spin flips effect have been observed. [24]

In the last chapter we study the ultrafast optical manipulation of a low T_c Josephson junction. This is, once again, in the direction of producing a manipulation of a quantum device without affecting its coherence. We begun studying this problem in order to give a theoretical support to the experimental groups involved in the Coherentia labs in Napoli [25,26].

The idea of shading laser radiation onto Josephson junctions, is of thirty years ago: the first experimental results [27] showed that a coupling between optical radiation and superconductivity was possible but the coherence of the superconductors were degraded because of the heating of the samples due the radiation.

The bolometric regime, that is when the sample 'feels' the radiation basically by mean of heating effects, has been extensively studied in the past [28].

Recent experimental techniques allow to release very low energy in short time windows (few tenths of fs) so that the coupling can preserve coherence, though in a non-equilibrium environment of carriers. The laser radiation excites electronic modes very high in energy and superconductivity plays no role in this: this very energetic electrons generate a cascade process which gives rise to a massive pair breaking, depending on the energy the the single photons. Wonderful theoretical papers have been published for the case of high energy photons (X rays), mainly by Larkin, Ovchinnikov and Kresin [29].

Some experiments have been performed with optical photons but at present, to our knowledge, no microscopic theories have been developed to describe them. In this experiential works some phenomenological theories [30–32] are usually invoked to describe the measurements.

We develop a microscopic theory, which shows that it is possible to stimulate in the superconductor a non-equilibrium dynamics without destroying the quantum coherence. This theory is based on non-equilibrium Keldysh Green's functions and allow for studying the response of the junction to such an optical stimulation. Within our non-equilibrium formalism we study the time evolution of the order parameter of the irradiated electrode and then the response of the whole junction by numerically analyzing the modified Josephson coupling. The order parameter can be manipulated in time in controlled way by appropriately tuning the duration of the radiation and the energy it releases [33].

Bibliography

- [1] G. E. Moore, *Electronics*, volume 38-8 (1965)
- [2] J. Birnbaum and R. S. Williams, *Physics Today*, volume 53-1, 38 (2000).
- [3] R. P. Feynman, *Int.J.Theor.Phys.* **21**, 467 (1982); R. P. Feynman, *Optics News* **11**,11 (1985).
- [4] P. W. Shor, Algorithms for quantum computation: Discrete logarithms and factoring, in *Proc. 35nd Annual Symposium on Foundations of Computer Science* (Shafi Golwasser, ed.), IEEE Computer Society Press (1994),124.
- [5] The criptography code RSA129 was invented in 1977 by Rivest, Shamit and Adleman at MIT. It consisted in founding the two prime numbers factorizing a number of 129 digits. This problem offers an exponential computational complexity and, with classical computer requires a very long computational time; it was first solved into 1995 by 1600 net connected computers working togheter for 8 months.
- [6] D. Deutsch, A. Barenco, A. Ekert, *Proc. R. Soc. London A* **449**, 669 (1995).
- [7] S. Lloyd, *Nature*, **406**,1047 (2000).
- [8] S. Loyd, *Science*, **261**, 1569 (1993), D. Di Vincenzo, *Science*, **270**, 255 (1995); A. Barenco, C. H. Bennett, R. Cleve, D. P. DiVincenzo, N. Margolus, P. Shor, T. Sleator, J. A. Smolin and H. Weinfurter, *Phys. Rev. A* **52**, 3457 (1995).
- [9] Y. Nakamura, Yu. Pashkin and J. L. Tsai, *Nature* **398**, 786 (1999).
- [10] J. E. Mooij, T. P. Orlando, L. Levitov, L. Tian, C. H. van der Wal and S. Lloyd *Science* **285**, 1036 (1999); C. H. van der Wal, A. C. J. ter Haar, F. K. Wilhelm, R. N. Schouten, C. J. P. M. Harmans, T. P. Orlando, S. Lloyd and J. E. Mooij *Science* **290** 773 (2000); I. Chiorescu, Y. Nakamura, C. S. P. Harmans, J. E. Mooji, *Science* **299** 1869 (2003).
- [11] J. M. Elzerman, R. Hanson, L. H. Willelms van Beveren, L. M. K. Vandersypen and L. Kouwenhoven, *Nature* **430**, 431 (2004).
- [12] N. J. Craig, J. M. Taylor, E. A. Lester, C. M. Marcus, M. P. Hanson, A. C. Gossard, *Science* **304**, 565, (2004); L. I. Glazman and R. C. Ashoori, *Science* **304** 524, 2004.

- [13] A. Wallraff, A. Lukashenko, J. Lisenfeld, A. Kemp, M. V. Fistul, Y. Koval and A. V. Ustinov *Nature* **425**, 155 (2003); D. Vion, A. Aassime, A. Cottet, P. Joyez, H. Pothier, C. Urbina, D. Esteve and M. H. Devoret, *Science* **296**, 286, (2002).
- [14] L. P. Kouwenhoven, D. G. Austing, S. Tarucha *Rep. Prog. Phys.* **64** (6), 701 (2001); L. P. Kouwenhoven and C. M. Marcus *Phys. World* **116**, 35 (1998); M. A. Kastner, *Ann.Phys.(N.Y.)* **9** , 885 (2000).
- [15] T. H. Oosterkamp, J. W. Janssen, L. P. Kouwenhoven, D. G. Austing, T. Honda and S. Tarucha, *Phys. Rev. Lett.* **82**, 2931 (1999).
- [16] P. Lucignano, B. Jouault, A. Tagliacozzo, *Phys. Rev. B***69**, 045314 (2004).
- [17] P. Lucignano, B. Jouault, A. Tagliacozzo, B. L. Altshuler submitted (2004).
- [18] E. Farhi, J. Goldstone, S. Gutmann, J. Lapan, A. Lundgreen and D. Preda, *Science* **292**, 472 (2001).
- [19] M. V. Berry, *Proc. R. Soc. London, A* **392**, 45 (1984).
- [20] G. Gaitan and S. R. Shenoy, *Phys. Rev. Lett.***76**, 4404 (1996).
- [21] G. Falci, R. Fazio, G. M. Palma, J. Siewert, V. Vedral, *Nature* **407**, 355 (2000).
- [22] Y. Aharonov, J. Anandan, *Phys. Rev. Lett.* **58**, 1593 (1987).
- [23] D. Giuliano, P. Lucignano, A. Tagliacozzo, “Spin manipulation in quantum dots by mean of electric field and voltage gates” in print in *Materials Science*.
- [24] E. Capozza, D. Giuliano, P. Lucignano, A. Tagliacozzo *Model hamiltonian and adiabatic evolution*, unpublished notes.
- [25] P. Lucignano Laurea Thesis “Interazione di radiazione laser ultraveloce con dispositivi a superconduttore” (2001), unpublished.
- [26] P. Lucignano, F. J. W. Hekking and A. Tagliacozzo, in “Quantum computing and Quantum bits in mesoscopic systems”, A. J. Leggett, B. Ruggero, P. Sivestrini ed.s, Kluwer Academic, Plenum Publishers N.Y. (2004).
- [27] L. R. Testardi, *Phys. Rev. B* **4**, 2189, 1971.
- [28] A. Barone and G. Paternó, *Physics and applications of Josephson effect*, Wiley New York, 1982.

- [29] Yu. N. Ovchinnikov and V. Z. Kresin *Eur. Phys. J. B* **32**, 297, (2003),
Yu. N. Ovchinnikov and V. Z. Kresin, *Phys. Rev. B* **58**,12416,(1998),
A. I. Larkin and Yu. N. Ovchinnikov *Zh. Eksp. Teor. Fiz* **55**,2262 (1968)
[*Sov. Phys. JETP* **28**, 1200, 1969].
- [30] A. V. Sergeev, M. Yu. Reizer, *J. Mod. Phys. B* **6** 635 (1996), M. Yu.
Reizer, *Phys. Rev. B* **39** 1602 (1989), A. V. Sergeev, M. Yu. Reizer, *Zh.*
Eks. Teor. Fiz. **90** 1096 (1986) [*Sov. Phys. JETP* **63** 616 (1986)]
- [31] M. Lindgren, M. Currie, C. Williams, T.Y. Hsiang, P. M. Fauchet,
R. Sobolewski, S. H. Moffat, R. A. Hughes, J. S. Preston and F. A.
Hegmann *Appl. Phys. Lett.* **74** 853 (1999)
- [32] A. D. Semenov, R. S. Nebosis, Yu. Gousev, M. A. Heusinger, K. F.
Renk, *Phys. Rev. B* **52** 581 (1995).
- [33] P. Lucignano, G. Rotoli, E. Santamato, A. Tagliacozzo, *Phys. Rev.*
*B***70**, 024520, 2004.

Science may set limits to knowledge, but should not set limits to imagination.

Bertrand Russell (1872-1970)

1

Quantum dots with spin orbit coupling

Abstract

We discuss the properties of two dimensional quantum dots with few interacting electrons in the presence of a magnetic field and an electric field orthogonal to the dot plane. The energy spectrum, the charge distribution and the spin distribution of the dots are discussed in detail. The Coulomb interactions between the electrons, with a large magnetic field $B = B^*$ applied in the z-direction (orthogonal to the dot), produce a fully spin polarized (FSP) ground state. The Rashba coupling can be tuned by using the electric field and induce the splitting of the levels corresponding to the FSP multiplet of total spin $S = N/2$. We find that the first excited state is a particular state which has a spin texture carrying one extra unit of angular momentum. This is reminiscent of the Quantum Hall Ferromagnet at filling one which has the skyrmion state as its first excited state. The spin orbit coupling can squeeze the flipped spin density at the center of the dot, can increase the gap in the spectrum and can tune the energy and the spin density of the first excited state. Far infrared radiation absorption can induce a transition from the ground state to the first excited state and monitor the crossover to the FSP state.

1.1 Introduction

Quantum dots (QD's) are semiconductor devices in which electrons are confined to a small area within a two dimensional electron gas by properly biasing voltage gates added to the structure [1, 2]. In an isolated quantum dot (QD) the confining potential gives rise to quantized single particle energy levels. However, electron-electron interaction determines the dot properties. In dots having a diameter of $\sim 100nm$, the level spacing and the Coulomb energy are of the order of the meV and most charging properties can be included within the Hartree-Fock (H-F) approximation, just like in atoms. Correlation effects do not significantly alter the charging properties, but may strongly influence the spin properties of the confined electrons. One

striking evidence of this is the fact that Hund's rule, which is typical of atoms, is often satisfied in dots [3]. However, the reduction of the energy scale by a factor of 10^{-3} with respect to atoms, enhances the sensitivity of the electrons in the dot to an external magnetic field.

Quantum dots, have been proposed as devices for the future quantum electronics. One of the possibilities is to operate on the spin of the trapped electrons as a qubit [4]. In a different proposal the QD controls the nuclear spins embedded in the crystal matrix via hyperfine coupling [5]. In both cases the polarization of the spins is expected to last long enough at low temperatures, so that the quantum computation can be carried out. Controlled spin transfer between electrons and nuclei has been demonstrated to be possible in a spin polarized two-dimensional electron gas (2DEG) [6]. In a 2DEG fully spin polarized quantum Hall states are used to manipulate the orientation of nuclear spins. Low lying skyrmion states at filling close to one are used to reset the nuclear spin system by inducing fast spin relaxation. In the presence of a magnetic field B orthogonal to the dot, the relaxation mechanism seems to be dominated by hyperfine interaction for $B < 0.5T$ and by spin-orbit (SO) coupling assisted by phonons for higher fields [7]. The inverse relaxation time $1/T_1$ has also been probed recently by transport across a single QD [8]. In the cylindrical geometry, orbital effects are dominant [9]. Indeed Zeeman spin splitting does not drive any spin polarization in these systems and can be often ignored ¹.

However correlations combine orbital and spin effects together and can be probed by magnetoconductance measurements in a pillar configuration [11, 12]. Spin properties are quite relevant to conductance, in view of the possibility of spin blockade [13, 14], Kondo effect [15, 16], or Berry phase induced tuning [17].

Quantum numbers labeling the dot energy levels are the number of electrons N , the total orbital angular momentum along z , M , the total spin S and the z -component of the spin S_z . By increasing the magnetic field B , both M and S increase. Finally, at $B = B^*$, a fully spin polarized (FSP) state is reached. The increasing of the total spin S was measured in a dot with about 30 electrons, a striking evidence of e-e correlations [18]. While, in the absence of interactions, the density of the FSP state becomes uniform over the dot area, which is contracted to a minimum, in the real case, the e-e interaction tends to reduce the density at the center of the disk, by

¹This is due to the fact that the Hamiltonian term coupling B_\perp to M is $\mu_B^* B_\perp M$ where $\mu_B^* = e\hbar/2m^*c$ is the effective Bohr magneton (m^* is the effective mass). On the other hand the Zeeman spin splitting term is $g^* \mu_B B_\perp S_z$, where g^* is the effective gyromagnetic factor for electrons in this geometry (very low in many semiconductor heterostructures) while μ_B is the Bohr magneton with the bare mass (spin is insensitive to band effects). The situation is similar to what happens in the QHE where ω_c includes the effective mass and Landau level separation is increased by a factor of ~ 20 , while Zeeman spin splitting, being reduced by a factor of 4, becomes negligible in comparison [10]

compressing the electrons at the dot edge (see Fig.1.4 [middle panel]). By further increasing B , the electron density reaches a maximum value. The dot becomes a so called “Maximum Density Droplet” (*MDD*) [19]. For larger B values, the *FSP* state is disrupted: the dot density reconstructs i.e. an annular local maximum of the density is produced at the edge of the dot [20] with breaking of azimuthal symmetry at the edge (de Chamon-Wen phase [21]).

Various numerical calculations [22] have investigated these subsequent electronic transformations which appear as crossing of levels with different quantum numbers. H-F calculations are known to incorrectly favor spin-polarized states [23]. Spin density functional calculations have been performed for dots including a larger number of electrons [24]. The density functional approach, with a good choice of the parameters of the potentials, can reach a significative agreement with the experiments, but it may introduce uncontrolled approximations. When the electron density is reduced, a Wigner molecule can be formed. Recently, this broken symmetry state has been studied in the absence of an external magnetic field, using Quantum Monte Carlo simulations, with a multilevel blocking algorithm which is free of the sign problem [25]. We use exact diagonalization for few electrons with azimuthal symmetry [14, 26] to discuss the spectral properties of the dot which is stabilized by the Coulomb interaction.

In what follows we discuss the spin properties of an isolated QD in presence of a magnetic field B in the z -direction, orthogonal to the dot disk (cylindrical symmetry is assumed). Electrons are confined to a two-dimensional ($2-d$) disk by a $2-d$ parabolic potential and interact via the full Coulomb repulsion whose strength is parametrized by $U = e^2/\kappa l$. Here l is the magnetic length due to the parabolic confinement in the presence of the magnetic field and κ is the static dielectric constant. The potential confining the electrons in the $x-y$ plane often is not symmetric for an inversion w.r. to the growth direction z , this implies the presence of an electric field in the z -direction which gives rise to the so called Spin Orbit (SO) Rashba term [27]. It provides a coupling between the orbital motion and the spin degree of freedom of the electrons and can be tuned, in a non-linear conductance measurement, when an extra bias voltage V_{sd} is applied to the contacts of a vertical structure. This possibility has been beautifully shown in *InGaAs*-based 2DEG [28] and in a recent experiment on large lateral QD, where the conductance has been tuned from the weak localization limit, without SO coupling, to the anti-localization limit, with SO [29]. Recent technological improvements allow to realize nanostructured materials in which the SO effects can be observed in transport measurement [30]. In the presence of SO, $J_z = M + S_z$ becomes the good quantum number. This modify the energy spectrum which is characterized by the presence of marked anti-crossings between levels coupled by the SO Hamiltonian [31].

The FSP ground state (GS) has $J_z = N(N-1)/2 - S$ (e.g. $J_z = 15/2$ for

$N = 5$), while the first excited state (denoted as DES state in the following) has $J_z = N(N - 1)/2 - S + 1$ (e.g. $J_z = 17/2$ for $N = 5$). The charge density is rather insensitive to the SO coupling, α . However, we show that the SO interaction by coupling the spin polarization to the orbital motion determines the spin properties of the GS and the first excited states in a surprising way. Indeed, by increasing α , the expectation value of the spin density of the GS, which was originally oriented in the z -direction, acquires a component in the dot plane, because the minority spin density is increased and pushed away from the center of the dot outward. Moreover the combined effect of U and α deforms substantially the spin density of the FES. A sharp minority spin polarization is present close to the dot center. The reversal of the spin polarization at the origin in the FES state w.r. to the FSP GS leads to an extra node in the spin density.

This situation is reminiscent of the case of the Quantum Hall Ferromagnet (*QHF*) [32] close to filling one. In that case, a true magnetic ordering is achieved, which is characterized by full spin polarization in the GS and by a topologically constrained first excited state, the Skyrmion (*SK*) state, with reversal of the spin at the origin, first studied in the $O(3)$ non linear σ model (*NLSM*) in $2 - d$ dimensions [33, 34]. There is evidence of skyrmion excitations in *GaAs* $2 - d$ electron gas systems close to filling one by magnetoabsorption spectroscopy [35]. We elaborate on the analogies and differences between the *FSP* dot and the *QHF*. In the *QHF* a topological quantization of charge occurs. By contrast the FES state has no topological features, because the geometrical compactification procedure cannot take place. We refer to the FES state as a “spin exciton” because there is some piling up of the charge at the center of the dot w.r.to the GS, together with the reversal of the spin polarization there. This spin exciton FES is found to be a universal property of the dot, that is independent of the number of particles confined. Within our numerical diagonalization scheme we have found this peculiar state for $N = 2, 3, 4, 5$.

We propose to probe this excited state using a Far Infrared Radiation (FIR) pumping [31]. A sharp absorption line is expected be found in exciting dots to the FES state, by transferral of energy and angular momentum with circularly polarized light. This amounts to adding a spin exciton to the dot. We find that the absorption intensity for circularly polarized FIR is strongly enhanced when the crossover to the FSP state is completed (see Fig.1.17). Moreover the spin density can be squeezed at the center of the dot by increasing the SO coupling α (see Fig.1.16). Meanwhile the gap between the GS and FES increases with α (as shown in Fig.1.8 for $N=3$).

1.2 FSP state and dot reconstruction

We consider N (we discuss in the following the cases $N = 2, 3, 4, 5$) electrons confined in two dimensions (spanned by the (ρ, φ) coordinates) by a parabolic potential of characteristic frequency ω_d . This is a model for an isolated disk shaped QD. A magnetic field B orthogonal to the disk is measured in units of $\hbar\omega_c$ (meV), where ω_c is the cyclotron frequency. The single particle Hamiltonian, for the i -th electron, in the effective mass approximation (m_e^*), in the absence of spin orbit coupling is:

$$H_{(i)} = \frac{1}{2m_e^*} \left(\vec{p}_i + \frac{e}{c} \vec{A}_i \right)^2 + \frac{1}{2} m_e^* \omega_d^2 r_i^2, \quad (1.1)$$

with $\vec{A}_i = B/2 (y_i, -x_i, 0)$, and e is minus the electron charge.

The single particle states ϕ_{nm} are the eigenfunctions of the $2-d$ harmonic oscillator with frequency $\omega_o = \sqrt{\omega_d^2 + \frac{\omega_c^2}{4}}$. They are labeled by n, m (with $n \in (0, 1, 2, 3, \dots)$ and $m \in (-n, -n+2, \dots, n-2, n)$). m is the angular momentum in the z direction:

$$\begin{aligned} \phi_{nm} &= \frac{e^{im\varphi}}{l\sqrt{\pi}} R_{n|m|}(t) = \\ \mathcal{C}_{nm} \frac{e^{im\varphi}}{l\sqrt{\pi}} e^{-\frac{\rho^2}{2l^2}} \left(\frac{\rho}{l} \right)^{|m|} L_{\frac{n-|m|}{2}}^{|m|} \left(\frac{\rho^2}{l^2} \right). \end{aligned} \quad (1.2)$$

Here $L_n^\alpha(t)$ (with $t = \rho^2/l^2$) is the generalized Laguerre polynomial with $n \geq 0$ [36], $l = \sqrt{\hbar/m^*\omega_o}$ is the characteristic length due to the lateral geometrical confinement in the dot inclusive of the B field effects and $\mathcal{C}_{nm} = \left[\frac{\left(\frac{n-|m|}{2}\right)!}{\left(\frac{n+|m|}{2}\right)!} \right]^{\frac{1}{2}}$ is a normalization factor.

The corresponding single particle energy levels are the so called Fock-Darwin levels [37],

$$\epsilon_{n,m} = (n+1)\hbar\omega_o - \frac{m}{2}\hbar\omega_c. \quad (1.3)$$

plotted in Fig.1.1. When the magnetic field is close to zero the spectrum reproduced the two dimensional harmonic oscillator spectrum with levels equally spaced in energy. By increasing the magnetic field there is the formation of the infinitely degenerate Landau bands which group levels having the same orbital angular momentum.

In the absence of SO, the full Hamiltonian for the dot, inclusive of the Coulomb interaction between the electrons (parametrized by U) is:

$$H = \sum_{i=1}^N H_{(i)} + \sum_{\substack{i < j \\ i, j=1}}^N U/|\vec{r}_i - \vec{r}_j|. \quad (1.4)$$

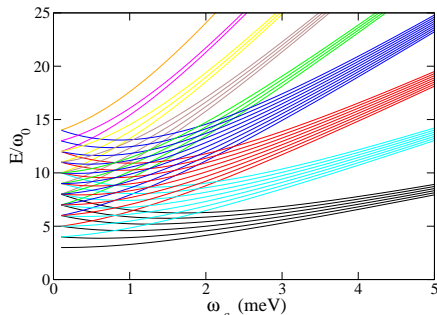


Figure 1.1: Single particle Fock and Darwin states of a parabolically confined two dimensional quantum dot

The orbital angular momentum $M = \sum_{i=1}^N m_{(i)}$, the total spin S and S_z (the projection of the spin along \hat{z}) are good quantum numbers.

We have performed Lanczos exact diagonalization of this system including Coulomb interaction between the electrons. The matrix elements of the unscreened Coulomb interaction use the single particle basis set, up to 28 orbitals. They can be calculated analytically and are parametrized by the strength of the interaction U . Our calculation is limited to very small particle numbers ($N < 7$), because the truncation of the Hilbert space influences the results for larger N . However, our convergency checks show that the numerical errors proliferate only at higher energies². In particular they affect the reliability of the level spin degeneracy. In any case, numerical errors are quite small if N is less or equal to 6. In the presence of the $e - e$ interaction the Fock and Darwin spectrum is slightly deformed: in fig 1.2 the energy spectrum of a $N = 2$ particles dot shows a different behavior of the levels vs the magnetic field with respect to the single particle spectrum. In particular, it shows many interesting crossings between states with different M . The most interesting one describes the very celebrated singlet triplet [19] transition which has never observed in real atoms but it is realizable in quantum dots because of their increased sensitivity at the magnetic fields. At low B field the ground state is a singlet state with $M = 0$ and $S_z = 0$, by increasing the magnetic field the ground state becomes the triplet state with $M = 1$ and $S_z = -1$.

In the absence of both interaction and magnetic field, the lowest lying single particle states are occupied with the minimum spin. The GS Slater determinant for $N=5$ is sketched pictorially in Fig.1.3a, where energy is intended on the vertical axis. Each box represents a single particle state labeled by n, m and arrows represent electron occupancy with spin projection along the quantization axis.

In Fig.1.4 [left panels], we show the lowest lying total energy levels at

²A new Lanczos routine has been improved in collaboration with B.Jouault in order to minimize the errors in the calculation of the energies of excited states. Preliminary results, not showed in this thesis, show a good agreement also for very excited levels with energy eigenvalues obtained performing an exact diagonalization (possible only for small Hilbert spaces)

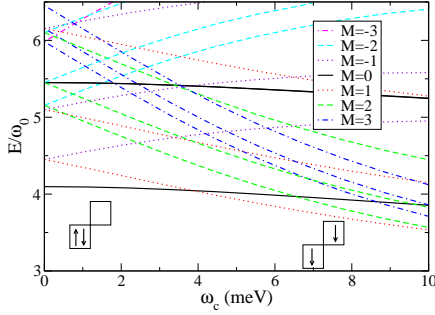


Figure 1.2: Energy levels vs magnetic field without SO coupling for the dot with $N = 2$ electrons at $U = 13 \text{ meV}$ and $\omega_d = 5 \text{ meV}$.

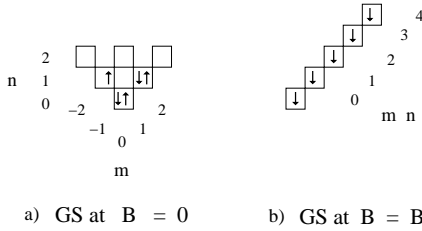


Figure 1.3: Slater determinants quoted in the text are depicted. Quantum numbers are $N = 5$, $S = 1/2$ for the state at $B = 0$ [a)] and $S = 5/2$ for the state at $B = B^*$, the magnetic field value at which the maximum absolute value of S is achieved [b)].

fixed angular momentum M , versus M , for $U = 13 \text{ meV}$. Magnetic field is $B = 5 \text{ meV}$ [top], $B = B^* = 7 \text{ meV}$ [middle], $B = 11.5 \text{ meV}$ [bottom]. At each M , the spin degeneracy is marked by dashes of different length: short dashes for $S = 1/2$ (doubly degenerate level), medium dashes for $S = 3/2$ (fourfold degeneracy) and long dashes for $S = 5/2$ (sixfold degeneracy). On the r.h.s. of the picture the radial charge density of the corresponding GS is plotted *vs* distance r from the dot center. Fig.1.4 ([left panels]) shows the crossing of levels with increasing B . Electron-electron correlations imply that when M increases, S also increases. At $B = B^* = 7 \text{ meV}$ the spin S reaches its maximum value $S = N/2$. The largest contribution to the GS wave function is given by the Slater determinant depicted in Fig.1.3b for $N=5$ corresponding to $M = \sum_0^{N-1} m = 10$. We concentrate on the state at $B = B^*$, the *FSP* GS. This corresponds to the “maximum density droplet” state discussed in the literature [19]. Qualitatively we can say that at $B = B^*$ the dot attains its smallest radius. As can be seen from the GS charge density, further increase of B leads to the so called reconstruction of the charge density of the dot. For $B > B^*$, the M of the GS increases further, but S is no longer at its maximum. In the bottom panel of Fig.1.4 it is shown that at $B = 11.5 \text{ meV}$ the GS energy is now achieved for $M = 13$ with a doublet ($S = 1/2$) state. The corresponding charge density of the dot, as depicted on the r.h.s, is strongly modified close to the edge [20]: it displays a node followed by an extra non zero annulus at a larger distance. In view of the fact that our expansion of the wave function only includes rotationally invariant components, the breaking of the azimuthal symmetry

is impossible. By contrast this is found to occur in density functional calculations and the corresponding GS is referred to as the de Chamom-Wen phase [21]. The GS at $B = B^*$ can be compared with a *FSP* quantum Hall state of an extended disk in the absence of lateral confinement (Quantum Hall Ferromagnet (QHF) at filling one). Fig. 1.3b) recalls the occupancy of the lowest Landau level (LLL) up to a maximum $m = N - 1$, except for the fact that in our case the single particle levels corresponding to the LLL are not all degenerate in energy. In the language of the quantum Hall effect the unperturbed levels are:

$$\epsilon_{\nu,m} = (2\nu + |m| + 1)\hbar\omega_o - \frac{m}{2}\hbar\omega_c \quad (1.5)$$

where $\nu = (n - |m|)/2$. LLL is for $\nu = 0$ and $m \geq 0$. The Slater determinant of Fig.1.3b) has a charge density which is flat as a function of the radius r , up to the disk edge, where it rapidly falls down to zero. In our case this feature is lost because of the presence of U , together with the fact that the number of electrons is small. We shall better discuss the comparison of the *FSP* GS with the *QHF* in the following.

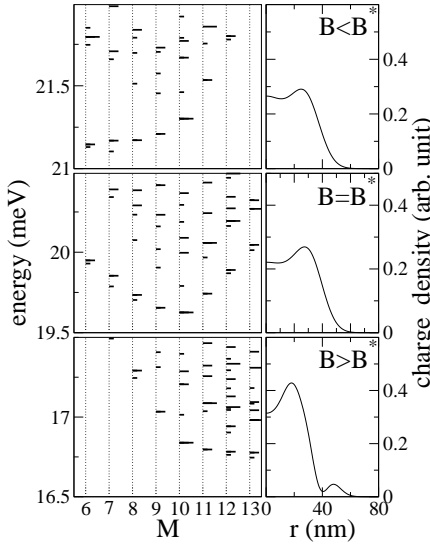


Figure 1.4: Energy levels without SO coupling for the dot with $N = 5$ electrons at $U = 13 \text{ meV}$ and $\omega_d = \text{meV}$. Magnetic field values are: (in units of $\hbar\omega_c$): $B = 5 \text{ meV}$ [top], $B = B^* = 7 \text{ meV}$ [middle], $B = 11.5 \text{ meV}$ [bottom]. The total M is on the x axis. The levels are drawn with short, medium or long dashes, depending on the total spin : $S = 1/2, 3/2, 5/2$

1.3 Inclusion of spin-orbit

We now add the spin orbit interaction to dot. This can be tuned by applying an electric field \mathbf{E} in the \hat{z} direction, which couples to the spin of the electrons in the dot with the so called Rashba (single particle) Hamiltonian [27]:

$$H_{so} = -\frac{\alpha}{\hbar} \left[\left(\vec{p} - \frac{e}{c} \vec{A} \right) \times \vec{\sigma} \right] \cdot \hat{z}. \quad (1.6)$$

Here $\vec{\sigma}$ are the Pauli matrices, α is the spin-orbit coupling parameter which is proportional to the electric field. α will be measured in units of $meV \cdot \text{\AA}$. \vec{A} is the vector potential due to the magnetic field B orthogonal to the dot plane: in the symmetric gauge it assumes the form $\vec{A} = B/2 (-y, x, 0)$. Expanding 1.6 in a 2D matrix form (using the Pauli matrixes) we can write

$$H_{so} = \alpha \left[\begin{pmatrix} 0 & \partial_x - i\partial_y \\ -(\partial_x + i\partial_y) & 0 \end{pmatrix} - \frac{eB}{2\hbar} \begin{pmatrix} 0 & x - iy \\ -(x + iy) & 0 \end{pmatrix} \right]. \quad (1.7)$$

We now rewrite the last equation in a second quantized form choosing an appropriate spinor basis (\uparrow, \downarrow). We denote the fermionic operators associated to ϕ_{nm} of Eq.(1.2) by $c_{nm\sigma}, c_{nm\sigma}^\dagger$ and we get:

$$H_{so} = \alpha \sum_{nm, n'm'} \left\{ \langle n'm' | -(\partial_x + i\partial_y) | nm \rangle c_{n'm'\downarrow}^\dagger c_{nm\uparrow} + \right. \quad (1.8)$$

$$\left. \langle n'm' | \partial_x - i\partial_y | nm \rangle c_{n'm'\uparrow}^\dagger c_{nm\downarrow} \right\} + \quad (1.9)$$

$$\frac{eB}{2\hbar} \left\{ \langle n'm' | x - iy | nm \rangle c_{n'm'\downarrow}^\dagger c_{nm\uparrow} + \right. \quad (1.10)$$

$$\left. \langle n'm' | x + iy | nm \rangle c_{n'm'\uparrow}^\dagger c_{nm\downarrow} \right\} .$$

The integration over the azimuthal angle φ have been done analytically. The Hamiltonian can be, then, rewritten in the following way:

$$H_{so} = \frac{\alpha}{l} \sum_{nn'} \sum_m \left(B_{n'm+1, nm} \left(1 - \frac{\omega_c}{\omega_0} \right) c_{n'm+1\downarrow}^\dagger c_{nm\uparrow} + \right. \quad (1.11)$$

$$\left. A_{n'm-1, nm} \left(1 - \frac{\omega_c}{\omega_0} \right) c_{n'm-1\uparrow}^\dagger c_{nm\downarrow} \right) ,$$

with

$$A_{n'm'nm} = \delta_{m'+1, m} \int_0^\infty dt R_{n'|m'}(t) \left(2\sqrt{t} \frac{\partial}{\partial t} + \frac{m}{\sqrt{t}} \right) R_{n|m}(t), \quad (1.12)$$

and

$$B_{n'm'nm} = \delta_{m'-1, m} \int_0^\infty dt R_{n'|m'}(t) \left(2\frac{\partial}{\partial t} \sqrt{t} + \frac{m'}{\sqrt{t}} \right) R_{n|m}(t). \quad (1.13)$$

Here $B_{nm, n'm-1} = A_{n'm-1, nm}^*$, what implies that the hamiltonian is hermitian. A pictorial sketch can help in understanding what happens in the presence of both an orthogonal magnetic field and a SO Rashba coupling. In the absence of an external orthogonal B field the Rashba coupling acts as an effective *in plane* magnetic field that forces a precession of the electron spins in the dot plane. An out of plane component of B tends to tilt the spin out of the plane acting, thus, in opposition to the Rashba coupling. Our

calculation confirms this intuitive idea that the SO coupling is weakened by an orthogonal magnetic field, in fact in 1.11 by increasing ω_c (that is increasing the orthogonal magnetic field B), the strength of the SO interaction decreases.

It is clear that while s_z and m are no longer separately conserved, their sum $j_z = s_z + m$ (with j_z half integer) is a good quantum number. We shall denote the single particle basis that diagonalizes the SO term by $w_{j_z}^\beta$ with $\beta = p, m$. The label β takes two possible values, say p, q and allows for the conservation of the number of degrees of freedom.

The SO interaction lifts the spin degeneracy. In Fig.1.5 we show the splitting of the multiplet with $N = 5$, $S = 5/2$, $M = 10$ at $B = B^* = 7 \text{ meV}$ and $U = 13 \text{ meV}$ vs the strength of the SO coupling α . The strength of U is responsible not only for the fact that the GS belongs to this multiplet, but also for the ordering in energy of the sequence: $J_z = 15/2, 17/2, 19/2, 21/2, 23/2, 25/2$ (from bottom to top). At small U values the sequence is $J_z = 25/2, 23/2, 21/2, 19/2, 15/2, 17/2$, as shown in Fig.1.6. With increasing of U , some level crossings occur.

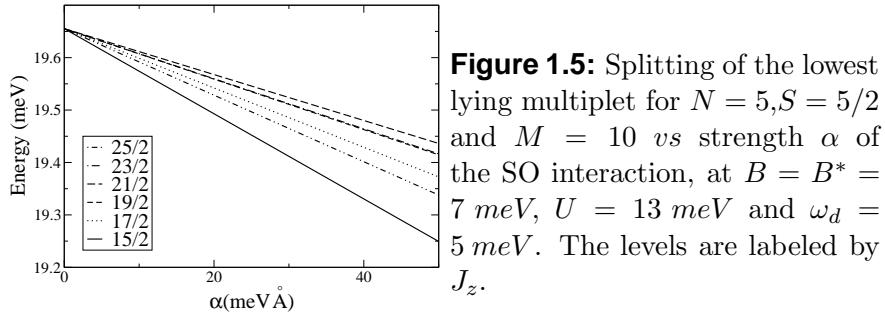


Figure 1.5: Splitting of the lowest lying multiplet for $N = 5, S = 5/2$ and $M = 10$ vs strength α of the SO interaction, at $B = B^* = 7 \text{ meV}$, $U = 13 \text{ meV}$ and $\omega_d = 5 \text{ meV}$. The levels are labeled by J_z .

The ordering at three different values of U is magnified in the bottom panels of Fig.1.6. The case with $U = 13 \text{ meV}$ is shown in the bottom right panel of Fig. 1.6. The lowest state in energy is for $J_z = 15/2$ followed by $J_z = 17/2, 19/2$ (almost degenerate with $25/2$), $25/2, 21/2, 23/2$. At $U = 13 \text{ meV}$ a sizeable gap is formed between the $J_z = 15/2$ GS and the first excited state $J_z = 17/2$. The other states of the multiplet are bunched together at higher energy.

In figure 1.7 we show the energy spectrum of a 2 particle dot in the presence of the SO coupling vs ω_c with $\omega_d = 5 \text{ meV}$, $U = 13 \text{ meV}$ and $\alpha = 250 \text{ meV \AA}$.

By mean of a comparison with Fig.1.2 some important features emerge. The level structure is qualitatively analogous to that obtained in Ref. [38], intended for an *InSb* dot, with Dresselhaus and cubic SO terms included. The singlet-triplet transition appearing in fig 1.2 as a crossing at $\hbar\omega_c \approx 4$ appears now here as a marked anti-crossing at $\hbar\omega_c \approx 4 \text{ meV}$, because of the SO coupling [31]. The states involved in the anti-crossing have $J_z = 0$ and

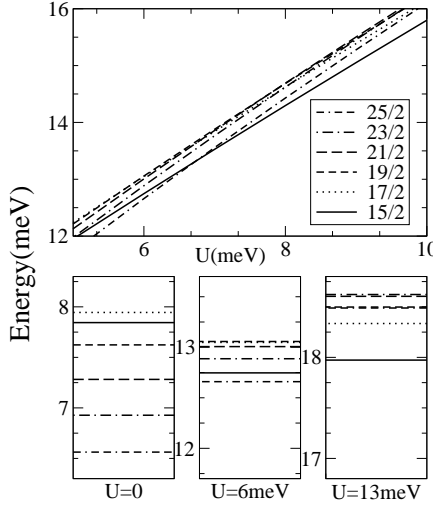


Figure 1.6: Energy levels with $N = 5$, $B = 7 \text{ meV}$, $\omega_d = 5 \text{ meV}$, and $\alpha = 100 \text{ meVÅ}$, for different U values. In the upper panel we show the crossings that allow the FSP polarized state to be the ground state when U is large. Ordering of the levels is magnified in the bottom panels for three different U values.

originate, in the absence of SO, from the singlet ($S = 0, S_z = 0, M = 0$) and the triplet ($S = 1, S_z = -1, M = 1$) states. Recently, the relaxation time T_1 for the flipping of the two-electron spin trapped in a vertical $GaAs$ QD, from the triplet to the singlet state, has been measured, by applying electrical pulses to the QD. T_1 has been estimated to be $> 200 \mu s$ at $T < 0.5 K$ [39]. Similarly to what found in Ref. [38], exchange interaction produces a small zero-field splitting between the first excited state (a triplet with $J_z = 2$) and the second excited state (a singlet with $J_z = 1$). Increasing B further the SO induces the crossing of the latter two states, so that lowest lying states are the GS ($S = 1, J_z = 0$) and the FES ($S = 1, J_z = 1$). As

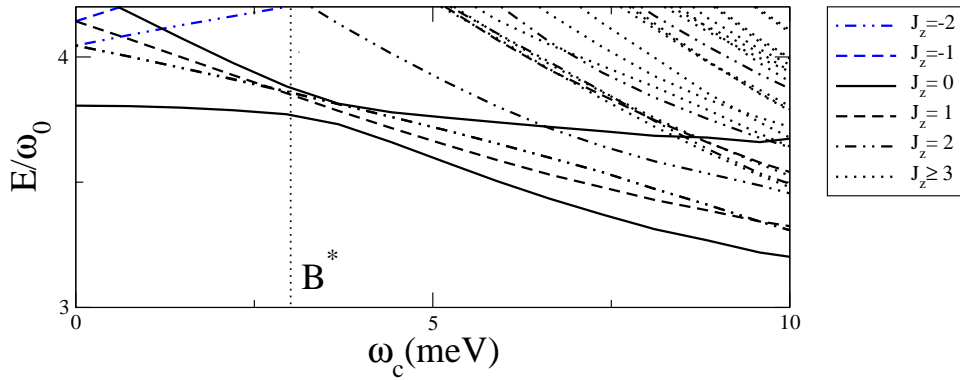


Figure 1.7: $N=2$ particles dot: energy spectrum vs magnetic field ω_c in the presence of the SO. $\omega_d = 5 \text{ meV}$, $U = 13 \text{ meV}$, $\alpha = 250 \text{ meVÅ}$. The GS is $J_z = 0$, the FES is $J_z = 1$.

seen from figures 1.8, 1.9, the same pattern can be found also for $N = 3, 4$.

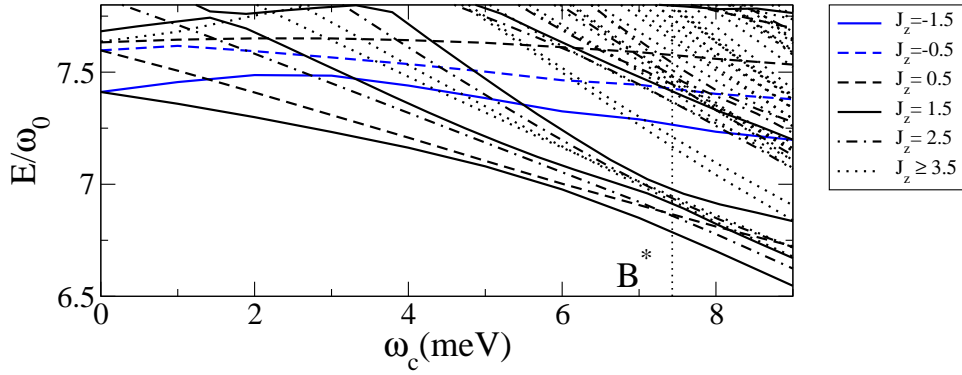


Figure 1.8: $N=3$ particles dot: energy spectrum vs magnetic field ω_c in the presence of the SO . $\omega_d = 7meV$, $U = 13meV$, $\alpha = 250meV\text{\AA}$. The GS is $J_z = 3/2$, the FES is $J_z = 5/2$.

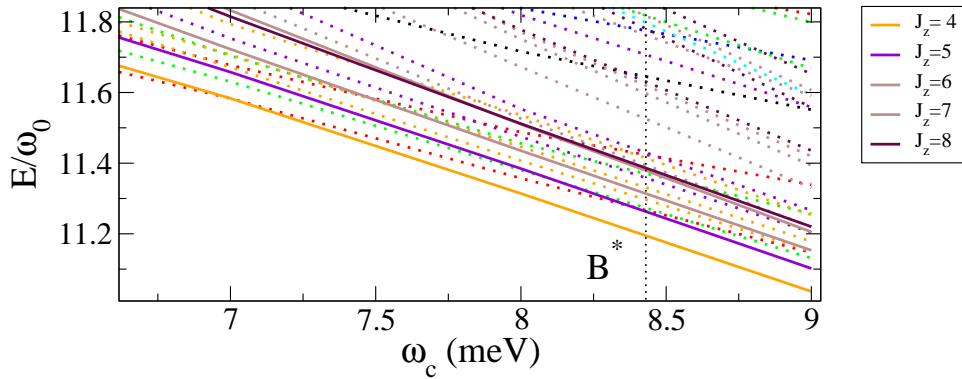


Figure 1.9: $N=4$ particles dot: energy spectrum vs magnetic field ω_c in the presence of the SO . The GS is $J_z = 4$, the FES is $J_z = 5$. $\omega_d = 7meV$, $U = 13meV$, $\alpha = 250meV\text{\AA}$.

However by increasing the number of particles the level structure becomes richer the anti-crossings between the levels seems to be masked. In fact, for $N = 4$, anti-crossings are less prominent and the level separation of the bunch of states in Fig.1.9 is much smaller, but a gap to the above develops at $\omega_c \approx 5.5\text{meV}$, between the GS ($S = 2, J_z = 4$) and the FES ($S = 1, J_z = 5$), originating from the $M = 6$ multiplet. The gap is strongly sensitive to the SO tuning and increases with increasing α (Fig.1.10). The SO coupling

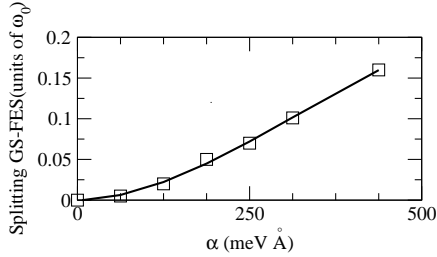


Figure 1.10: GS-FES spin gap vs α at $\omega_c = 8\text{meV}$ for a 3 particles ($N = 3$) dot with $\omega_d = 7\text{meV}$, $U = 13\text{meV}$, $\alpha = 250\text{meV}\text{\AA}$.

tends to shift the \downarrow spin density with respect to the \uparrow one radially (see Fig. 1.13 and [26]). The shift can occur easily for the GS when $N = 2$ and provides a reduction of the $e - e$ interaction by leaving an isolated spin at the center of the dot. When $N > 2$, the confinement potential together with the $e - e$ repulsion contrasts such a spin redistribution and the final result is that the z -component of the total spin density is diminished at the center of the dot. In particular, $\sigma_z(r)$ tends to flatten in the GS for $N = 3, 4$ (see Fig.1.11). Correspondingly the radial component $\sigma_r(r)$ increases in the

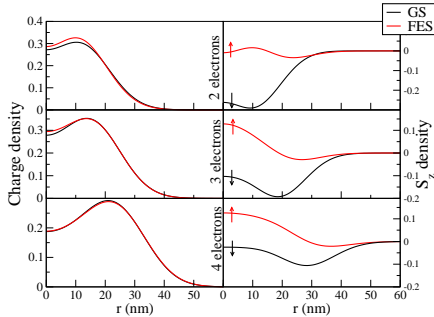


Figure 1.11: Spin and charge density of the ground state (black) and the first excited state (red) for the dot with $N=2$ [top], $N=3$ [middle], $N=4$ [bottom]. $\omega_d = 7\text{meV}$, $U = 13\text{meV}$, $\alpha = 250\text{meV}\text{\AA}$.

case of $N = 3, 4$ at any distance from the center and not only at the dot boundary as it happens for $N = 2$ (see Fig.1.11).

In what follows discuss the charge density and the spin polarization of the GS in the presence of strong $e - e$ correlations. As it appears from Fig. 1.12 [top panel], the charge density of the GS is only mildly changed when we increase the SO coupling. By contrast, the spin density is quite sensitive to the addition of SO, up to saturation. Now the z -component of the total spin is no longer a good quantum number and some admixture with down spin electrons appears. Indeed the role of the Rashba term is to rotate the average electron spin. In particular, down spin electrons are pushed

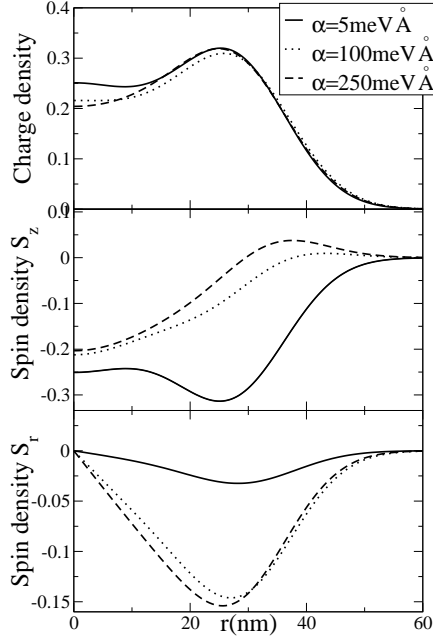


Figure 1.12: Charge density, azimuthal spin density S_z , in plane spin density S_r , in the radial direction, in the GS ($N = 5$, $J = 15/2$) at various SO couplings: $\alpha = 5, 100, 250 \text{ meV}\text{\AA}$. Here $B = 7 \text{ meV}$, $U = 13 \text{ meV}$ and $\omega_d = 5 \text{ meV}$

away from the center of the dot, giving rise to the spin density components $S_z(\vec{r})$ (orthogonal to the dot plane), and $S_r(\vec{r})$ (in the plane of the dot), which are plotted in Fig.1.12 [middle and bottom panels, respectively]. It is remarkable that the spin density $S_z(\vec{r})$ changes sign at the edge of the dot for large SO coupling. This is confirmed by a plot of the occupation numbers $n_{nm\sigma} = \langle GS | c_{nm\sigma}^\dagger c_{nm\sigma} | GS \rangle$ with $n = m$. They are shown in Fig.1.13 for both $N = 4$ and $N = 5$ for comparison. Of course, the change of N would

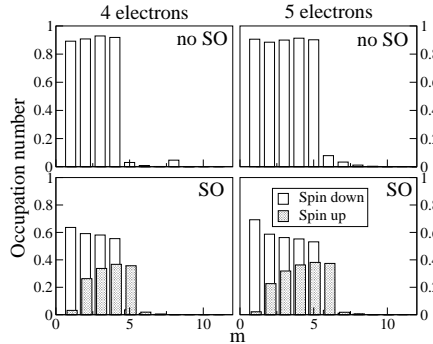


Figure 1.13: Occupation numbers $n_{n=m,m,\sigma}$ in the GS with $N = 4(5)$ electrons (left(right)) without SO (top) and with SO ($\alpha = 100 \text{ meV}\text{\AA}$) (bottom). Other parameter values are $B = 7 \text{ meV}$, $U = 13 \text{ meV}$, $\omega_d = 5 \text{ meV}$. White bars refer to spin down, grey bars refer to spin up. The FSP GS of the dot with $N = 4(5)$ electrons has total spin $S = 2(5/2)$ and the z -component of the total angular momentum $J_z = (15/2)$.

also imply an effective change of the confinement potential ω_d (what we do not do). However, all what we want to show here is that our findings

depend on the strength of B only, and not on the number of electrons being even or odd. A similar feature occurs in the de Chamon-Wen phase, in the absence of SO: when crossing the edges, the spins tilt away from their bulk direction [40]. The reversal of the spins in the tail at the dot boundary is a peculiarity of the Rashba interaction, but the spin/charge density is very small there and does not influence the dot properties.

1.4 Spin and charge density in the multiplet $S = 5/2, M = 10$

In the previous Section we have shown that at $B = B^*$ the GS with $N = 5$ electrons belongs to the $S = 5/2, M = 10$ multiplet. The SO coupling lifts its degeneracy as shown in Fig.1.5. The size of U strongly influences the energy of each state, by producing crossings of levels. At $U = 13 \text{ meV}$ the lowest lying states with increasing energies are (see Fig.1.6[right bottom panel]):

$|GS \rangle \equiv |N = 5; J_z = 15/2 \rangle$: this is the fully spin polarized GS .

$|FES \rangle \equiv |N = 5; J_z = 17/2 \rangle$: the ‘spin exciton‘.

This ordering of energy levels is the following: lowest energy is for $J_z = L_z - S_z$, higher energy is for $J_z = L_z + S_z$. Besides affecting the energy of the states, the effect of U is to enhance the transfer of weight from the majority (“down”) to the minority (“up”) spin population. This is shown in Fig.1.14, where the occupation numbers $n_{n=m,\sigma}$ are reported for the states $|GS \rangle$, $|FES \rangle$ and another reference level $|b \rangle \equiv |N = 5; J_z = 25/2 \rangle$ for $U = 0$ [left panels] and $U = 13 \text{ meV}$ [right panels], respectively. A striking feature characterizes the spin densities of these states (see Fig.1.14, 1.15): the dominant spin density is reversed in the $|b \rangle$ state, with respect to the $|GS \rangle$. The state $|FES \rangle$, which is the first excited state, interpolates between the two. Spin occupancy is not significantly modified for larger r . While at $U = 0$ the flipping of the spin at the origin with respect to the GS is full, in the interacting case some up-spin is left at the center. This allows for a smoother radial dependence of the spin and charge density expectation values. Eventually, this is the reason why this state turns out to be the lowest excited state in the FSP system. In Fig.1.15 we show the charge and spin densities of the complete GS multiplet for $N = 5$ at $\alpha = 100 \text{ meV\AA}$, $U = 13 \text{ meV}$ and $B = B^*$. The situation is quite peculiar: by looking at $\langle S_z \rangle$ [middle panel], we see that the GS has a down spin density everywhere in the dot, except for a tiny little reversed tail at the boundary. By contrast, the state b $J_z = 25/2$ has an up spin density at any r . Intermediate between the two, the FES state displays a reversed spin at the center of the dot but the spin polarization changes into down

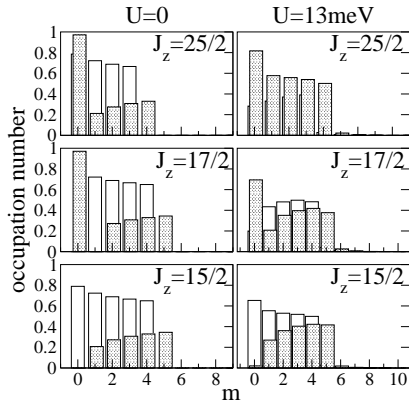


Figure 1.14: The occupation numbers $n_{n=m,m,\sigma}$ in the state at $J_z = 15/2, 23/2, 25/2$ for small U [left], and large U [right]. White bars refers to spin down, grey bars refers to spin up. We stress that at $U = 0$ the ordering of the levels, corresponding to the three panels on the left is changed with respect to the ones on the right ($U = 13 \text{ meV}$). (see Fig. 1.6 [bottom panels]).

when approaching the edge, to restore the spin density of the GS . There is a node in the middle! The other states (17/2, 19/2 and 21/2) are rather featureless and they do not share these features. The trend is confirmed by looking at the projection of the spin density in the plane of the dot $S_r = \hat{r} \cdot \vec{S}$ (see Fig.1.15[bottom panel]). This is the complementary information with respect to $S_z(r)$. When $S_r(r)$ is strongly non zero, then $S_z(r)$ is heavily reduced.

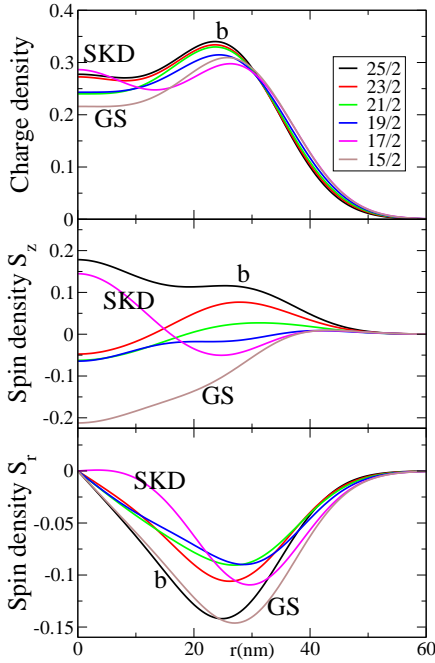


Figure 1.15: Charge density, azimuthal spin density S_z , in plane spin density S_r , in the radial direction, at various J_z . Parameters are $N = 5$, $\alpha = 100 \text{ meV \AA}$, $U = 13 \text{ meV}$ and $\omega_d = 5 \text{ meV}$

An analogous interpolation occurs for the charge density. There is a piling up of the charge at the origin (see Fig.1.15[top panel]), corresponding to a locally dominant down spin density. The FES is a collective excitation

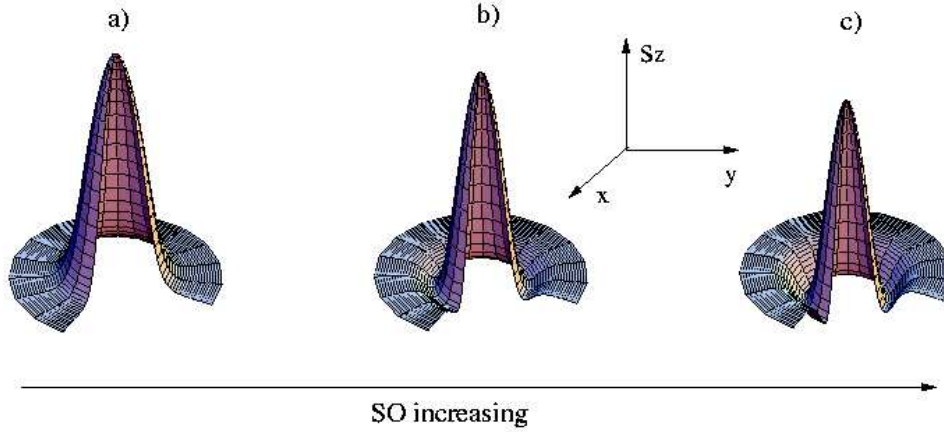


Figure 1.16: $N=3$ particles dot: FES spin density (arb.units) for a) $\alpha = 150 \text{ meV \AA}$, b) $\alpha = 250 \text{ meV \AA}$, c) $\alpha = 350 \text{ meV \AA}$. By increasing the SO there is a squeezing close to the center and some reduction of $\langle \sigma_z \rangle$.

of the QD, which we call a “spin exciton”. So in the FES the SO enforces a spin texture with $\langle S_z \rangle$ flipped at the origin with respect to the GS and healing back gradually away from the center up to the QD boundary, where the spin density points radially in the dot plane [26]. Remarkably, the SO coupling acts on this spin excitation as a squeezing factor: that is the larger is α the closer the spin distribution of the FES is to the center of the dot, as can be seen in Fig 1.16. The FES for $B > B^*$ has J_z increased by one with respect to the GS. But, the difference of the angular momentum expectation values $\Delta \langle M \rangle \equiv \langle M \rangle_{FES} - \langle M \rangle_{GS}$ is found to be vanishingly small.

To justify the last statement, we note that in a disk shaped dot, a radial change of $\Delta \langle M \rangle$ requires a change of $n(r)$ as well, but, as a matter of fact, we find that the charge distribution in the dot at the FSP point is rather insensitive to excitation and to the strength of the SO coupling (see Figs 1.11, 1.12). While the radial charge density $n(r)$ appears to be compressible at fields $B < B^*$ and $B > B^*$, it is approximately incompressible at $B \sim B^*$ [41]. When $B \gg B^*$, the charge distribution of the dot reconstructs [20,26].

The spin excitation gives rise to an extra collective magnetization $\hat{z} \cdot \Delta \vec{M}(r) \approx \langle 2\mu_B \Delta \sigma_z(r) \rangle$, where $\Delta \sigma_z(r)$ is the difference in z -component of the local spin density between the FES and the GS and $\mu_B = e\hbar/2m_e c$. The radial spin density $\sigma_z(r)$ appears in Fig.1.11 (for $N = 2, 3, 4$).

We have estimated the possible extra magnetic flux ϕ associated to the spin excitation, by integrating numerically the vector potential, induced by the spin polarization of the dot, $a_\vartheta(r)$, along the circle of radius R at the dot boundary γ ($\phi = \int_\gamma R d\vartheta a_\vartheta(R)$). This is given by:

$$a_{\vartheta}(r) = 2\mu_B \int_0^{2\pi} d\vartheta' \int_0^R \frac{dr' \hat{r}' \times \hat{z}}{|\vec{r}' - \vec{r}|} \frac{\partial \Delta S_z(r')}{\partial r'}, \quad (1.14)$$

where \hat{r} is a radial unit vector. The calculation yields a very tiny fraction of the flux quantum $\phi_o = \hbar c/e$, but it is remarkable that, at $B \approx B^*$, we find the same value of ϕ for $N = 2, 3, 4$. This is consistent with the fact that the FES has essentially one spin flipped at the origin and no change in orbital angular momentum independently of the number of electrons on the dot.

1.5 FIR absorption

The ground state and the first excited state are spaced by an energy of the order of meV , so our idea is to study the possibility to drive, with a far infrared radiation (FIR), a transition between these two states by choosing in an appropriate way the polarization of the radiation field. In particular the transition under analysis requires an increasing of the total angular momentum of $\Delta J_z = 1$ that impose us to choose a right hand circularly polarized radiation. In order to probe the effect of the FIR on the FSP dot we have to go beyond the generalized Kohn theorem.

Our aim is twofold:

- We want to monitor, with the FIR, the crossover of the QD, embedded in an orthogonal magnetic field, in the presence of SO coupling, to the FSP state. In fact, as seen in Figs. 1.17 a),b), when the dot becomes fully spin polarized the transition probability increases suddenly.
- In addition, the possibility to drive, with the FIR, a transition between the GS and the FES of the FSP dot is quite appealing in that it allow manipulating the spin properties of the dot in an unusual way.

We study in detail such transition by focusing on the importance of the spin orbit coupling in what follows.

1.5.1 Kohn Theorem

Far infrared radiation is a common tool in large scale QD arrays (e.g. *In* QD's [42] or field-effect confined *GaAs* QD [43]). Apparently, experiments of far infrared spectroscopy on QD's seems not to reveal their very rich energy levels structure [44–46], by contrast only two excitation frequencies seems to be singled out, this phenomenon has been completely understood [47] as a consequence of the generalized Kohn theorem.

Maksym and Chakraborty [47] (and well before Laughlin [48] in a 2-D electron gas) had showed that the full Hamiltonian of a parabolic quantum dot, in the absence of Rashba coupling can be decoupled into center of mass and relative coordinates.

The coupling Hamiltonian in the dipole approximation for a space independent electric field $\vec{E} = \vec{E}_0 \exp(-i\omega t)$ is:

$$H_{int} = \sum_{j=1}^N e\vec{E}_0 \cdot r_j e^{-i\omega t}, \quad (1.15)$$

by choosing the center of mass coordinate as $\vec{R} = \sum_i \vec{r}_i / N$ and the total charge as $Q = Ne$ it can be rewritten as:

$$H_{int} = Q\vec{E}_0 \cdot \vec{R} e^{-i\omega t}. \quad (1.16)$$

Now we can rewrite also the dot Hamiltonian in the absence of SO coupling as a function of center of mass coordinate and the $3(N-1)$ coordinates relative to it. These are conveniently chosen to be $\vec{\rho}_i = \vec{r}_i - \vec{R}$ where $i = 1, \dots, n_e - 1$. It reads

$$H = \frac{1}{2M}(\vec{P} + Q\vec{A})^2 + \frac{1}{2}M\omega_0^2 R^2 + H_{rel}(\vec{\rho}_i), \quad (1.17)$$

with $\vec{P} = \sum_i \vec{p}_i / N$, \vec{A} is the vector potential of the cm and $M = Nm^*$.

The Hamiltonian 1.17 is separated into two pieces: the second one is H_{rel} and only depends on the relative coordinates $\vec{\rho}_i$. The first one does not contain any terms due to the interaction and depends only on the center of mass coordinates \vec{R} and \vec{P} , it is fully equivalent to the single particle Hamiltonian except for a renormalization of the coefficients that does not affect at all the energy eigenvalues.

In the dipole approximation the perturbing Hamiltonian due to the FIR is expressed only in terms of the center of mass coordinate 1.16: this means that the radiation would couple only to the single particle modes without affecting any relative motion! This is a simple explanation of the generalized Kohn theorem. In the range of validity of the Kohn theorem the FIR transition between the two states (the GS and FES are not Kohn modes for the FSP dot) studied here would be typically forbidden and only the two Kohn modes at frequencies $\omega_{\pm} = 1/2(\sqrt{4\omega_0^2 + \omega_c^2} \pm \omega_c)$ would be observed. In the past, some exotic ways to excite non center of mass modes of QD's with a FIR have already been proposed: the best results, as far as we know, have been obtained both in theory [43] and in experiments [49] by hypotizing a non parabolicity of the confining potential. Indeed, plasma modes have been spotted just below the upper Kohn frequency ω_+ [43].

However modern technology allow to realize devices in which a strong spin orbit coupling is present: this offers new chances to go beyond the generalized Kohn theorem. In fact in the presence of a strong SO coupling the hypothesis of the generalized Kohn theorem breaks down: the full dot Hamiltonian can no longer be decoupled because the Rashba term explicitly couples relative and center of mass coordinate (next chapter section 3 and

[2]) and does not allow for the decoupling of the Hamiltonian. So it is possible and interesting to study this ‘non center of mass’ transition.

1.5.2 Coupling Hamiltonian and FIR spectra

We write the coupling Hamiltonian in a slightly different way:

$$H_{FIR} = \sqrt{(2)}\mathcal{A}_0(\omega)\hat{\epsilon}_R \cdot \vec{p} e^{i\omega t} + h.c. \quad (1.18)$$

where $\mathcal{A}_0(\omega) = A_0(\omega)/\sqrt{2}[\exp(-i\omega t) + c.c.]$ (and $A_0(\omega)$ is the envelope function of the wavepacket in the ω -space, which we suppose to be very peaked around the ω frequency to simulate a monochromatic radiation) and $\epsilon_R = \hat{x} + i\hat{y}$ is the unit vector characterizing a right hand circularly polarized radiation. Typical wavelength of FIR are $1 \div 100 \mu m$ while typical dot size are usually less than $100 nm$: this assures that, in this case, dipole approximations holds to a high degree of accuracy.

By writing this Hamiltonian in a second quantized form we have:

$$H_{FIR} = \frac{A_0(\omega)}{\sqrt{2}i} \sum_{n,n',m,\sigma} \left[A_{n'm-1nm} c_{n'/m-1\sigma}^\dagger c_{nm\sigma} e^{i\omega t} - B_{n'm+1,nm} c_{n'/m+1\sigma}^\dagger c_{nm\sigma} e^{-i\omega t} \right], \quad (1.19)$$

where $A_{n'm-1nm}$ and $B_{n'm+1,nm}$ have been already defined in Eqs 1.12 and 1.13. It appears clearly that the radiation releases energy and exchanges orbital angular momentum to the dot. In particular the adsorption of a photon increases the total angular momentum of one unity by releasing one quantum of angular momentum. As explained before in order to excite the dot from GS to FES we do not need orbital but spin angular momentum. Once again the Rashba Hamiltonian provide the right coupling in order to couple orbital and spin motion: in this way the angular momentum released to the dot is transferred into spin angular momentum. This mechanism allow to wash out the spin gap between the two states under examination by using the radiation, that is we can switch the dot to an ‘opposite’ spin configuration by mean of fast radiation. Moreover, if we turn off the FIR we can let it relax back to the ground state with the original spin polarization.

We have calculated the dipole matrix element squared for the transition from GS to FES vs B. Our results are shown in Fig. 1.17 (a) for $N = 2$ and 1.17 (b) for $N = 4$, respectively. The dispersion of the absorption peaks is artificial, but their detailed shape would yield direct access to the coupling constants and to the level mixing introduced by the SO terms. We find an increase of the expected intensity at the FSP point which marks the crossover to the new states. As expected, the crossover sharpens with increasing N .

In conclusion, it is possible to stimulate the transition between the ground state and the FES by mean of circularly polarized FIR radiation. The transition from the ground state is strongly favoured after the dot

appears to be fully spin polarized. This way to manipulate spins seems to be very appealing. In fact we do not deal with single spins as in recent proposals for spin based quantum computers (in that case the coupling to the environment can easily destroy the coherence) [50] but we propose to change the spin polarization of whole dot. This is very interesting because the spin configuration of the QD is certainly stabilized by the electron electron interaction within the dot.

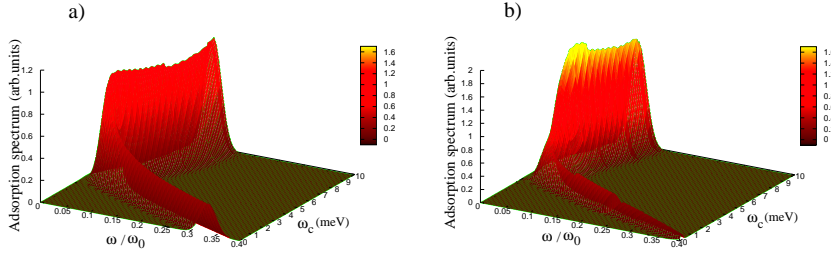


Figure 1.17: Absorption spectrum vs magnetic field for a) $N=2$ particles, b) $N=4$ particles

In the next Section we show that the spin exciton recalls the first excited state of a *QHF* with some important differences, though.

1.6 Comparison between the dot and a QHF disk

The case of the dot in the *FSP* state can be compared with that of a disk shaped Quantum Hall Ferromagnet at filling one. The comparison is in order, because the physics of the dot turns into that of a quantum Hall disk by increasing the magnetic field, as long as the ratio $\omega_d/\omega_c \rightarrow 0$. Of course, while the infinite quantum Hall system is marked by a phase transition to the spin polarized state, the dot, being a system with a finite number of particles, undergoes a crossover to the *FSP* state which is not a broken symmetry state. This is confirmed by the presence of the tiny minority spin tail at the edge of the dot.

We now, recall, some properties of the Hartree Fock description of the GS and first excited state of the QHF, which applies to filling close to (but less than) one.

Similarly, some analytical approximations leading to a simplified H-F-like approach for the dot with SO coupling will be discussed in the following to highlight the analogies between the two systems.

1.6.1 Quantum Hall Ferromagnet

In describing the QH state on a disk it is customary to label one particle states with $\nu = (n - |m|)/2$ and m, σ , corresponding to the eigenvalues $\epsilon_{\nu, m, \sigma}$ given in Eq.(1.5). The LLL includes the wave functions ϕ_{nm} given by Eq.(1.2) for $\nu = 0$ and $m \geq 0$. In this case all Laguerre polynomials $L_0^{|m|}(t) = 1$. If there is no confinement potential ($\omega_d = 0$), all ϵ_{0m} are degenerate. We rename the LLL wave functions $f_{0m}\chi_\sigma$ (here χ_σ denotes the spin 1/2 wave function) and associate the single particle fermion operators $\hat{a}_{\nu=0m\sigma}$ to them. In the *QHF* at filling one, the LLL sub-band with, say, spin down, is fully occupied: the GS is a fully spin polarized state:

$$\left| QHF, 0 \right\rangle = \prod_{0 \leq m \leq N-1} \hat{a}_{0m\downarrow}^\dagger \left| \emptyset \right\rangle \quad (1.20)$$

Here $|\emptyset\rangle$ is the vacuum state. The lowest lying branch of excitations of the QHF are spin waves. These involve electrons in the down spin LLL sub-band and holes in the up spin LLL sub-band.

It was pointed out long ago [51] that, if the filling is slightly less than one, the first excited state can be a very special collective excitation with $S < N/2$ and an extra node in the spin density. The spin polarization is reversed at the center, but gradually heals to the dominant spin background over a distance of many magnetic lengths (*SK* state). This excitation can be traced back to the *skyrmion*, the topological excitation of the *O(3) NLσM in 2-d* [33]. A disk of infinite radius in coordinate space can be compactified to a sphere S^2 in \mathcal{R}^3 having the origin in the south pole and the point at infinity in the north pole. A similar compactification can be performed in the order parameter configurational space. An uniform magnetization “down” is represented by a vector pointing to the south pole everywhere on S^2 . The skyrmion is a finite action configuration on S^2 , satisfying the classical Eq.s of motion for the magnetization of the *NLσM*, conserving $\vec{J} = \vec{S} + \vec{M}$ and belonging to a non trivial homotopy class. If the topological charge is $Q = 1$, the shape of the magnetization field is $\vec{s}(\vec{r}) = \hat{r}$, where \hat{r} is the normal to S^2 at each point. Q is the flux of $\vec{s}(\vec{r})$ through the sphere of unit radius. The spin polarization is “up” at the south pole and turns over continuously in space, until it reaches “down” at the north pole. That is, the spin polarization is flipped at the origin of the disk with respect to the GS and turns smoothly over away from it in the radial direction.

Within Hartree-Fock [52], the Slater determinant $|S, K\rangle$ that describes this state conserves total J_z . To construct it, a canonical transformation is

performed on the fermion operators:

$$\begin{aligned}\hat{q}_j &= u_j \hat{a}_{0j-\frac{1}{2}\uparrow} + v_j \hat{a}_{0j+\frac{1}{2}\downarrow}, & j \in \left(\frac{1}{2}, \dots, \infty\right) \\ \hat{p}_{-\frac{1}{2}} &= \hat{a}_{00\downarrow} \\ \hat{p}_j &= -v_j \hat{a}_{0j-\frac{1}{2}\uparrow} + u_j \hat{a}_{0j+\frac{1}{2}\downarrow}, & j \in \left(\frac{1}{2}, \dots, \infty\right),\end{aligned}\quad (1.21)$$

Normalization requires that $|u_j|^2 + |v_j|^2 = 1$. Note that the operator $\hat{p}_{-\frac{1}{2}}$ still belongs to the LLL as it destroys a particle in the $f_{\nu=0, m=0}\chi_{\downarrow}$ state. We denote by $f_j^{p/q}$ the single particle orbitals corresponding to the operators of Eq.(1.21) and we use them in Appendix 1A.

The generic Slater determinant built by means of these operators is:

$$|S, K\rangle = \prod_{j=\frac{1}{2}}^{\infty} \left(\hat{p}_{j-1}^{\dagger}\right)^{n_j^p-1} \left(\hat{q}_j^{\dagger}\right)^{n_j^q} |\emptyset\rangle \quad (1.22)$$

n_j^{β} are the occupation numbers of the single particle states ($n_j^p = \langle p_j^{\dagger} p_j \rangle$, $n_j^q = \langle q_j^{\dagger} q_j \rangle$), with $\sum_{j,\beta} n_j^{\beta} = N$. The state of Eq.(1.22) is labeled by the total spin S and by K . S_z is no longer a good quantum number and is substituted by

$$K = S + \frac{1}{2} \sum_{j=1/2}^{N-1/2} (n_j^q - n_{j-1}^p) \quad (1.23)$$

The state of Eq.(1.22) with $S = N/2, K = 0$ is the *FSP QHF* ground state of Eq.(1.20), if the only non zero occupation numbers are $n_j^q = 1$ for $j \in (\frac{1}{2}, \dots, N/2)$ with $u_j = 1$ for $j \in (\frac{1}{2}, \dots, N/2)$. This state corresponds to the *FPS* GS of Fig.1.3b) for the QD case.

For the hard core model the HF equations can be solved analytically [52]. The lowest lying skyrmion state is $|N/2, 1\rangle$, with

$$|u_j|^2 = 1 - |v_j|^2 = \frac{\xi^2}{\xi^2 + (j + \frac{1}{2})} \quad (1.24)$$

leading to the spin density $\vec{s}(\vec{r})$ defined in terms of the arbitrary length scale ξ ($r^2 = x^2 + y^2$) [34] (see Appendix 1A for a detailed discussion):

$$s_x(\vec{r}) = -\frac{2x\xi}{r^2 + \xi^2}; \quad s_y(\vec{r}) = \pm \frac{2y\xi}{r^2 + \xi^2}; \quad s_z(\vec{r}) = -\frac{r^2 - \xi^2}{r^2 + \xi^2}. \quad (1.25)$$

The \pm refer to the sign of the topological charge $Q = \pm 1$. In the real *QHF* the length ξ is governed by the relative strength of the Zeeman and the Coulomb energies.

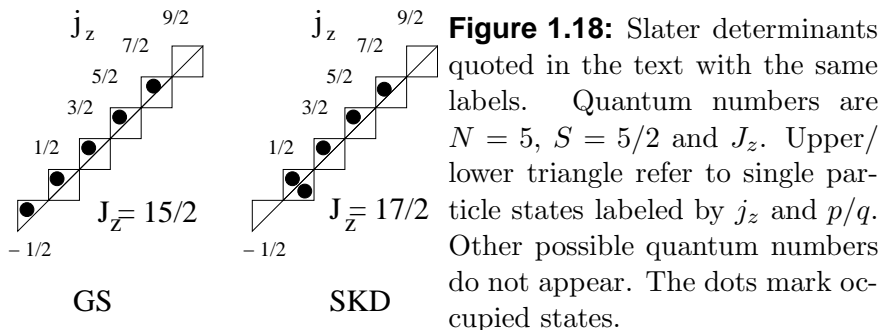
1.6.2 Dot with spin-orbit coupling

In this Subsection we give arguments supporting our claim that the FES of the dot corresponds to the state $|N/2, 1\rangle$ in the *QHF* limit, that is in the limit of zero confinement potential and filling one. Indeed, the radial distribution of the spin density of the FES recalls the one of Eq.(1.25) except for a very shallow tail at the boundary. Away from the center the spin polarization of the *FES* state lines up gradually with the one of the GS as it happens for the case of the Skyrmion. As in the *SK* case, $S_z(r)$ has an extra node at $r = \xi$. In the presence of SO, the length scale ξ is no longer arbitrary, but is fixed by the strength of the SO coupling. In the case of the *QHF* on a disk, both rotations in real space around the z -axis and rotations in spin space are good symmetries, so that M as well as S_z are conserved. This implies that an allowed *SK*-like excited state of the real system has to be obtained by projecting the state of Eq.(1.22) onto the subspace of definite M and S_z . This is not necessary in the QD with SO interaction, because the SO Hamiltonian term only conserves J_z as the state $|S, K\rangle$ does. In the following we show that a simplified H-F-like approach for the dot case with SO coupling shows features similar to the ones described by Eq.s (1.21), (1.24) and Eq.s (1.22), (1.25). Let us first discuss SO coupling in the dot at $U = 0$. The vector space required to diagonalize the SO coupling and to obtain the eigenfunctions $w_{j_z}^\beta$ exceeds the LLL space enormously (in practice we always use the basis of Eq.(1.2) and never calculate the $w_{j_z}^\beta$'s explicitly). As a simple analytical approximation, we can restrict ourselves to the LLL for sake of simplicity. We have checked numerically that this approximation is largely satisfactory away from the level crossings. In this case, diagonalization of the SO interaction factorizes the problem into a collection of 2×2 matrices. What the SO does is to mix single particle states with different m and opposite spins in the way that the transformation of Eq.(1.21) shows. Indeed, j_z ($j_z \equiv j$ in the following) is conserved. Within the LLL, two (m, σ) values contribute to each half integer j : (m, \uparrow) and $(m + 1, \downarrow)$. The unperturbed energy levels involved, ϵ_{0m} and ϵ_{0m+1} , are given by Eq.(1.5). Let the off-diagonal matrix element including the SO coupling be α . Then the eigenvalues are:

$$\lambda_j^{p/q} = \frac{1}{2}(\epsilon_{0m} + \epsilon_{0m+1}) \pm \sqrt{\frac{\delta^2}{4} + \alpha^2}, \quad (1.26)$$

where $\delta = \epsilon_{0m+1} - \epsilon_{0m} = \omega_o - \omega_c/2$. The diagonalization implies a rotation in the 2-vector space $\{f_{0m}\chi_\uparrow, f_{0m+1}\chi_\downarrow\}$ of an angle γ given by $\tan 2\gamma = -2\alpha/\delta$. The single particle states obtained in this way coincide with $f_j^{p/q}$ defined after Eq.(1.21). The mixing of the two states (m, \uparrow) and $(m + 1, \downarrow)$ is j -independent, within our approximations, because δ is. This implies that the rotation angle γ keeps roughly constant in the radial direction, because average radial distribution of an electron of angular momentum j is

$\sim l\sqrt{j+1}$. We can now construct the Slater determinants representing the



states lower lying in energy. The states corresponding to the ones obtained numerically in the previous sections are depicted in Fig.(1.18). In analogy to Fig.(1.3) we use boxes to allocate electrons. Each box is cut into a lower and an upper triangle with respect to the diagonal, corresponding to the q and the p state of a given j_z , respectively. A dot marks which of the orbitals is occupied. We have analyzed the Slater determinants which contribute mostly to the states obtained at the end of the Lanczos procedure, giving the average occupation numbers of Fig.(1.14). Their largest components indeed contain the determinants shown in Fig.(1.18). Another analogy between our finite system (dot) and the quantum Hall disk can be found on symmetry grounds. The SK state of the QHF is the first excited state of a spontaneously broken symmetry, which is the spin $SU(2)$. In the dot case, once again, there is a reduction of the symmetry of system because the SO couples the spin and orbital motion thus conserving J_z and reducing the old symmetry $SO(3) \times SU(2)$ (orbital and spin) to a smaller group $SO(3)$. In a sense, we could say that in the finite system again there is a breaking of the $SU(2)$ symmetry but it is not a spontaneous symmetry breaking because the SO provides it. All these are close similarities between the dot and the QH disk. However relevant differences can be immediately recognized. While the skyrmion shows a very smooth tilting of the spin orientation with increasing distance from the center of the disk (see Eq.(1.24)), the rotation angle γ for the dot is uniform in the radial direction. This feature is partly compensated by the addition of the Coulomb repulsion. Indeed, $U \neq 0$ predominantly affects the occupations close to the center of the dot disk, while its influence fades out away at larger distances. This fact introduces a radial variation of the tilting of the spin polarization. According to Eq.(1.25), the skyrmion has a linear variation with radial distance of S_r , close to the origin. By contrast, our numerical results reported in Fig.(1.12 [bottom panel]) show a quadratic increase at small r 's. The role of U is quite substantial, by locating the energy of the FES state intermediate between those of the GS and of the b state. Needless to say, another relevant and obvious difference

between *FES* and *SK* is the absence of any conserved topological charge in the dot. In the *QHF* the conservation of Q is implemented on symmetry grounds, by mapping the QH disk onto a sphere. This mapping cannot be extended to the dot, because, as seen from Fig.(1.15), the direction of the magnetization at the boundary is not unique. Magnetization is not defined at $\vec{r} \rightarrow \infty$: the point at infinity is a singular point in the magnetization configurational space.

1.7 Discussion

In a disk shaped quantum dot with few electrons in the presence of a magnetic field $B = B^*$ orthogonal to the dot the interactions drive the system to a fully spin polarized state with $S = N/2$. At $B > B^*$, the total spin is again drastically reduced and the charge density reconstructs at the disk boundary. We have discussed on exact diagonalization results of a QD with $N = 2, 3, 4, 5$ electrons and studied the effect of SO coupling possibly due to an external electric field orthogonal to the dot disk. The effect of the Rashba interaction can modify both qualitatively and quantitatively the energy spectrum of the dot and its spin configuration. As an example the single triplet transition of the $N=2$ electrons dot, in the presence of spin orbit appear as a marked anti-crossing at the corresponding energy. We focus on the fully spin polarized dot (*FSP*) with $N = 2, 3, 4, 5$. There are analogies between the dot state at $B = B^*$ and the Quantum Hall Ferromagnet at filling one. We claim that such analogies are universal properties of the dot in the sense that all the effects studied are present in the dot independently of the number N of confined particles. However by increasing the number of particles both the polarization of the dot and the formation of a very peculiar FES become stabilized by the e-e interaction U . In fact we require a sizeable interaction strength U to stabilize the *FSP* GS. As an example, in the $N = 5$ particles case, when the SO coupling is increased, level crossings occur in the splitted $S = 5/2$ multiplet, until the state with minimum $J_z = M - S_z = 15/2$ becomes the GS. The first excited state (*FES* state) has $J_z = 17/2$. When compared to the GS, the *FES* state has some charge transferred to the dot center and a very peculiar spin texture. Indeed, the z -component of the spin density at the center of the dot is opposite to the one of the GS and rotates continuously over away from the center, by acquiring the same profile as the one of the GS at the dot boundary. This winding requires an extra node in the spin density, which is absent in the other multiplet states. According to these properties, the *FES* state can be viewed as carrying one spin exciton. Both our numerical results, and our approximate analytical speculation show how essential the combined role of the SO coupling and of the $e - e$ interaction is in stabilizing this state. Our calculation parametrizes the interaction strength U , but it ignores the

screening of the $e - e$ interaction altogether. This should be reconsidered in view of the fact that vertical QD's are separated on the top and the bottom from the contact metals by barriers with a typical width of 70\AA . Even for $N = 5$ this is smaller than the inter-electron spacing. However, we believe that the exciton state is robust when the screening is included. Indeed, the flipping of the spin is concentrated at the center of the dot and is governed by the $e - e$ interaction at short range, which should be largely insensitive of screening effects.

The FES state recalls the skyrmion excitation which takes place in a disk shaped QHF at filling one. The statement could be puzzling, in view of the fact that the SO coupling is essential to the FES state, but it is never invoked when discussing Quantum Hall properties. However field theory models ($NL\sigma M$) use the conservation of J to prove the existence of the skyrmion state. In a real isolated QH disk M, S_z would keep finite and separately conserved. In this case only the component of the SK state that conserves given values of M, S_z would be present in the excitation spectrum. Nonetheless the difference is washed out in the limit of an infinite disk size. This is the continuous limit which leads to the $NL\sigma M$. In the case of the dot, the compactification of both the coordinate space and the magnetization space cannot be performed because the direction of the magnetization is not defined at $\vec{r} \rightarrow \infty$. Therefore no state can be constructed that conserves J_z only, without conserving M and S_z separately. The spin orbit coupling opens up this possibility. However, no topological charge can be associated to the FES state in the dot.

Our calculation shows that for realistic values of the dot confining potential ($\omega_d = 5meV$), of the Coulomb interaction strength ($U = 13meV$) and of the SO coupling $\alpha \sim 100meV\text{\AA}$ [30], the FSP GS and the FES state are well spaced levels and their spacing monotonically increases by increasing α . The other levels of the multiplet appear at higher energies and are rather close to each other. This means that, at $B = B^*$, the dot opens a sizeable spin gap between the GS and the FES state, that can be tuned with an applied gate. This spin gap cannot be washed out by thermal fluctuations, if the temperature is low enough ($\sim 50mK$). The gap can be probed by optically pumped NMR as in quantum wells [32]. Spin-lattice relaxation of ^{71}Ga nuclear spins in the dot, driven by the hyperfine coupling to the dot electrons should be very much reduced, thus leading to a large T_1 .

The extremely low spin relaxation expected for this excitation, could allow for a coherent manipulation of the spin exciton using teraHertz radiation [53–55]. In general, we believe that the system studied here can be relevant to the coherent manipulation of QD states. This is appealing in view of quantum information processing [56–58]. Indeed, a spectrum like the one discussed in this chapter should produce sharp optical absorption lines. Photoluminescence induced by a pump and probe laser technique has been studied in disk shaped *In Ga As* QD's with evidence for Rabi oscilla-

tions [59].

In our case, a circularly polarized pulse of one single chirality has been used to excite the spin exciton discussed here. We have found that it is possible to stimulate the transition between the ground state and this spin excitation by mean of circularly polarized FIR radiation. The effect of the radiation is twofold: first of all the transition, from the ground state is strongly favoured after the dot appears to be fully spin polarized. It means that the FIR spectrum can be used to monitor the crossover to the FSP state. Moreover by increasing the number of particles, the crossover appear to be sharper, that is, we are going in the direction of a phase transition because the increased number of particles and the strong magnetic field make the system closer to the 'thermodynamic' limit in the QH sense. Then the second effect is to manipulate in a controlled way the spins of the dot. This new way to manipulate spins seems to be very appealing. In fact we do not deal with single spins, as in recent proposals for spin based quantum computers (in that case the coupling to the environment can easily destroy the coherence) [50], but we propose to change the spin polarization of whole dot. This is very interesting because the spin configuration of the QD is certainly stabilized by the electron electron interaction within the dot.

Appendix 1A

QHF Spin Density

In this appendix we show that the state $|N/2, 1\rangle$ given by Eq.(1.22) with u_j given by Eq.(1.24) leads to the skyrmion spin density of Eq.(1.25).

The wave functions for the QH disk associated to the operators $\hat{a}_{0m\sigma}$ are given in Eq.(1.2). In the LLL ($\nu = (n - |m|)/2 = 0$) all Laguerre polynomials $L_0^m(t) = 1$. To construct the field operator, we associate a spinorial wave function $f_j^{p/q}(\vec{r})$ to the operator \hat{p}_j/\hat{q}_j following Eq.(1.21):

$$f_j^p(\vec{r}) = \begin{pmatrix} -v_j f_{0j-\frac{1}{2}}(\vec{r}) \\ u_j f_{0j+\frac{1}{2}}(\vec{r}) \end{pmatrix}, \quad j \in (\frac{1}{2}, \dots, \infty), \quad (1.27)$$

$$f_j^q(\vec{r}) = \begin{pmatrix} u_j f_{0j-\frac{1}{2}}(\vec{r}) \\ v_j f_{0j+\frac{1}{2}}(\vec{r}) \end{pmatrix}, \quad j \in (\frac{1}{2}, \dots, \infty). \quad (1.28)$$

We take u_j and v_j real. The field operator is:

$$\hat{\psi}(\vec{r}) = \sum_{j=\frac{1}{2}}^{\infty} \left(f_{j-1}^p(\vec{r}) \hat{p}_{j-1} + f_j^q(\vec{r}) \hat{q}_j \right). \quad (1.29)$$

The spin density operator is $\hat{s}(\vec{r}) = \Re e \left\{ \hat{\psi}^\dagger(\vec{r}) \vec{\sigma} \hat{\psi}(\vec{r}) \right\}$, to be evaluated on the state $|N/2, 1\rangle$. Let us consider $s_x(\vec{r})$ first. All the f^q orbitals are unoccupied in the state $|N/2, 1\rangle$, except for $j = \frac{1}{2}$: this term, would give a contribution $\sim 2\xi/(\xi^2 + 1)r * \exp(-r^2)$ which rapidly vanishes away from the center. So the term including the \hat{q}_j operators giving an exponentially vanishing contribution can be neglected.

The contribution to $s_x(\vec{r})$ given by the \hat{p}_j operators is:

$$\begin{aligned} & \sum_{j=\frac{1}{2}}^{\infty} \begin{pmatrix} -v_j f_{0j-\frac{1}{2}}^*(\vec{r}) & u_j f_{0j+\frac{1}{2}}^*(\vec{r}) \end{pmatrix} \begin{pmatrix} 0 & 1 \\ 1 & 0 \end{pmatrix} \begin{pmatrix} -v_j f_{0j-\frac{1}{2}}(\vec{r}) \\ u_j f_{0j+\frac{1}{2}}(\vec{r}) \end{pmatrix} \\ & = - \sum_{j=\frac{1}{2}}^{\infty} 2u_j v_j f_{0j-\frac{1}{2}}^*(\vec{r}) f_{0j+\frac{1}{2}}(\vec{r}) \quad . \end{aligned} \quad (1.30)$$

Using Eq.(1.24) we get ($\vec{r} \equiv (r, \varphi)$):

$$\begin{aligned} & -2\xi \sum_{j=\frac{1}{2}}^{\infty} \Re e \left\{ e^{i\varphi} \frac{r^{j-\frac{1}{2}} r^{j+\frac{1}{2}}}{(j-\frac{1}{2})!^{\frac{1}{2}} (j+\frac{1}{2})!^{\frac{1}{2}}} \frac{(j+\frac{1}{2})^{\frac{1}{2}}}{\xi^2 + (j+\frac{1}{2})} e^{-r^2} \right\} \\ & = -2\xi \quad r \cos \varphi \sum_{j=\frac{1}{2}}^{\infty} \frac{(r^2)^{j-\frac{1}{2}} e^{-r^2}}{(j-\frac{1}{2})!} \frac{1}{\xi^2 + (j+\frac{1}{2})}. \end{aligned} \quad (1.31)$$

Because the maximum of the first factor occurs for $j + \frac{1}{2} \sim r^2$ we evaluate the denominator of the second factor by substituting $j + \frac{1}{2} \rightarrow r^2$, what allows us to perform the sum explicitly. By noting that $r \cos \varphi = x$ we obtain $s_x(\vec{r})$ as given by Eq.(1.25).

$$s_x(\vec{r}) = -\frac{2x\xi}{r^2 + \xi^2} . \quad (1.32)$$

A similar calculation applies for $s_y(\vec{r})$.

$$s_y(\vec{r}) = \pm \frac{2y\xi}{r^2 + \xi^2} . \quad (1.33)$$

In the case of $s_z(\vec{r})$, the extra factor is $v_j^2 - u_j^2 = [(j + \frac{1}{2}) - \xi^2]/[(j + \frac{1}{2}) + \xi^2]$ and φ disappears.

$$s_z(\vec{r}) = -\frac{r^2 - \xi^2}{r^2 + \xi^2} . \quad (1.34)$$

Bibliography

- [1] L. P. Kouwenhoven, D. G. Austing, S. Tarucha Rep. Prog. Phys. **64** (6), 701-736 (2001); L. P. Kouwenhoven and C. M. Marcus Phys. World **116**, 35-39 (1998); M. A. Kastner, Ann. Phys.(N.Y.) **9** , 885 (2000).
- [2] L. Jacak, P. Hawrilack, A. Wójs, Quantum Dots, Springer-Verlag Berlin (1998).
- [3] S. Tarucha, D. G. Austing, T. Honda, R. J. van der Hage, and L. P. Kouwenhoven, Phys. Rev. Lett. **77**, 3613 (1996).
- [4] D. Loss and D. P. Di Vincenzo, Phys. Rev. A **57**,120 (1998).
- [5] B. E. Kane, Nature,**393**,133 (1998).
- [6] J. H. Smet, R. A. Deutschmann, F. Ertl, W. Wegscheider, G. Abstreiter, K. von Klitzing Nature,**415**,281 (2002).
- [7] A. V. Khaetskii and Y. Nazarov, Phys. Rev **B64**, 125316 (2001), Y. B. Lyanda - Geller, I. L. Aleiner and B. L. Altshuler, Phys. Rev. Lett.**89**, 107602 (2002).
- [8] A. K. Hüttel, J. Weber, A. W. Holleitner, D. Weinmann, K. Eberl and R. H. Blick Phys. Rev. B **69**, 073302 (2004).
- [9] Y. Ishikawa and H. Fukuyama, Journ. of Phys. Soc. Japan **68**(7), 2405 (1999)
- [10] A. H. MacDonald,in NATO ASI:'Quantum transport in semiconductor submicron structures', B.Kramer ed.(Kluwer Berlin, 1996).

- [11] W. G. van der Wiel, T. H. Oosterkamp, J. W. Janssen, L. P. Kouwenhoven, D. G. Austing, T. Honda, S. Tarucha., *Physica B* **256**, 173 (1998).
- [12] T. Schmidt, M. Tewordt, R. H. Blick, R. J. Haug, D. Pfannkuche, K. v. Klitzing, A. Frster and H. Lth , *Phys. Rev. B* **51**,5570 (1995).
- [13] H. Imamura, H. Aoki and P. A. Maksym, *Phys. Rev. B* **57**,R4257 (1998); D. Weinmann, W. Häusler and B. Kramer, *Phys. Rev. Lett.* **74**, 984 (1995).
- [14] B. Jouault, G. Santoro, A. Tagliacozzo, *Phys. Rev. B* **61**, 10242 (2000).
- [15] I. L. Aleiner, P. W. Brouwer and L. I. Glazman, *Phys. Rep.* **358**, 309 (2002).
- [16] D. Giuliano, B. Jouault, A. Tagliacozzo, *Europhys. Lett.* **58**, 401 (2002).
- [17] D. Giuliano, P. Sodano, A. Tagliacozzo, *Phys. Rev. B* **67**, 155317 (2003).
- [18] O. Klein, C. de C. Chamon, D. Tang, D. M. Abusch-Magder, U. Meirav, X. -G. Wen and M. A. Kastner S. J. Wind, *Phys. Rev. Lett.* **74**, 785(1995); O. Klein, D. Goldhaber-Gordon, C. d. C. Chamon and M. A. Kastner , *Phys. Rev. B* **53**,4221(1996).
- [19] T. H. Oosterkamp, J. W. Janssen, L. P. Kouwenhoven, D. G. Austing, T. Honda and S. Tarucha, *Phys. Rev. Lett.* **82**, 2931 (1999).
- [20] L. P. Rokhinson, L. J. Guo, S. Y. Chou and D. C. Tsui, *Phys. Rev. Lett.* **87**, 166802 (2001).
- [21] C. de Chamon and X. G. Wen, *Phys. Rev. B* **49**, 8227 (1994); S. M. Reimann, M. Koskinen, M. Manninen, B. R. Mottelson, *Phys. Rev. Lett.***83**,3270 (1999).
- [22] for a review see: S. M. Reimann and M. Manninen, *Rev.Mod.Phys.* **74**, 1283 (2002).
- [23] D. Pfannkuche, V. Gudmindsson and P. A. Maksym, *Phys. Rev. B* **47**, 2244 (1993).
- [24] M. Stopa, *Phys. Rev. B* **54**, 13767 (1996).
- [25] R. Egger, W. Häusler, C. H. Mak and H. Grabert *Phys. Rev. Lett.* **82** 3320 (1999); R. Egger, W. Häusler, C. H. Mak *Phys. Rev. Lett.* **83** 462 (1999).
- [26] P. Lucignano, B. Jouault, A. Tagliacozzo, *Phys. Rev. B***69**, 045314 (2004).

- [27] E. I. Rashba, Fiz. Tverd. Tela **2**, 1224 (1960) [Sov.Phys. - Solid State **2**, 1109 (1960), Y. A. Bychkov, E. I. Rashba, J. Phys. **C17**, 6039 (1984).
- [28] F. E. Meijer, A. F. Morpurgo, T. M. Klapwijk, T. Koga and J. Nitta cond-mat/0406106.
- [29] J. B. Miller, D. M. Zumbhl, C. M. Marcus, Y. B. Lyanda-Geller, D. Goldhaber-Gordon, K. Campman and A. C. Gossard Phys. Rev. Lett. **90** 076807 (2003).
- [30] In *In Ga As* α is about $70meV \text{ \AA}$ at zero electric field. It can be increased by applying a gate voltage. (J. Nitta, T. Akazaki, H. Takayanagi and T. Enoki, Phys. Rev. Lett, **78**, 1335 (1997); D. Grundler, Phys. Rev. Lett. **84**, 6074 (1999)).
- [31] P. Lucignano, B. Jouault, A. Tagliacozzo, B. L. Altshuler submitted (2004).
- [32] R. Tycko, S. E. Barrett, G. Dabbagh, L. N. Pfeiffer, and K. W. West, Science **268**, 1460 (1995).
- [33] A. A. Balavin and A. M. Polyakov, JETP Lett. **22**, 245(1975); A. M. Polyakov, Phys.Lett. **59B**, 79 (1975).
- [34] R. Rajaraman *Soliton and instantons*, North Holland, Amsterdam (1982).
- [35] E. H. Aifer, B. B. Goldberg and D. A. Broido, Phys. Rev. Lett. **76**, 680(1996).
- [36] M. Abramowitz, I. A. Stegun, Handbook of Methemathical Functions with Formulas, Graphs and Mathematical Tables, Dover (New York 1972).
- [37] V. Fock, Z. Phys **47**, 446 (1928); C. G. Darwin Proc. Cambridge Phil. Soc. **27**, 86, (1931).
- [38] C. F. Destefani, S. E. Ulloa and G. E. Marques, Phys. Rev. B **69**, 125302 (2004) (see Fig.3).
- [39] T. Fujisawa, D. G. Austing, Y. Tokura, Y. Hirayama and S. Tarucha, Nature, **419**, 278 (2002).
- [40] A. Karlhede, S. A. Kivelson, K. Lejnell and S. L. Sondhi, Phys. Rev. Lett. **77**, 2061 (1996).
- [41] In a vertical B field, a sequence of compressible and incompressible regions was found in much larger dots using Hartree self-consistent schemes. V. Gudmundsson, A. Brataas, C. Steinbach, A.

- G. Mal'shukov, K. A. Chao and D. Heitmann, *Physica Scripta* **T69**, 150 ,(1997).
- [42] M. Fricke, A. Lorke, J. P. Kotthaus, G. Medeiros-Ribeiro and P. M. Petroff, *Europhys. Lett.* **36**,197 (1996); P.Junker, U.Kops, U.Merkt, T.Darnhofer and U Rossler, *Phys. Rev. B* **49**, 4794 (1994).
- [43] R. Krahne, V. Gudmundsson, G. Heyn, D. Heitmann *Phys. Rev. B* **63**, 195303, (2001).
- [44] C. Sikorski and U. Merkt *Phys. Rev. Lett.* **62** 2164 (1989).
- [45] L. Brey, N. F. Johnson and B. I. Halperin *Phys. Rev. B* **40** 10647 (1989)
- [46] D. A. Broido, K. Kempa and P. Bakshi *Phys. Rev. B* **42** 11400 (1990); P.Bakshi, D. A. Broido and K. Kempa *Phys. Rev. B* **42** 7416 (1990).
- [47] P. A. Maksym and T. Chakraborty, *Phys. Rev. Lett.* **65**, 108, (1990).
- [48] R. B. Laughlin, *Phys. Rev. B* **27** 3383, (1983).
- [49] P. Junker, U. Kops, U. Merkt, T. Darnhofer and U. Rossler *Phys. Rev. B* **49** 4794 (1994).
- [50] D. Loss, D. Di Vincenzo, *Phys. Rev. A* **57**, 120(1998); H. A. Engel, D. Loss, *Phys. Rev. Lett.* **86**, 4648(2001).
- [51] B. I. Halperin, *Helv. Phys. Acta* **56**,75 (1983).
- [52] H. A. Fertig, L. Brey, R. Ct, A. H. MacDonald, A. Karlhede, S. L. Sondhi , *Phys. Rev. B* **55**, 10671 (1997) ; M. Abolfath, J. J. Palacios, H. A. Fertig, S. M. Girvin and A. H. MacDonald *Phys. Rev. B* **56**, 6795 (1997).
- [53] T. Takagahara *J. of Luminescence* **87-89**, 308 (2000).
- [54] D. D. Awszalom, J. M. Kikkawa, *Phys.Today.* **52**, 33 (1999).
- [55] B. E. Cole, J. B. Williams, B. T. King, M. S. Sherwin and C. R. Stanley, *Nature* **410**,60 (2001).
- [56] P. Chen,C. Permarocchi and L. J. Sham, *Phys. Rev. Lett.* **87**, 067401 (2001).
- [57] G. Chen, N. H. Bonadeo, D. G. Steel, D. Gammon, D. S. Katzer, D. Park and L. J. Sham, *Science* **289**, 1906 (2000).
- [58] N.H. Bonadeo, J. Erland, D. Gammon, D. Park, D.S. Katzer and D.G. Steel, *Science* **282** , 1473 (1998).
- [59] H. Kamada, H. Gotoh, J. Temmyo, T. Takagahara and H. Ando., *Phys. Rev. Lett.* **87**,246401 (2001).

Discovery consists in seeing what everybody has seen and thinking what nobody has thought.

Albert Szent-Györgyi (1893-1986)

2

Adiabatic control and Berry phase

Abstract

By adiabatically cycling some external control parameters it is possible that the many-body wave function of a quantum dot acquire a geometrical Berry phase. We introduce an effective low energy Hamiltonian capable to describe the singlet triplet anti-crossing in the two electron dot in the presence of the Rashba coupling and we calculate explicitly such a geometrical phase. This can be detected both in the adiabatic (Berry) and in the non-adiabatic regime (Ahronov-Anandan) by reading the conductance oscillations of a quantum mesoscopic ring.

2.1 Introduction

Manipulating in a controlled fashion the phase of a quantum electronic system is presently one of the most relevant challenges in nanophysics, especially in view of possible applications to quantum computing [1]. Probably, the most promising route to achieve such a task is provided by coherent solid-state devices. For instance, a superconducting Josephson qubit has already been realized as a Cooper pair box, that is, a small superconducting island, weakly coupled to a charge reservoir via a Josephson junction [2]. The quantum state of the box can be tuned to a coherent superposition of the charge-zero and the charge-one states. The possibility of realizing superpositions of flux states has been considered, as well [3]. Entanglement in a semiconducting device made out of two dots, one on top of each other (“quantum dot molecule”) has been recently optically measured [4].

Usually, quantum algorithms assume that the system dynamically evolves through a sequence of unitary transformations, or that a set $\vec{\lambda}$ of external control parameters of the Hamiltonian H smoothly changes in time [5]. In particular, if adiabatic evolution is realized across a closed path γ in the parameter space, close enough to an accidental level degeneracy, the nontrivial topology of the space makes the state of the system to acquire a “geometrical” phase Γ , referred to as “Berry Phase” [6]. The value of Γ may be

controlled by properly choosing γ .

Following this idea, geometric adiabatic evolution has recently been proposed as a way to operate with superconducting devices without destroying phase coherence [7, 8]. Another possibility is using semiconducting nanodevices, like single-electron transistors or Quantum Dots (QD). The QD state can be finely tuned, by means of external magnetic and electric fields acting on the dot, or on the coupling between the dot and the contacts [9]. Moreover, accidental level degeneracies are quite common in QD's, as seen both theoretically, and experimentally [10–13]. Also, double dots have been proposed as possible qubits [14].

In the two electron quantum dot the single triplet crossing becomes an anti crossing in the presence of a Rashba coupling. In other words by mean of the magnetic field we can tune the dot at the singlet triplet crossing. Then by cyclically modulating in time an electric field orthogonal to the dot plane, and as a consequence the Rashba coupling, we can manipulate the dot close enough to the level degeneracy point. The nontrivial topology of the space allows the many body wave function to acquires a “geometrical” phase Γ . This phase is in general an Ahronov Anandan phase [15] and in the adiabatic limit a “Berry Phase” [6]. In order to properly describe this situation we introduce an effective low energy Hamiltonian by projecting the full Hamiltonian onto the singlet and the triplet states involved in the anti-crossing. Such a projection gives us a simple two level Hamiltonian that, in the adiabatic limit recalls the celebrated two level Berry Hamiltonian. Solving this simple model in the next section we shall show that the many body wave function of the dot acquires a geometrical phase.

In the second part of the chapter we shall try to describe a possible transport experiment that allows for reading out such a geometrical phase. The studied device, in this case, is not a quantum dot but a quantum ring. The choice of the ring allows us to simplify the calculations and gives us a very clear physical picture as it will be explained in the following. Moreover such a structure is capable of producing a geometrical phase without any time dependent parameter because the electrons themselves by moving into the arms of the ring experience time dependent external fields varying according to semiclassical equations of motions. Some evidences of geometric phases will be described, particularly in the non adiabatic regime, that is, when a strong spin orbit and a weak magnetic fields are present.

2.2 Berry Phase in QM

In this section we shall briefly review the basics of the quantum mechanics in the adiabatic approximation and introduce the concept of the topological Berry phase. Imagine a quantal system whose Hamiltonian H is slowly¹

¹We shall come back later in much detail on the meaning of “slowly”

altered in time, it follows from the adiabatic theorem [16] that at any instant the system will be in an eigenstate of the instantaneous H . If the Hamiltonian is returned to its original form, the system will return to its original state as well, apart from a phase factor. This phase factor contains a circuit dependent component $e^{i\Gamma}$ in addition to the familiar dynamical phase $e^{-iEt/\hbar}$.

In what follow we will briefly review how it is possible to calculate such new phase Γ following the same approach of the wonderful original paper by Berry [6] who first introduced this phase within a general framework.

Let the Hamiltonian be changed by mean of a set of external control parameters $\vec{\lambda}$ which depend on time. Let us suppose that these parameters are changed in time in such way that $\vec{\lambda}(t=0) = \vec{\lambda}(t=T)$, that is the excursion of the system describes a closed path in the parameters space, this path will be denoted as γ . After a certain period T the Hamiltonian comes back into itself. The system evolves according to Schrödinger's equation (from now on, in this section, we shall put $\hbar = 1$ except in some important results):

$$i\frac{\partial}{\partial t}|\psi(t)\rangle = H(\vec{\lambda}(t))|\psi(t)\rangle, \quad (2.1)$$

if the time evolution of the parameters is sufficiently slow, the system is in an eigenstate of the Hamiltonian at each time:

$$H(\vec{\lambda})|n(\vec{\lambda})\rangle = E_n(\vec{\lambda})|n(\vec{\lambda})\rangle, \quad (2.2)$$

with energies $E_n(\vec{\lambda})$ and eigenvectors $|n(\vec{\lambda})\rangle$.

First of all, let us discuss what does *adiabatical* evolution of a quantum mechanical system means in this framework.

We expand the wave function solving the time dependent Schrödinger equation on the basis $|n(\vec{\lambda}(t))\rangle$ of the instantaneous eigenstates of the Hamiltonian:

$$|\psi(t)\rangle = \sum_{n=1}^N c_n(t) e^{-i\int_0^t E_n(\vec{\lambda}(t')) dt'} |n(\vec{\lambda}(t))\rangle, \quad (2.3)$$

and calculate $i\partial_t|\psi(t)\rangle$:

$$\begin{aligned} i\partial_t|\psi(t)\rangle = \sum_n \left(i\partial_t c_n(t) + c_n(t) E_n(\vec{\lambda}(t)) \right) e^{-i\int_0^t E_n(\vec{\lambda}(t')) dt'} |n(\vec{\lambda}(t))\rangle + \\ + i \sum_n c_n(t) e^{-i\int_0^t E_n(\vec{\lambda}(t')) dt'} \partial_t |n(\vec{\lambda}(t))\rangle. \end{aligned} \quad (2.4)$$

Now we multiply Eq.2.1 onto $\langle n(\vec{\lambda}(t))|$ and using Eq.2.4, we get:

$$\begin{aligned} \frac{d}{dt}c_n(t) = -\langle n(\vec{\lambda}(t))|\partial_t|n(\vec{\lambda}(t))\rangle c_n(t) + \\ + \sum_{m \neq n} \langle n(\vec{\lambda}(t))|\partial_t|m(\vec{\lambda}(t))\rangle c_m(t) e^{-i\int_0^t (E_n(t') - E_m(t')) dt'}. \end{aligned} \quad (2.5)$$

Differentiating eq.2.2 with respect to t and projecting onto $\langle n(\vec{\lambda}(t))|$ we find:

$$\langle n(\vec{\lambda}(t))|\partial_t|m(\vec{\lambda}(t))\rangle = -\dot{\vec{\lambda}} \frac{\langle n(\vec{\lambda}(t))|(\nabla_{\vec{\lambda}}H(t))|m(\vec{\lambda}(t))\rangle}{E_n(t) - E_m(t)}. \quad (2.6)$$

Now imagine integrating the second term of the right hand side of Eq.2.5, using 2.6 and assume that everything except the exponential is approximately constant in time. We see that the admixture of other state, to a given state n will be small if

$$\left| \frac{1}{\omega_{mn}} \left\langle \frac{\partial H}{\partial t} \right\rangle \right| \ll E_n(t) - E_m(t) \quad (2.7)$$

where $\hbar\omega_{mn} = E_m - E_n$. In other words *if the change of the Hamiltonian over on Bohr period for the transition $|n\rangle \rightarrow |m\rangle$ is small w.r. to the level spacing $E_m - E_n$ of the system, the off-diagonal contribution to Eq.2.5 can be neglected.* In this case the coefficients $c_n(t)$ can be decoupled and satisfy the equation:

$$\frac{d}{dt}c_n(t) = -\langle n(\vec{\lambda}(t))|\partial_t|n(\vec{\lambda}(t))\rangle c_n(t). \quad (2.8)$$

This is the core of the adiabatic approximation [17].

Let us prepare the system in the state $|n(\vec{\lambda}(t=0))\rangle$ and adiabatically evolve by H in such a way that at the time t it is into the state $|n(\vec{\lambda}(t))\rangle$. The wave function ψ solving the time dependent Schrödinger equation can be written as

$$|\psi(t)\rangle = \exp\left\{-i\int_0^t dt' E_n(\vec{\lambda}(t'))\right\} \exp\{i\Gamma_n(t)\} |n(\vec{\lambda}(t))\rangle. \quad (2.9)$$

The first phase is the usual dynamical phase. We shall focus our attention on the second contribution Γ which we shall show to be a non integrable phase: it cannot be written as a function of $\vec{\lambda}$ and in particular is not single valued under continuation on the circuit γ , that is $\Gamma(T) \neq \Gamma(0)$ where T is the time needed to enclose the path γ in the parameters space. After the time T the total wavefunction can be written as

$$|\psi(T)\rangle = \exp\left\{-i\int_0^T dt' E_n(\vec{\lambda}(t'))\right\} \exp\{i\Gamma_n(\gamma)\} |\psi(0)\rangle, \quad (2.10)$$

where the geometrical phase is

$$\Gamma_n(\gamma) = i \int_{\gamma} \langle n(\vec{\lambda})|\nabla_{\vec{\lambda}} n(\vec{\lambda})\rangle \cdot d\vec{\lambda}. \quad (2.11)$$

By applying Stokes theorem, the last expression can take the form

$$\Gamma_n(\gamma) = - \iint_{\gamma} d\vec{S} \cdot \vec{V}_n(\vec{\lambda}), \quad (2.12)$$

where $d\vec{S}$ is the area element in $\vec{\lambda}$ space and

$$\vec{V}_n(\vec{\lambda}) = \Im m \{ \nabla \times \langle n | \nabla n \rangle \}. \quad (2.13)$$

So V_n is the curl of a vector which depends on the choice of the phase of the single-value eigenstate $|n(\vec{\lambda})\rangle$. The dependence on phase is of the following kind: if $|n\rangle \rightarrow \exp\{i\mu(\vec{\lambda})\}|n\rangle$ then $\langle n | \nabla n \rangle \rightarrow \langle n | \nabla n \rangle + i\nabla\mu$. Thus the vector is not unique but its curl is. The quantity \vec{V}_n is analogous to a 'magnetic field' in the parameter space whose 'vector potential' is $\Im m \langle n | \nabla n \rangle$. In the following we shall show that close to the degeneracies of the Hamiltonian such vector potential acquires the form of a magnetic monopole potential. Some geometric identities can be applied to Eq. 2.13:

$$\nabla \times \langle n | \nabla n \rangle = \langle \nabla n | \times | \nabla n \rangle = \sum_{m \neq n} \langle \nabla n | m \rangle \times \langle m | \nabla n \rangle \quad (2.14)$$

and using 2.6, Eq. 2.13 acquires the form:

$$\vec{V}_n(\vec{\lambda}) = \Im m \sum_{m \neq n} \frac{\langle n(\vec{\lambda}) | \nabla_{\vec{\lambda}} H(\vec{\lambda}) | m(\vec{\lambda}) \rangle \times \langle m(\vec{\lambda}) | \nabla_{\vec{\lambda}} H(\vec{\lambda}) | n(\vec{\lambda}) \rangle}{(E_m(\vec{\lambda}) - E_n(\vec{\lambda}))^2}. \quad (2.15)$$

Easily $\Gamma_n(\gamma)$ is zero if γ encloses no area. It is independent of how the circuit is traversed, provided that the time evolution of the parameters is slow enough that adiabatic approximation still holds. The energy denominator shows that if the circuit γ lies close to a point $\vec{\lambda}^*$ in the parameters space at which the state n is involved in a degeneracy, then $V_n(\vec{\lambda}^*)$, and hence $\Gamma(\gamma)$, is dominated by the term m corresponding to the other states involved. So let us suppose that the degeneracy involves only two states $|+\rangle$ and $|-\rangle$, and $E_+(\vec{\lambda}) \geq E_-(\vec{\lambda})$. For $\vec{\lambda} \sim \vec{\lambda}^*$ the Hamiltonian can be expanded to first order in $\vec{\lambda} - \vec{\lambda}^*$ and

$$\vec{V}_+(\vec{\lambda}) = \Im m \frac{\langle +(\vec{\lambda}) | \nabla_{\vec{\lambda}} H(\vec{\lambda}) | -(\vec{\lambda}) \rangle \times \langle -(\vec{\lambda}) | \nabla_{\vec{\lambda}} H(\vec{\lambda}) | +(\vec{\lambda}) \rangle}{(E_+(\vec{\lambda}) - E_-(\vec{\lambda}))^2}, \quad (2.16)$$

and easily $\vec{V}_- = -\vec{V}_+$ and $\Gamma_-(\gamma) = -\Gamma_+(\gamma)$. We can choose $E_{\pm}(\vec{\lambda}^*) = 0$ and $\vec{\lambda}^* = 0$. So, close to the crossing between the two levels, the Hamiltonian can be written as a simple two by two matrix which in general (in the absence of symmetries) takes the form

$$H(\vec{\lambda}) = \frac{1}{2} \begin{pmatrix} Z & X - iY \\ X + iY & -Z \end{pmatrix}. \quad (2.17)$$

The eigenvalues are $E_+(\vec{\lambda}) = -E_-(\vec{\lambda}) = 1/2 R$ where $R^2 = X^2 + Y^2 + Z^2$. The degeneracy at $\vec{\lambda}^* = 0$ is realized if at the same time $X = Y = Z = 0$,

that is the degeneracy has co-dimension three. By noting that $\vec{\nabla}H = 1/2\hat{\sigma}$ it is easy to calculate the Berry's phase. By using Eq. 2.16 we obtain

$$\vec{V}_+ = \frac{\hat{R}}{2R^2}, \quad (2.18)$$

and Eq. 2.12 tells us that the Berry phase is the flux through the surface enclosed by γ of the magnetic field of a monopole with strength $-1/2$ located at the degeneracy. In fact

$$\Gamma_{\pm} = \mp \frac{1}{2} \Omega_{\gamma}, \quad (2.19)$$

where Ω_{γ} is the solid angle that γ subtends at the degeneracy: it is in a sense a measure of the view of the circuit as seen from the degeneracy.

2.3 Two electron Quantum Dot: A Possible $SU(2)$ Berry Phase

In this section we shall introduce a low energy effective Hamiltonian to describe the two electron quantum dot properties close to the singlet triplet crossing. To this aim let us start by discussing again Figs. 1.2 and 1.7. In order to help the reader, these figures are drawn again in the following.

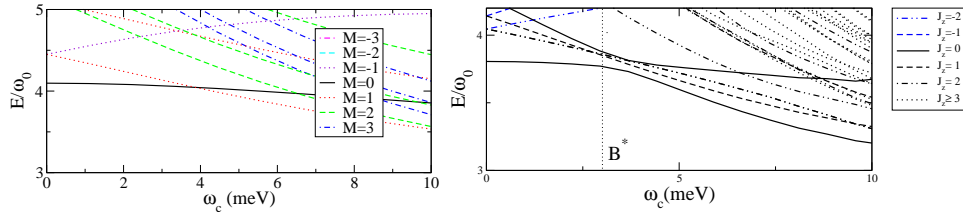


Figure 2.1: $N=2$ particles dot: (Left box) energy spectrum vs magnetic field ω_c in the absence of the SO . $\omega_d = 5meV$, $U = 13meV$, (Right box) energy spectrum vs magnetic field ω_c in the presence of the SO . Same parameter values and $\alpha = 250meV\text{\AA}$

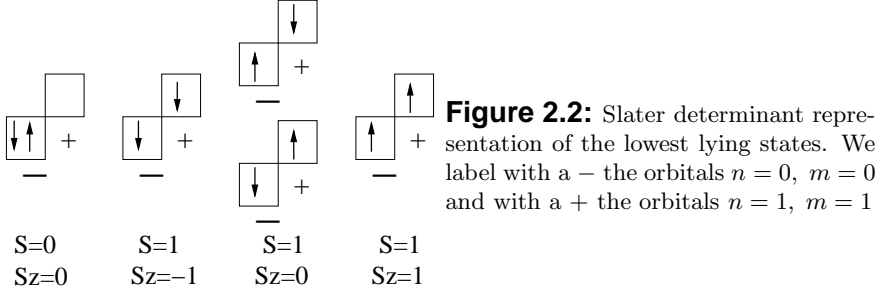
As explained in Chapter 1 the singlet triplet crossing typical of the 2 electron quantum dot (left panel) without spin orbit coupling appears as a marked anti-crossing in the case of a quantum dot with SO coupling.

The low lying states are (here we label the states by using the total spin momentum S and the spin projection along the z axis S_z : $|S, S_z\rangle$ which are good quantum numbers when the SO is absent):

- $|0, 0\rangle$, that is $M = 0$, $S = 0$, $S_z = 0$, $J_z = 0$, it is the singlet ground state at low B ,

and then there are the three triplet states :

- $|1, -1\rangle$, that is $M = 1, S = 1, S_z = -1, J_z = 0$ it is the ground state at high B ,
- $|1, 0\rangle$, that is $M = 1, S = 1, S_z = 0, J_z = 1$ it is higher up in energy and completes the $S = 1$ spin multiplet together with the previous and next state,
- $|1, 1\rangle$, $M = 1, S = 1, S_z = 1, J_z = 2$.



In Fig. 2.2 we represent these states by using the single particle Slater determinants representation. We label the $n = 0, m = 0$ “orbital” with - and the $n = 1, m = 1$ “orbital” with +. So it is possible to describe the low lying states by mean of appropriate fermionic operators for the dot $\hat{d}_{n,\sigma}$ with $n = +, -$ and $\sigma = \uparrow, \downarrow$. So the following correspondences arise

$$\begin{aligned}
 |0, 0\rangle &= \hat{d}_{-, \uparrow}^\dagger \hat{d}_{-, \downarrow}^\dagger |0\rangle, \\
 |1, -1\rangle &= \hat{d}_{-, \downarrow}^\dagger \hat{d}_{+, \downarrow}^\dagger |0\rangle, \\
 |1, 0\rangle &= \frac{1}{\sqrt{2}} \left(\hat{d}_{-, \uparrow}^\dagger \hat{d}_{+, \downarrow}^\dagger + \hat{d}_{+, \uparrow}^\dagger \hat{d}_{-, \downarrow}^\dagger \right) |0\rangle, \\
 |1, 1\rangle &= \hat{d}_{-, \uparrow}^\dagger \hat{d}_{+, \uparrow}^\dagger |0\rangle,
 \end{aligned} \tag{2.20}$$

where $|0\rangle$ is the dot state with the two levels \pm empty. In this framework we can write the low energy dot Hamiltonian as:

$$H_{dot} = \sum_{n,s} \epsilon_n \hat{d}_{n,s}^\dagger \hat{d}_{n,s} - E_s \vec{S}^2 - E_z S^z + H_{SO}, \tag{2.21}$$

where the parameters ϵ_n and E_s are chosen in order to reproduce the real spectrum in the presence of $e - e$ interaction and

$$\vec{S} = \sum_{n,s,s'} \hat{d}_{n,s}^\dagger \frac{\vec{\sigma}_{s,s'}}{2} \hat{d}_{n,s'}. \tag{2.22}$$

H_{SO} is the projection of the Rashba Hamiltonian onto this 4 - d space spanned by the vectors 2.20:

$$H_{SO} = V_{so} \hat{d}_{+, \downarrow}^\dagger \hat{d}_{-, \uparrow} + h.c. . \tag{2.23}$$

From the last equation it is clear that the spin orbit only couples the two states $|0, 0\rangle$ and $|1, -1\rangle$ thus conserving the total angular momentum, $J_z = 0$; moreover the other two states $J_z = 1, 2$ are not coupled by H_{SO} .

Now it is convenient to map the Hilbert space spanned by the four states of Eq.(2.20) onto a pseudo-spin Hilbert space which basis is constructed starting from two spins $\frac{1}{2}$: \vec{S}_1 and \vec{S}_2 and of the corresponding basis $|S_+, S_+^z\rangle$ with $\vec{S}_\pm = \vec{S}_1 \pm \vec{S}_2$ [18-20]. The one-to-one correspondence between the four low energy states of the dot and of the two fictitious spins is:

$$\begin{aligned} |0, 0\rangle &= \frac{1}{\sqrt{2}} (|\uparrow_1, \downarrow_2\rangle - |\downarrow_1, \uparrow_2\rangle) , \\ |1, -1\rangle &= |\downarrow_1, \downarrow_2\rangle , \\ |1, 0\rangle &= \frac{1}{\sqrt{2}} (|\uparrow_1, \downarrow_2\rangle + |\downarrow_1, \uparrow_2\rangle) , \\ |1, 1\rangle &= |\uparrow_1, \uparrow_2\rangle . \end{aligned} \quad (2.24)$$

This correspondence allows one to represent any operator acting on the states 2.20 in terms of the spin-1/2 operators $\vec{S}_{1,2}$ acting on the 2.24 basis. By comparing the matrix elements directly one can write:

$$\mathcal{P} \sum_s d_{ns}^\dagger d_{n's} \mathcal{P} \Rightarrow n \delta_{n,n'} \left[\vec{S}_1 \cdot \vec{S}_2 - \frac{1}{4} + n \right] , \quad (2.25)$$

$$\mathcal{P} \sum_{ss'} d_{ns}^\dagger \frac{1}{2} \vec{\sigma}_{ss'} d_{n's'} \mathcal{P} \Rightarrow \frac{1}{2} \delta_{n,n'} \vec{S}_+ + \delta_{n,-n'} \frac{1}{2\sqrt{2}} \left[\vec{S}_- + 2in\vec{T} \right] , \quad (2.26)$$

where $\mathcal{P} = \sum_{S,S^z} |S, S^z\rangle \langle S, S^z|$ is the projector onto the states 2.20, $\vec{S}_\pm = \vec{S}_1 \pm \vec{S}_2$ and $\vec{T} = \vec{S}_1 \times \vec{S}_2$. Equations 2.25, 2.26 have to be intended in the sense that the operators on the left hand side obey the same algebra as those on the right hand side. The states 2.20 are eigenstates of the operators \vec{S}_+ and $\vec{S}_1 \cdot \vec{S}_2$ while \vec{S}_- and \vec{T} describe transitions between the singlet and one component of the triplet. Some important relations among these operators are reported in appendix 2A while some details about how to calculate the matrix elements of Eq.s 2.25, 2.26 are shown in Appendix 2B. In this new representation, close to B^* , the low energy Hamiltonian takes the form [21]:

$$H_{dot} = K \vec{S}_1 \cdot \vec{S}_2 - \mu B S_+^z + \frac{1}{2\sqrt{2}} \left(V_{so} \left(\vec{S}_- + 2in\vec{T} \right) + h.c. \right) . \quad (2.27)$$

The second term is the Zeeman spin splitting, the first term takes into account the kinetic part of the confined electrons and together both terms are responsible for the single triplet crossing at B^* which appears in the absence of SO coupling.

In Appendix A the commutation relations are reported which show that while $\vec{S}_1 \cdot \vec{S}_2$ and \vec{S}_+ commute, they do not commute with \vec{S}_- and \vec{T} , nor

\vec{S}_- and \vec{T} commute between themselves. This proves that the SO couples the center of mass coordinate with the relative ones. Hence Kohn's theorem does not apply in the case of dots with spin orbit coupling and microwave radiation shed onto the dot probes interactions as well (see chapter 1 section 5).

As seen in Fig. 2.1 the SO does not couple states $|1, 1\rangle$ and $|1, 0\rangle$ with $|0, 0\rangle$ and $|1, -1\rangle$, nor between themselves. For what the SO is concerned they are frozen out. If we just retain the two states involved in the anti-crossing, we can further simplify the problem which boils down to a single spin 1/2: \tilde{S} . The correspondence between the states is

$$|0, 0\rangle \rightarrow |\uparrow\rangle, \quad (2.28)$$

$$|1, -1\rangle \rightarrow |\downarrow\rangle. \quad (2.29)$$

Defining as $\mathcal{P}' = \sum_s |s\rangle\langle s|$ as the projector on the two state basis we have:

$$\begin{aligned} \mathcal{P}' S_+^z \mathcal{P}' &\Rightarrow \tilde{S}^z - \frac{1}{2}, \\ \mathcal{P}' \vec{S}_1 \cdot \vec{S}_2 \mathcal{P}' &\Rightarrow -\tilde{S}^z - \frac{1}{4}, \\ \mathcal{P}' S_-^{\pm} \mathcal{P}' &\Rightarrow \sqrt{2} \tilde{S}^{\pm}, \\ \mathcal{P}' T^{\pm} \mathcal{P}' &\Rightarrow \pm \frac{i}{\sqrt{2}} \tilde{S}^{\pm}. \end{aligned} \quad (2.30)$$

It follows that the effective Hamiltonian of Eq.(2.27), rewritten in the new representation, reads (for further details see appendix 2A-B-C)

$$H_{\tilde{S}} = -\frac{1}{2}\left(\frac{K}{2} - \mu B\right) - (K + \mu B)S^z + \left(V_{so}\tilde{S}^- + V_{so}^*\tilde{S}^+\right), \quad (2.31)$$

where the terms in the last parenthesis are due to the spin orbit coupling and the first two terms allow for the kinetic and magnetic part of the Hamiltonian. We can now define an effective magnetic field \tilde{b} as follows:

$$\tilde{b}_+ = \tilde{b}_x + i\tilde{b}_y = V_{so}, \quad (2.32)$$

$$\tilde{b}_- = \tilde{b}_x - i\tilde{b}_y = V_{so}^*, \quad (2.33)$$

$$\tilde{b}_z = -(K + \mu B). \quad (2.34)$$

In terms of \tilde{b} the last Hamiltonian can be written in the form:

$$H_{dot} = -\frac{1}{2}\left(\frac{K}{2} - \mu B\right) + \vec{b} \cdot \vec{S}. \quad (2.35)$$

This maps, apart from a shift $-\frac{1}{2}\left(\frac{K}{2} - \mu B\right)$ of the energies which we shall neglect in the following, the two-electron Hamiltonian of Eq.(2.27) onto a simple spin Hamiltonian completely, close to the anti-crossing point.

The dot state may be controlled by properly tuning the external control parameters B and \mathcal{E} . The adiabatic cycle is realized by keeping B fixed, and by slowly periodically varying \mathcal{E} , with time period T ; because of this cycling a time dependent spin-orbit coupling term arises, involving the spin of electrons at the dot. Such an interaction may give raise to a Berry phase at the QD.

2.3.1 Solution of the low energy spin Hamiltonian

Here we discuss the simple Hamiltonian 2.31. We show that, in the adiabatic limit, the the dot can acquire a Berry phase which could be measured in transport experiment as explained in the following sections. By a simple shift of the energies the Hamiltonian 2.31 can be written in the simple form:

$$H_{\tilde{S}} = \vec{b} \cdot \vec{S}. \quad (2.36)$$

Let us suppose that the spin orbit coupling is generated by a slowly varying electric field, that is $V_{so} = \mathcal{E}e^{i\omega_o t}$. Under this assumption the matrix Hamiltonian in the 2-d basis $\{|\uparrow\rangle, |\downarrow\rangle\}$ is:

$$\hat{H}(t) = \frac{1}{2} \begin{bmatrix} -(K + \mu B) & \mathcal{E}e^{-i\omega_o t} \\ \mathcal{E}e^{i\omega_o t} & (K + \mu B) \end{bmatrix}, \quad (2.37)$$

a description of the vector \tilde{b} in polar coordinates allow us to write $\tilde{b}\cos(\theta) = |K + \mu B|$ and $\tilde{b}\sin(\theta) = |\mathcal{E}|$, here we introduce θ as measured from the $-\hat{z}$ direction

$$\hat{H}(t) = \frac{|\tilde{b}|}{2} \begin{bmatrix} \cos \vartheta & \sin \vartheta e^{-i\omega_o(t)} \\ \sin \vartheta e^{i\omega_o(t)} & -\cos \vartheta \end{bmatrix}, \quad (2.38)$$

where $|\tilde{b}| = \sqrt{(K + \mu B)^2 + |V_{so}|^2}$, $\omega_o = 2\pi t/T$. T is the period of adiabatic evolution and, clearly, the criterion for adiabaticity will be $|\tilde{b}|T \gg 1$, as $|\tilde{b}|/2$ is the scale of the transition frequency between the two levels of the system.

The path lies along a parallel on the sphere in parameter space of radius $|\tilde{b}|/2 = r$. ϑ is fixed during adiabatic evolution.

In order to construct the adiabatic Hamiltonian, $\hat{H}_A(t)$, let us diagonalize $\hat{H}(t)$ at fixed t . The eigenvalues are given by $\epsilon = \pm r$, while the corresponding eigenvectors take the form:

$$|+, t\rangle = \begin{pmatrix} \cos \frac{\vartheta}{2} \\ \sin \frac{\vartheta}{2} e^{i\omega_o t} \end{pmatrix}, \quad |-, t\rangle = \begin{pmatrix} -\sin \frac{\vartheta}{2} e^{-i\omega_o t} \\ \cos \frac{\vartheta}{2} \end{pmatrix}. \quad (2.39)$$

The matrix of the eigenvectors, diagonalizing \hat{H} at time t , is

$$\hat{B}(t) \equiv \begin{bmatrix} \cos \frac{\vartheta}{2} & -\sin \frac{\vartheta}{2} e^{-i\omega_o t} \\ \sin \frac{\vartheta}{2} e^{i\omega_o t} & \cos \frac{\vartheta}{2} \end{bmatrix}. \quad (2.40)$$

In order to properly define the adiabatic Hamiltonian, we shall consider the Schrödinger equation with Hamiltonian \hat{H} :

$$\left\{ i \frac{\partial}{\partial t} - \hat{H}(t) \right\} |\Psi(t)\rangle = 0.$$

It is convenient to strip off from the state $|\Psi(t)\rangle$ its adiabatic evolution, operating with \hat{B}^\dagger , so to get:

$$\left[i \frac{\partial}{\partial t} - \hat{B}^\dagger(t) \hat{H}(t) \hat{B}(t) + \hat{B}(t)^\dagger i \frac{\partial}{\partial t} \hat{B}(t) \right] \hat{B}^\dagger(t) |\Psi(t)\rangle = 0. \quad (2.41)$$

By definition, \hat{B} diagonalizes $\hat{H}(t)$. Therefore, we may rewrite Eq.(2.41) in a 2×2 matrix form as:

$$\left[\left(\begin{array}{cc} i \frac{\partial}{\partial t} & 0 \\ 0 & i \frac{\partial}{\partial t} \end{array} \right) - \left(\begin{array}{cc} r & 0 \\ 0 & -r \end{array} \right) - \omega_o \left(\begin{array}{cc} \sin^2 \frac{\vartheta}{2} & \sin \frac{\vartheta}{2} \cos \frac{\vartheta}{2} e^{-i\omega_o t} \\ \sin \frac{\vartheta}{2} \cos \frac{\vartheta}{2} e^{i\omega_o t} & -\sin^2 \frac{\vartheta}{2} \end{array} \right) \right] |u(t)\rangle = 0, \quad (2.42)$$

where we have defined $|u(t)\rangle = \hat{B}^\dagger(t) |\Psi(t)\rangle$.

From Eq.(2.42), we see that, in the ‘‘adiabatic basis’’, the total Hamiltonian is given by the sum of an ‘‘adiabatic’’ contribution, obtained by neglecting offdiagonal contributions:

$$\hat{H}_A(t) = \left(\begin{array}{cc} r + \omega_o \sin^2(\vartheta/2) & 0 \\ 0 & -r - \omega_o \sin^2(\vartheta/2) \end{array} \right), \quad (2.43)$$

plus an extra term $\Delta \hat{H}$, whose meaning we are now going to figure out. Indeed, let us consider the projectors $\hat{P}_\pm(t) = |\pm, t\rangle \langle \pm, t|$:

$$\begin{aligned} \hat{P}_+(t) &= \left(\begin{array}{cc} \cos \frac{\vartheta}{2} & \\ \sin \frac{\vartheta}{2} e^{i\omega_o t} & \end{array} \right) \left(\begin{array}{cc} \cos \frac{\vartheta}{2} & \sin \frac{\vartheta}{2} e^{-i\omega_o t} \\ & \end{array} \right) = \\ &= \left(\begin{array}{cc} \cos^2 \frac{\vartheta}{2} & \cos \frac{\vartheta}{2} \sin \frac{\vartheta}{2} e^{-i\omega_o t} \\ \cos \frac{\vartheta}{2} \sin \frac{\vartheta}{2} e^{i\omega_o t} & \sin^2 \frac{\vartheta}{2} \end{array} \right) \\ \hat{P}_-(t) &= \left(\begin{array}{cc} -\sin \frac{\vartheta}{2} e^{-i\omega_o t} & \\ \cos \frac{\vartheta}{2} & \end{array} \right) \left(\begin{array}{cc} -\sin \frac{\vartheta}{2} e^{i\omega_o t} & \cos \frac{\vartheta}{2} \\ & \end{array} \right) = \\ &= \left(\begin{array}{cc} \sin^2 \frac{\vartheta}{2} & -\cos \frac{\vartheta}{2} \sin \frac{\vartheta}{2} e^{-i\omega_o t} \\ -\cos \frac{\vartheta}{2} \sin \frac{\vartheta}{2} e^{i\omega_o t} & \cos^2 \frac{\vartheta}{2} \end{array} \right). \end{aligned} \quad (2.44)$$

It follows that:

$$[\hat{P}_\pm, P_\pm] = \frac{\omega_o}{2} \sin \vartheta \left(\begin{array}{cc} -\sin \vartheta & \cos \vartheta e^{-i\omega_o t} \\ \cos \vartheta e^{i\omega_o t} & \sin \vartheta \end{array} \right), \quad (2.45)$$

and it is easy to see that

$$\Delta \hat{H} = \hat{B}^\dagger(t) \left(\frac{i}{2} \sum_{\sigma=\pm} \left[\frac{d\hat{P}_\sigma}{dt}(t), \hat{P}_\sigma(t) \right] \right) \hat{B}(t). \quad (2.46)$$

In the next section, we shall derive the exact propagator $\hat{U}(t)$, by exactly integrating the full Schrödinger equation in the adiabatic basis.

2.3.2 The exact propagator

The adiabatic propagator in the basis $|\pm, t\rangle$ is simply given by:

$$\hat{U}_A(t) = \begin{pmatrix} e^{-i(r+\omega_o \sin^2(\theta/2))t} & 0 \\ 0 & e^{i(r+\omega_o \sin^2(\theta/2))t} \end{pmatrix} \quad (2.47)$$

We now derive the exact propagator $\hat{U}(t)$. In the adiabatic basis we have found the following formula for $\hat{H}(t)$:

$$\hat{H}(t) = \begin{pmatrix} r + \omega_o \sin^2 \frac{\vartheta}{2} & \omega_o \sin \frac{\vartheta}{2} \cos \frac{\vartheta}{2} e^{-i\omega_o t} \\ \omega_o \sin \frac{\vartheta}{2} \cos \frac{\vartheta}{2} e^{i\omega_o t} & -r - \omega_o \cos^2 \frac{\vartheta}{2} \end{pmatrix}. \quad (2.48)$$

The propagator $\hat{U}(t)$ is simply defined as the operator that provides us with

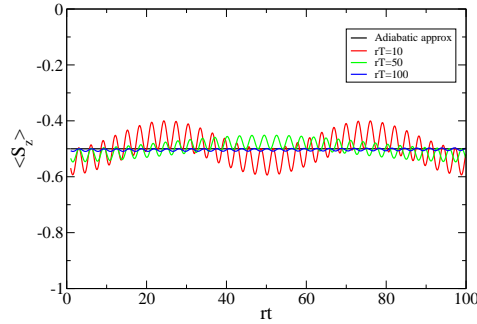


Figure 2.3: Average value of the spin projection along the z axis using the adiabatic propagator (black curve) and the exact propagator for different values of the product rT . When rT is very large the average value $\langle \tilde{S}_z \rangle$ is very close to the one calculated in the adiabatic approximation

a state at time t , upon acting on a state at $t = 0$:

$$\hat{U}(t)|\Psi(t=0)\rangle = |\Psi(t)\rangle.$$

The calculation of the full propagator is performed in appendix 2D, and the result is

$$U(t) = \begin{pmatrix} (\cos(\epsilon t) - i\gamma \sin(\epsilon t))e^{i\alpha t} & -i\beta \sin(\epsilon t)e^{i\alpha t} \\ -i\beta \sin(\epsilon t)e^{-i\alpha t} & (\cos(\epsilon t) + i\gamma \sin(\epsilon t))e^{-i\alpha t} \end{pmatrix}. \quad (2.49)$$

Where the coefficients α , β , γ are defined in appendix 2D. It is easily verified that in the adiabatic limit, ($T \rightarrow \infty$), $U(t) \rightarrow U_A(t)$. That is, the larger is the product rT , the better is the approximation of substituting \hat{U} with \hat{U}_A . It can be checked in plot 2.3 where it shows the average value of the spin projection along the z $\langle \tilde{S}_z \rangle$ calculated both using the adiabatic and the exact propagators.

2.3.3 Calculation of the Berry phase

By definition, the differential Berry phase for the system lying within either state $|\pm, t\rangle$ is given by:

$$\frac{d\Gamma_{\pm}}{dt}(t) = i\dot{\vec{\lambda}} \cdot \langle \pm, t | \frac{\partial}{\partial \vec{\lambda}} | \pm, t \rangle, \quad (2.50)$$

where $\vec{\lambda}$ is the set of parameters of the system. For the particular case we have in mind, since we are using polar coordinates in parameter space. Therefore, we have:

$$\vec{\lambda} = (r, \vartheta, \varphi),$$

and, along the particular path we have chosen, we obtain:

$$\frac{d\vec{\lambda}}{dt} = (0, 0, \frac{2\pi}{T}), \quad (2.51)$$

and easily

$$\frac{d\Gamma_{+}}{dt}(t) = -\frac{2\pi}{T} \sin^2(\vartheta/2), \quad (2.52)$$

and

$$\frac{d\Gamma_{-}}{dt}(t) = \frac{2\pi}{T} \sin^2(\vartheta/2). \quad (2.53)$$

Therefore we get, for instance:

$$\Gamma_{\pm}(t) = \mp \frac{2\pi t}{T} \sin^2(\vartheta/2). \quad (2.54)$$

Obviously by integrating this phase over one period we obtain that the Berry phase is

$$\Gamma_{\pm}(T) = \mp 2\pi \sin^2 \vartheta/2, \quad (2.55)$$

and easily if the circuit in the parameter space enclose no surface (i.e. $\vartheta = 0$) the Berry phase is absent.

2.4 Detection of the Berry phase: a possible transport experiment

In this section we describe a possible transport experiment which can allow to detect the Berry phase accumulated by the wave function of the electrons traveling through a quantum ring. The choice of a ring simplifies the calculations, with respect to the dot case, and the results obtained give us a very clear physical picture.

In order to study the transport through the ring we have to apply two contacts to it. The simplified geometry that we are going to study is sketched in Fig. 2.4. We assume that the contacts are located symmetrically with respect to the center: this assumption simplifies our calculations but does not alter qualitatively the generality of our results.

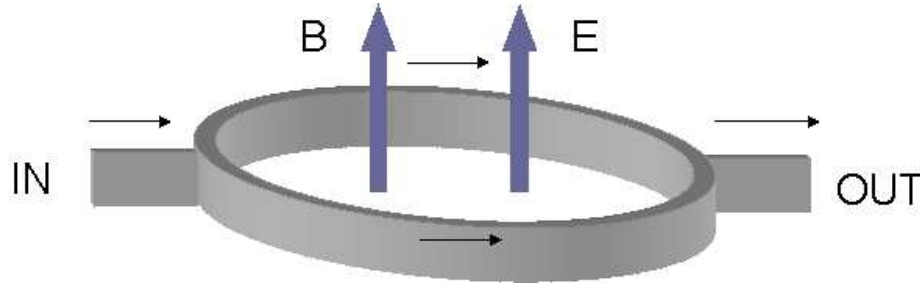


Figure 2.4: Sketch of a possible transport experiment across a quantum ring

The conductance in the framework of a Landauer-Buttiker like approach [22,23], is proportional to the probability T that one electron traveling into the dot from the left contact, jumps out from the dot through the right contact, no matter how long it stays into the ring:

$$G = \frac{e^2}{\hbar} \sum_{\sigma, \sigma'} T_{\sigma, \sigma'}, \quad (2.56)$$

where σ is the spin of the incoming electron and σ' the spin of the outgoing one. The transmission probability T , for an electron injected with energy E_{in} , is a function of the transmission amplitude:

$$A(\varphi_f, \mu_f; \varphi_0, \mu_0 | E_{in}) = \int_0^\infty e^{i \frac{E_{in} t_f}{\hbar}} \langle \vec{r}_f \mu_f t_f | \vec{r}_0 \mu_0 0 \rangle dt_f. \quad (2.57)$$

Here we have considered a particle injected at the point \vec{r}_o with a spin μ_o at the time t_o which exits from the point \vec{r}_f with the spin μ_f at the time t_f . The transmission probability is calculated by mean of an exact description for the electrons in the ring [24]. In order to do that, we calculate the exact quantum mechanical propagator for a spinful electron in a closed ring by

means of a Feynman path integral approach. This is not enough, however, when a source and drain contacts are attached to the ring. We shall discuss the results in a saddle point approximation what amounts to consider the orbital motion of the particle as semiclassical. As the contacts are not 'ideal' they will offer a finite barrier for the incoming electrons. Each contact will be considered as perfectly equal the other. In our semiclassical framework an electron moving across the ring 'sees' a certain reflection amplitude r and transmission amplitude t or, in other words, it will be back reflected with a probability r^2 and it will be transmitted with a probability t^2 .

2.4.1 Model Hamiltonian for the electron on the ring

The electrons in the ring are considered to move on a strictly one dimensional trajectory. The neglect of the actual finite transverse dimension of the arms of the ring can be performed, to a good level of accuracy, because the mixing between lateral sub bands alter only quantitatively and not qualitatively the conductance of this devices as shown in Ref. [25].

We write down the Hamiltonian for the electrons in the ring: we want to describe a low electron rate transport experiment, so we can neglect, from now on, the electron correlations within the ring and consider a single electron injected in the ring at the Fermi energy. The Hamiltonian thus reads:

$$H = \frac{1}{2m} \left(\vec{p} + \frac{e}{c} \vec{A} \right)^2 - \frac{1}{2} \hbar \omega_c \sigma_Z + \hat{H}_{so}, \quad (2.58)$$

$$H_{so} = \frac{\alpha}{\hbar} \left(\hat{z} \times \left(\vec{p} + \frac{e}{c} \vec{A} \right) \right) \cdot \vec{\sigma},$$

where α is the spin orbit coupling constant inclusive of the effect of an external electric field orthogonal to the ring plane; as introduced in chapter 1, ω_c is the cyclotron frequency and $\vec{\sigma}$ is the vector of the Pauli matrices. In the symmetric gauge, by using cylindrical coordinates the vector potential $\vec{A} = \frac{\phi}{2\pi R} \hat{\varphi}$ (where ϕ is the flux through the ring, R is its radius, and φ a the orbital coordinate on the ring). So the Hamiltonian takes the form:

$$H = \frac{\hbar^2}{2mR^2} \left(\hat{l} + \frac{\phi}{\phi_0} \right)^2 + \frac{1}{2} \hbar \omega_c \sigma_Z + H_{so}.$$

As usual $\hat{l} = -i \frac{\partial}{\partial \varphi}$, and $\phi_0 = \frac{hc}{e}$ is the flux quantum. Again we can define:

$$\vec{\Pi} = \frac{\hbar}{R} \left(\hat{l} + \frac{\phi}{\phi_0} \right).$$

Moreover H_{so} can be rewritten as:

$$H_{so} = \alpha [\Pi_x \sigma_y - \sigma_x \Pi_y] = -\alpha \begin{pmatrix} 0 & \Pi_y + i\Pi_x \\ \Pi_y - i\Pi_x & 0 \end{pmatrix},$$

so by applying straightforward transformations and by symmetrizing the operators (in order to assure the hermiticity of the Hamiltonian), the spin orbit contribution can be written as

$$H_{so} = -\frac{\alpha}{2R} \left[\left(e^{-i\varphi} \left(\hat{l} + \frac{\phi}{\phi_0} \right) + \left(\hat{l} + \frac{\phi}{\phi_0} \right) e^{-i\varphi} \right) \sigma_{++} + \left(e^{i\varphi} \left(\hat{l} + \frac{\phi}{\phi_0} \right) + \left(\hat{l} + \frac{\phi}{\phi_0} \right) e^{i\varphi} \right) \sigma_{--} \right], \quad (2.59)$$

where we have introduced the usual operators $\sigma_{\pm} = (\sigma_x \pm i\sigma_y)/2$.

2.4.2 Topology of the ring

The topology of our problem is non trivial: the electrons moving into a ring see a multiply connected space $\mathbf{Q} = \mathbf{R}^2 - C$ where C is the ring center. The usual evolution operator, defined as the integral kernel $\mathcal{K}(\vec{r}, \vec{r}', t)$ (in this subsection we shall neglect spin indexes) such that

$$\psi(\vec{r}, t) = \int d\vec{r}' \mathcal{K}(\vec{r}, \vec{r}', t) \psi(\vec{r}', 0), \quad (2.60)$$

onto our space acquires the form [26]:

$$\mathcal{K}(\vec{r}, \vec{r}', t) = \sum_{n=-\infty}^{+\infty} \mathcal{K}_n(\vec{r}, \vec{r}', t), \quad (2.61)$$

where n represents the n -th homotopy class (or in another language n is the winding number) labeling for $n > (< 0)$ electrons traveling anticlockwise (clockwise), in the dot. The path integral will be calculated onto a covering space (\mathbf{U}, π) , which allow to avoid the complications due to the multiple connection. \mathbf{U} is the *log* Riemann surface and π the projection of \mathbf{U} onto \mathbf{Q} , defined as follows:

$$\mathbf{U} \ni \tilde{\mathbf{r}} = (r, \theta) \quad R < r < +\infty; \quad -\infty < \theta < +\infty.$$

And the application π is defined as:

$$\begin{aligned} \pi : \mathbf{U} &\rightarrow \mathbf{Q}; & (r, \theta) &\rightarrow (r, \theta - 2n\pi), \\ & & 0 \leq \theta - 2n\pi &\leq 2\pi \quad n \in \mathbb{Z}. \end{aligned}$$

The difference between \mathbf{Q} and its covering \mathbf{U} is in the definition of the θ angle: in the n^{th} sheet of the Riemann surface $\theta \rightarrow \theta + 2\pi n$.

On such Riemann surface the problem appears simplified because paths that in \mathbf{Q} belong to different homotopy classes are now, in \mathbf{U} , different paths. Indeed they have the same starting point but different finishing points that lie on different sheets of the new space. So the kernel now read:

$$\theta \rightarrow \theta + 2\pi \Rightarrow \mathcal{K}_n \rightarrow \mathcal{K}_{n+1},$$

and the calculations of the n^{th} kernel \mathcal{K}_n is performed onto the space with trivial connection \mathbf{U} .

2.4.3 Path-integral of a spinful particle on the ring

The transition amplitude of a particle that comes into the ring in the point r_o with a spin μ_o at the time t_o and exit from the point r_f with the spin μ_f at the time t_f is expressed as:

$$\langle \vec{r}_f \mu_f t_f | \vec{r}_o \mu_o t_o \rangle, \quad (2.62)$$

where we use the notation $|\vec{r} \mu\rangle = |\vec{r}\rangle \otimes |\mu\rangle$. Eq. 2.62 has to be intended as:

$$\langle \vec{r}_f \mu_f t_f | \vec{r}_o \mu_o 0 \rangle = \langle \vec{r}_f \mu_f | U(t_f, 0) | \vec{r}_o \mu_o \rangle, \quad (2.63)$$

where, for simplicity, we have posed $t_o = 0$.

Because we consider a strictly one dimensional ring, no dependence on the radius enters the Hamiltonian, so we can write the previous amplitude only in terms of angular coordinates on the ring:

$$\langle \varphi_f \mu_f t_f | \varphi_o \mu_o 0 \rangle = \langle \varphi_f \mu_f | e^{-iHt_f} | \varphi_o \mu_o \rangle. \quad (2.64)$$

The full path integral procedure is reported in appendix 2E for electrons belonging to a well defined homotopy class n (that is $\varphi_n - \varphi_0 = \pi(2n - 1)$). The transition amplitude is:

$$\langle \varphi_f \mu_f t_f | \varphi_o \mu_o 0 \rangle \equiv e^{it_f \frac{\alpha^2 m}{2}} \int_{\varphi_o}^{\varphi_f} \mathcal{D}[\varphi(t)] e^{i \int_0^{t_f} \left(\frac{m}{2} R^2 \dot{\varphi}^2(t) - \frac{\phi}{\phi_0} \dot{\varphi}(t) \right)} \langle \mu_f | \hat{T} e^{i \int_0^{t_f} C[\varphi(t)]} | \mu_o \rangle, \quad (2.65)$$

where \hat{T} indicates the chronologically ordered product and $\hat{C}[\varphi(t)]$ is the matrix:

$$\hat{C}[\varphi(t)] = \left[-\frac{1}{2} \hbar \omega_c \sigma_z + e^{-i\varphi(t)} \alpha \sigma_+ \left(\dot{\varphi}(t) R m + \frac{1}{2R} \right) + e^{i\varphi(t)} \alpha \sigma_- \left(\dot{\varphi}(t) R m - \frac{1}{2R} \right) \right]. \quad (2.66)$$

The first phase factor in Eq. (2.65) originates from the Rashba coupling, the second one is the usual kinetic energy and the third one, after the integration, will provide the Ahronov-Bohm phase. The quantum evolution of the spin is calculated, in the following, for a particular saddle point field $\varphi_{cl}(t)$ evaluated in the next subsection. The spin propagator appearing as a last piece in Eq.2.65 will provide an additional geometrical phase. The full evolution kernel, from Eq.2.61, is

$$\sum_n e^{it_f \frac{\alpha^2 m}{2}} \int_n \mathcal{D}[\varphi(t)] e^{i \int_0^{t_f} \left(\frac{m}{2} R^2 \dot{\varphi}^2(t) - \frac{\phi}{\phi_0} \dot{\varphi}(t) \right)} \langle \mu_f | \hat{T} e^{i \int_0^{t_f} C[\varphi(t)]} | \mu_o \rangle, \quad (2.67)$$

where n labels the different homotopy classes.

2.4.4 Saddle point approximation

As outlined before, the transition amplitude for electrons injected in the ring at the energy E_{in} is:

$$A(\varphi_f, \mu_f; \varphi_0, \mu_0 | E_{in}) = \int_0^\infty e^{i\frac{E_{in}t_f}{\hbar}} \langle r_f \mu_f t_f | r_0 \mu_0 0 \rangle dt_f. \quad (2.68)$$

The matrix element $\langle r_f \mu_f t_f | r_0 \mu_0 0 \rangle$ can be evaluated in the saddle point approximation. This approximation allow us to find the path which gives the main contribution to Eq.2.65. As in classical mechanics, the saddle point path satisfies the classical Lagrange equation:

$$\frac{\partial \mathcal{L}}{\partial \varphi} - \frac{d}{dt} \frac{\partial \mathcal{L}}{\partial \dot{\varphi}} = 0. \quad (2.69)$$

Where the whole Lagrangian from Eq.2.65 has to be intended as:

$$\begin{aligned} \mathcal{L}(\dot{\varphi}) = & \frac{m}{2} R^2 \dot{\varphi}^2 - \frac{\Phi}{\Phi_0} \dot{\varphi} - \frac{1}{2} \omega_c \sigma_Z + e^{-i\varphi} \sigma_+ (\dot{\varphi} R \alpha m + \frac{\alpha}{2R}) + \\ & + e^{-i\varphi} \sigma_+ (\dot{\varphi} R \alpha E m - \frac{\alpha}{2R}). \end{aligned}$$

By simply substituting in Eq.2.69 we have:

$$m r^2 \ddot{\varphi} + i \frac{\alpha}{2R} (e^{-i\varphi} \sigma_+ + e^{i\varphi} \sigma_-) = 0. \quad (2.70)$$

It appears that $\prod_{i=1}^N e^{\frac{\epsilon}{\hbar} \hat{C}_i}$ contributes to the equation of motion (2.70) only up to $\frac{\alpha}{2R}$ (momentum quantum fluctuation). If we suppose that R is the radius of a mesoscopic structure, these terms can be neglected. So the equation of motion oversimplifies and reads:

$$m R^2 \ddot{\varphi} = 0 \Rightarrow \dot{\varphi}_{cl} = cost = \frac{\varphi_f - \varphi_0}{t_f} = \frac{\pi(2n-1)}{t_f}, \quad (2.71)$$

where $\varphi(0) = \varphi_0$ and $\varphi(t_f) = \varphi_f$, and the pedix cl reads for 'classical'. So the transition amplitude, in the saddle point approximation, is:

$$\begin{aligned} \langle \varphi_f \mu_f t_f | \varphi_0 \mu_0 0 \rangle_{cl} \simeq & \lim_{N \rightarrow +\infty} \left(\sqrt{\frac{m R^2}{2\pi\epsilon}} \right)^N e^{-i\frac{\phi}{\Phi_0}(\varphi_f - \varphi_0)} e^{it_f \frac{\alpha^2 m}{2}} \times \\ & \langle \mu_f | \hat{U}_{cl}(t_f, 0) | \mu_0 \rangle \int d\varphi_1 \dots d\varphi_{N-1} e^{\epsilon \sum_{i=1}^N \frac{m}{2} R^2 \dot{\varphi}_i^2}, \end{aligned}$$

where

$$\hat{U}_{cl}(t_f, 0) = \prod_{i=1}^N e^{\frac{\epsilon}{\hbar} \hat{C}_i^{cl}}, \quad (2.72)$$

is the spin evolution operator evaluated along the classical path.

The term $e^{-i\frac{\phi}{\phi_0}(\varphi_f - \varphi_0)}$ is the so-called Ahronov-Bohm phase. The Rashba term does not give any additional Ahronov-Bohm phase because the effective magnetic field it originates lies in the plane. As a last step we have to evaluate the expression:

$$\begin{aligned} \lim_{N \rightarrow +\infty} \left(\sqrt{\frac{mR^2}{2\pi\epsilon}} \right)^N \int d\varphi_1 \dots d\varphi_{N-1} e^{\frac{1}{\hbar} \sum_{i=1}^N \frac{m}{2} R^2 \dot{\varphi}_{i-1}^2} = \\ = \sqrt{\frac{m}{2i\pi\hbar t_f}} e^{i\frac{mR^2}{2t_f}(\varphi_f - \varphi_0)^2}. \end{aligned}$$

In conclusion the transition amplitude, in the saddle point approximation, is:

$$\begin{aligned} \langle \varphi_f \mu_f t_f | \varphi_0 \mu_0 0 \rangle_{cl} \simeq \sqrt{\frac{m}{2i\pi t_f}} e^{i\frac{mR^2}{2t_f}(\varphi_f - \varphi_0)^2} e^{-i\frac{\phi}{\phi_0}(\varphi_f - \varphi_0)} e^{i t_f \frac{\alpha^2 m}{2}} \times \\ \langle \mu_f | \hat{U}_{cl}(t_f, 0) | \mu_0 \rangle. \quad (2.73) \end{aligned}$$

Moreover the contacts are located at an angular distance of π and the solution obtained is valid for a path belonging to a certain homotopy class n where $\varphi_f - \varphi_0 = \pi(2n - 1) = \varphi_n$.

Eq. (2.73) is the transition amplitude for an electron which travels through the dot in a time t_f , it is not properly what we need in order to calculate the transmission probability which, of course, does not depend on time, but expresses the probability that an incoming particle jumps out from the ring, no matter how long it does stay onto it.

So we can fix the winding number n and the injection energy, and integrate over all the possible final times up to a very long time $t_f = \infty$. Obviously not all the values of the injection energy are allowed but only discrete values will be available corresponding to the eigenstates of the single particle Hamiltonian on the ring as pointed out in [25]. Finally, the transmission probability amplitude can be expressed as:

$$\begin{aligned} A(\varphi_f, \mu_f; \varphi_0, \mu_0 | E_{in}) = \int_0^\infty e^{i\frac{E_{in} t_f}{\hbar}} \sqrt{\frac{m}{2i\pi t_f}} e^{i\frac{mR^2}{2t_f}(\varphi_f - \varphi_0)^2} e^{-i\frac{\phi}{\phi_0}(\varphi_f - \varphi_0)} \times \\ e^{i t_f \frac{\alpha^2 m}{2}} \langle \mu_f | \hat{U}_{cl}(t_f, 0) | \mu_0 \rangle dt_f \quad (2.74) \end{aligned}$$

For each n there will be a particular traveling time which will give a greater contribution to the total amplitude. This allow us to perform a stationary phase approximation. To impose the stationary phase condition on Eq.2.73 we should solve:

$$\frac{d}{dt_f} \left[\left(\frac{\alpha^2 m}{2\hbar^3} + E_{in} t_f \right) + \frac{mR^2}{2\hbar t_f} \pi^2 (2n - 1)^2 \right] = 0,$$

where we have made use of Eq. (2.4.4). Easily (omitting the pedix f and replacing it with the label n):

$$t_n = \frac{\pi(2n-1)\tau_0}{\sqrt{\frac{(k_{so}R)^2}{4} + \tilde{E}_{in}}}, \quad (2.75)$$

where we have introduced the time scale $\tau_0 = mR^2/\hbar$, the momentum $k_{so} = 2m\alpha/\hbar^2$ and the dimensionless injection energy $\tilde{E}_{in} = E_{in}/(\hbar^2/(mR^2))$. Now it clearly emerges that, for each homotopy class, there is a particular time t_n which mostly contributes to the transmission.

This time increases with n . So we can substitute this time into the equation (2.73) and sum over all the possible homotopy classes n from $-\infty$ to $+\infty$. Now the reader could argue that negative n should also mean negative time: nevertheless in the framework of our calculation the time is only an indication of the traveling direction and positive and negative n has only to be intended as anticlockwise or clockwise rotation directions in the ring.

We then obtain the total transition amplitude between (φ_0, μ_0) e (φ_f, μ_f) ,

$$A(\mu_f; \mu_0 | E_{in}) = \sum_{n=-\infty}^{\infty} \sqrt{\frac{m}{2i\pi t_n}} e^{i\frac{E_{in}t_n}{\hbar}} e^{i\frac{mR^2}{2t_n}(\pi(2n-1))^2} e^{-i\frac{\phi}{\phi_0}(\pi(2n-1))} \quad (2.76)$$

$$e^{i t_n \frac{\alpha^2 m}{2}} \times \langle \mu_f | \hat{U}_{cl}(t_n, 0) | \mu_0 \rangle,$$

we have omitted the injection and ejection angle which have been fixed to be 0 and $(2n-1)\pi$ for each winding number n .

This semiclassical approach allows us to estimate the angular velocity of the electrons rounding n times in the ring:

$$\dot{\varphi}^{cl} = \frac{\varphi_f - \varphi_0}{t_f} = \frac{\varphi_n}{t_n} = \frac{\sqrt{\frac{(k_{so}R)^2}{4} + \tilde{E}_{in}}}{\tau_0}. \quad (2.77)$$

This clearly states that the velocity is constant independent of n ; the period of evolution in the ring:

$$T^{cl} = \frac{2\pi}{\dot{\varphi}^{cl}} = \frac{2\pi\tau_0}{\sqrt{\frac{(k_{so}R)^2}{4} + \tilde{E}_{in}}}. \quad (2.78)$$

Taking into account Eq.(2.75), the characteristic time can be also expressed in terms of the evolution period T :

$$t_n = T^{cl} \left(\frac{2n-1}{2} \right).$$

Eq.2.77 can be also improved by introducing the scattering center at the contacts (introduced the previous subsection) with semiclassical reflection amplitude r and transmission amplitude t such that:

$$A(\mu_f; \mu_0 | E_{in}) = t^4 \sum_{n \neq 0, n = -\infty}^{\infty} (r^2)^{2|n|-1} \sqrt{\frac{m}{2i\pi t_n}} e^{\frac{iE_{in}t_n}{\hbar}} e^{i\frac{mR^2}{2t_n}(\pi(2n-1))^2} \times e^{-i\frac{\phi}{\phi_0}(\pi(2n-1))} e^{it_n \frac{\alpha^2 m}{2}} \langle \mu_f | \hat{U}_{cl}(t_n, 0) | \mu_0 \rangle. \quad (2.79)$$

Now easily $T_{\mu_0, \mu_f} = |A(\mu_f; \mu_0)|^2$. Using a semiclassical picture, one can imagine that each electron can jump out of the ring in infinitely different ways, that is after $1/2$ round trip, after $3/2$ round trips, after $5/2$, and so on. Each of this different paths is associated to a characteristic weights and 'times'. It is worth noting that the prefactor $\sqrt{\frac{m}{2i\pi t_n}}$ is proportional to $\sqrt{1/(2n-1)\pi}$: this means that paths with high winding numbers, corresponding to electrons which experience multiple reflections into the ring, gives a vanishing contribution to the transition amplitude and, as a consequence, to the conductance. Therefore we expect the main contribution to the conductance to be given by electrons performing a low number of round trips in the ring.

The last step to calculate the transmission probability is the evaluation of the spin dynamics

$$\langle \mu_f | \hat{U}_{cl}(t_n, 0) | \mu_0 \rangle = \langle \mu_f | e^{-\frac{i}{\hbar} \int_0^{t_n} \hat{C}^{cl} dt} | \mu_0 \rangle, \quad (2.80)$$

where, from Eq.(2.122):

$$\hat{C}^{cl} = \left[-\frac{1}{2} \hbar \omega_c \sigma_z + e^{-i\varphi^{cl}} \sigma_+ \left(\dot{\varphi}^{cl} R \frac{\alpha E}{\hbar} m + \frac{\alpha E}{2R} \right) + e^{i\varphi^{cl}} \sigma_- \left(\dot{\varphi}^{cl} R \frac{\alpha E}{\hbar} m - \frac{\alpha E}{2R} \right) \right]. \quad (2.81)$$

Here R is the radius of a mesoscopic ring $\sim 50 \div 100nm$ this allow us to neglect the term $\frac{\alpha E}{R}$ and consider only $\dot{\varphi}^{cl} R \frac{\alpha E}{\hbar} m$. So, once again the spin evolution seems to be regulated by the simple 2 by 2 Hamiltonian of Eq.2.36

$$\hat{H}_S = \vec{b} \cdot \vec{S},$$

by simply using the following correspondences:

$$b \cos \theta \rightarrow -\frac{1}{2} \hbar \omega_c, \quad b \sin \theta \rightarrow \dot{\varphi}^{cl} R \frac{\alpha E}{\hbar} m.$$

In other words our semiclassical picture allow us to describe 'classically' the orbital dynamics and the spin dynamics in a fully quantum mechanical way. Interestingly, here, the real external fields are time independent but, because of the periodic motion of the electrons in the ring, they 'see' effective time dependent external fields which allow us to treat with the spin dynamics as

in the usual Berry Hamiltonian. The solution of the spin dynamics is the same as reported into the previous section (for details see also the appendix D) and eventually shows a geometrical phase due to the non trivial topology of the parameter space.

So the transmission amplitude of Eq.2.80 can be obtained both in the adiabatic approximation and in an exact form by using all the results of appendix 2D and giving the appropriate meaning to all the symbols.

At this point we are able to evaluate the conductance and Eq.2.56 can be rewritten as

$$G = \frac{e^2}{h} \left[|A(\uparrow; \uparrow)|^2 + |A(\uparrow; \downarrow)|^2 + |A(\downarrow; \downarrow)|^2 + |A(\downarrow; \uparrow)|^2 \right] \quad (2.82)$$

where the evaluation of the single transmission amplitudes of 2.79 have been calculated by numerically evaluating the summation over the winding numbers of Eq.2.79 .

2.4.5 Conductance oscillations

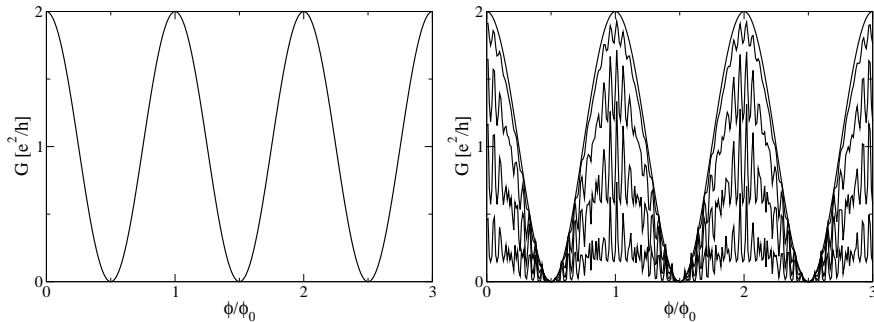


Figure 2.5: Conductance vs ϕ/ϕ_0 for (left panel) ideal coupling with the contacts $r = 0$ and (right panel) more realistic contacts $r \neq 0$ for different values of the reflection amplitude at the contacts

The results showed in figures 2.5, 2.6 are in agreement with the other semiclassical analytical [25] and numerical [27] theoretical predictions. Moreover our improved path integral approach allow us to include also the quantum fluctuations which mainly contributes in the case of non ideal contacts, that is, with reflection amplitudes different from zero.

In fig 2.5[left panel] the dimensionless conductance is plotted vs ϕ/ϕ_0 in the absence of the Rashba coupling and with ideal contacts. The conductance shows the well known Ahronov-Bohm oscillations [28]. In Fig. 2.6[right panel] we represent again the dimensionless conductance vs ϕ/ϕ_0 but for different values of the reflection amplitude r at the contacts. We suppose that the two contacts are perfectly equal each other and the incoming electrons can be back-reflected with a probability r^2 and transmitted

with a probability $t^2 = 1 - r^2$. For $r = 0$, upper curve, we reproduce the perfect coupling conditions and we can observe the same behavior as in Fig. 2.5[left panel]. Moreover, by increasing the reflection amplitude, the electrons with higher order winding numbers ($n > 1$) generate higher harmonics oscillations.

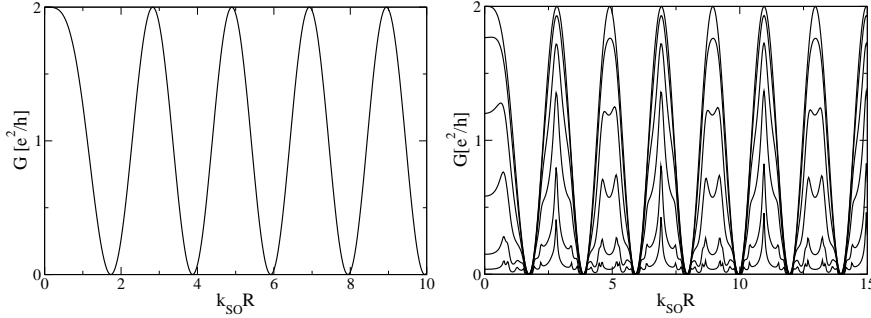


Figure 2.6: Conductance vs $k_{SO}R$ for (left panel) ideal coupling with the contacts $r = 0$ and (right panel) more realistic contacts $r \neq 0$ for different values of the reflection amplitude at the contacts

In fig 2.6[left panel] the dimensionless conductance is plotted vs the parameter $k_{SO}R$ in the absence of the orthogonal magnetic field and with ideal contacts. The conductance shows some quasi-periodic oscillations and, remarkably, reproduces the zeros at $k_{SO}R = \sqrt{3}, \sqrt{15}, \sqrt{35}, \dots$ predicted by other authors [25, 27].

In Fig. 2.6[right panel] we represent again the dimensionless conductance vs $k_{SO}R$ but for different values of the reflection amplitude r at the contacts. Once again, for $r = 0$, upper curve, we reproduce the perfect coupling conditions and again we can observe the same behavior as in Fig. 2.6[left panel]. By increasing the reflection amplitude, the electrons with higher order winding numbers ($n > 1$) makes further interference effect thus generating oscillations at higher harmonics in the conductance. As expected, by increasing r also the oscillations amplitude decrease and there is no conductance at all in the case of a totally reflecting barrier with $r = 1$. Nevertheless the superimposed oscillations at $r \neq 0$ does not appear to be perfectly periodic as in the case of Fig. 2.5: in this case a variable number of secondary peaks appear in correspondence to different values of the SO coupling. This is due to beating effects between the SO phases and a geometric Ahronov-Anandan [15] phase which comes from the spin evolution operator. In the non adiabatic regime, that is, at low magnetic fields, some unexpected phenomena can emerge. In particular in Figs 2.7 and 2.8 we can see the conductance for a single incoming spin channel \uparrow for two different values of the SO coupling: $k_{SO}R = 2$ and $k_{SO}R = 6$ respectively. Once the spin orientation of the incoming electron is fixed to be \uparrow , two conductance channels can be studied that are $G^{\uparrow, \uparrow}$ and $G^{\uparrow, \downarrow}$ for outgoing electrons

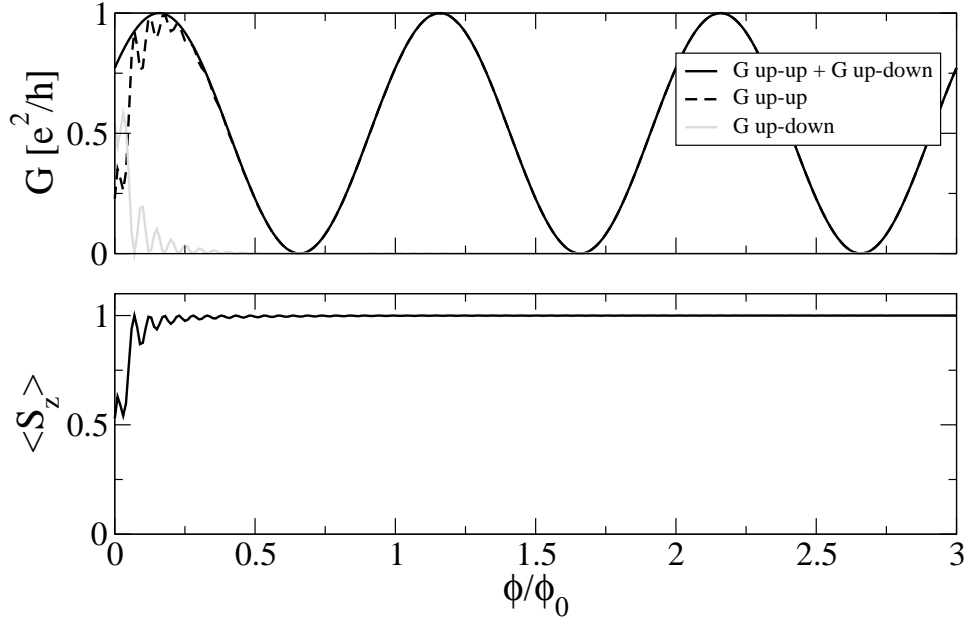


Figure 2.7: Conductance vs ϕ/ϕ_0 for ideal coupling with the contacts $r = 0$ and corresponding average value of the outgoing spin $\langle S_z \rangle$.

with spin up and down respectively. A clear correspondence between these two conductance channels and the average value of the spin of the outgoing electron emerges. Interestingly, in correspondence to minima of the $G^{\uparrow,\uparrow}$ there are maxima of $G^{\uparrow,\downarrow}$ and the spin projection along the z axis for the outgoing electrons reaches its minimum. For weak spin orbit coupling this is a clear indication of the Rashba spin precession but does not allow for spin flippings (Fig. 2.7). If we increase the SO coupling, the flipping of the outgoing spins is possible as depicted in figure 2.8. Moreover in both cases by increasing the magnetic field (in other words we are restoring the adiabaticity) orthogonal to the ring plane both the simple precession and the spin flip phenomena tends to disappear because the spins are forced to be aligned in the direction of the magnetic field.

2.5 Discussion

In mesoscopic quantum structures it is possible to drive the system through an adiabatic sequence of unitary transformations which does not alter the energetical ordering of the eigenstates of the Hamiltonian but affects their phase. This way of controlling such devices is very interesting because can allow for reading the coherence of the quantum states of a mesoscopic device by simply looking at its quantum mechanical phase, for instance, in the framework of transport experiment.

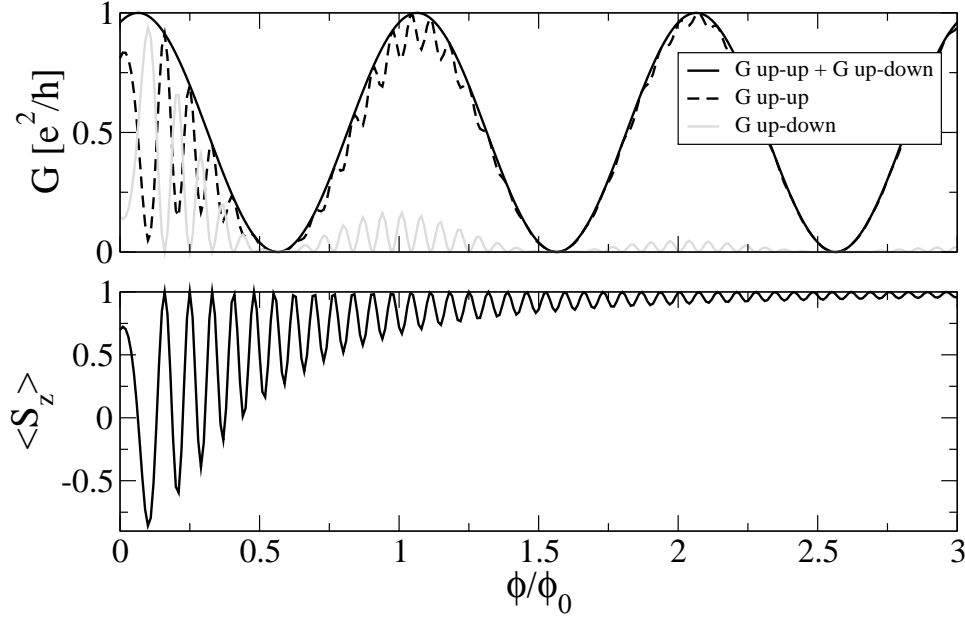


Figure 2.8: Conductance vs ϕ/ϕ_0 for ideal coupling with the contacts $r = 0$ and corresponding average value of the outgoing spin $\langle S_z \rangle$.

In this chapter we have first dealt with the case of a two electron quantum dot close to the single triplet crossing. The case under examination seems to be very interesting because it fulfill in a wonderful way all the requirements needed to obtain a topological Berry phase. In the presence of a Rashba spin orbit coupling a gap develops between the two states involved in the crossing which, thus, becomes an anti-crossing. If the electric field is cyclically modulated in time it can periodically tune the gap and drive the dot in such a way that the many body wave function of the electrons can acquire a topological phase. In fact the level splitting, close to the singlet triplet transition, can be finely tuned in order that its product times the period of the quantum evolution satisfies the adiabaticity condition. By introducing an effective low energy Hamiltonian [21] we show that the project outlined before can be actually realized into a parabolically confined two electron quantum dot in the presence of a magnetic field orthogonal to the dot plane and of an additional electric field that can allow for the modulation of the Rashba coupling.

Provided that a quantum topological phase can be induced onto the wave function of the dot, the second point faced into this chapter concerns with the possibility to observe this phase.

Our main idea is that evidences of such a geometrical phase can be found by studying the conductance oscillations of a mesoscopic quantum ring. The ring geometry allows us to simplify the calculation of the conduc-

tance through with respect to the case of the dot.

In the framework of a ballistic Landauer Buttiker approach we perform a path integral calculation which allows us to calculate the conductance of the dot. The geometrical phase, now, emerges from the quantum mechanics of the spins, which moving into the ring, experience time dependent effective fields although the real fields are fixed. This is a nice way to induce a topological phase and allow us to explore both adiabatic and non adiabatic regimes by choosing the strength of the external fields.

In the non adiabatic regime again a topological phase arise [15], which gives back the Berry phase [6] only in the adiabatic limit.

Moreover in the non adiabatic regime some interesting spin flip phenomena have been studied that should be measured experimentally giving an estimation of the nonadiabaticity of the quantum evolution.

Appendix 2A

Some properties of the operators **S** and **T**

Using

$$[S_i^\alpha, S_j^\beta] = \delta_{ij} \sum_{\gamma} \epsilon_{\alpha\beta\gamma} S_i^\gamma,$$

it is possible to proof the following commutation relations between the operators $\vec{S}_{\pm} = \vec{S}_1 \pm \vec{S}_2$ and $\vec{T} = \vec{S}_1 \times \vec{S}_2$.

$$(\vec{S} \cdot \vec{T}) - (\vec{T} \cdot \vec{S}) = 4i (\vec{S}_1 \cdot \vec{S}_2), \quad (2.83)$$

$$[\vec{S}_-, (\vec{S}_1 \cdot \vec{S}_2)] = -2i\vec{T}, \quad (2.84)$$

$$[\vec{T}, (\vec{S}_1 \cdot \vec{S}_2)] = \frac{i}{2}\vec{S}_-. \quad (2.85)$$

These relations allow to relate \vec{S}_- and \vec{T} by mean of the unitary transformation:

$$2\vec{T} = e^{-i(\pi/2)(\vec{S}_1 \cdot \vec{S}_2)} \vec{S}_- e^{i(\pi/2)(\vec{S}_1 \cdot \vec{S}_2)}, \quad (2.86)$$

since $(\vec{S}_1 \cdot \vec{S}_2)$ commutes with \vec{S}_+ application of this transformation to the identity

$$[S_{\pm}^\alpha, S_{\mp}^\beta] = i \sum_{\gamma} \epsilon_{\alpha\beta\gamma} S_{\mp}^\gamma, \quad (2.87)$$

leads to the equations

$$[S_+^\alpha, T^\beta] = i \sum_{\gamma} \epsilon_{\alpha\beta\gamma} T^\gamma, \quad [T^\alpha, T^\beta] = \frac{i}{4} \sum_{\gamma} \epsilon_{\alpha\beta\gamma} S_+^\gamma. \quad (2.88)$$

Appendix 2B

Mapping of the low energy effective Hamiltonian onto the two spin 1/2 model

In order to properly map the dot Hamiltonian onto the two spin basis we have to project the operators from the original Hartree Fock $4-d$ basis of Eq 2.20 to the $4-d$ two spin S_1, S_2 basis of Eq.2.24. Defining $\mathcal{P} = \sum_{S,S^z} |S, S^z\rangle \langle S, S^z|$ as the projector on the original basis 2.20, the following correspondences arise 2.26:

$$\mathcal{P} \sum_s d_{ns}^\dagger d_{n's} \mathcal{P} \Rightarrow n \delta_{n,n'} \left[\vec{S}_1 \cdot \vec{S}_2 - \frac{1}{4} + n \right], \quad (2.89)$$

$$\mathcal{P} \sum_{ss'} d_{ns}^\dagger \frac{1}{2} \vec{\sigma}_{ss'} d_{n's'} \mathcal{P} \Rightarrow \frac{1}{2} \delta_{n,n'} \vec{S}_+ + \delta_{n,-n'} \frac{1}{2\sqrt{2}} \left[\vec{S}_- + 2in\vec{T} \right]. \quad (2.90)$$

In order to properly understand the mapping, we sketch the way used to calculate the correspondence between matrix elements in the two different basis. As a simple example we now calculate the correspondence between two matrix elements according to Eq.2.89.

First we have to calculate the matrix elements of $\sum_s d_{ns}^\dagger d_{n's}$ between the states of the old basis, as a simplification we shall do it only for the singlet state $\hat{d}_{-\uparrow}^\dagger \hat{d}_{-\downarrow}^\dagger$. Such a matrix element can be written as:

$$\langle \hat{d}_{-\uparrow} \hat{d}_{-\downarrow} \left| \sum_s d_{ns}^\dagger d_{n's} \right| \hat{d}_{-\uparrow}^\dagger \hat{d}_{-\downarrow}^\dagger \rangle, \quad (2.91)$$

and only nonzero contributions from the summations are:

$$\langle \hat{d}_{-\uparrow} \hat{d}_{-\downarrow} \left| d_{-\uparrow}^\dagger d_{-\uparrow} + d_{-\downarrow}^\dagger d_{-\downarrow} \right| \hat{d}_{-\uparrow}^\dagger \hat{d}_{-\downarrow}^\dagger \rangle = 2. \quad (2.92)$$

Now in the two spin basis the corresponding matrix element is again:

$$\frac{1}{\sqrt{2}} (\langle \downarrow_1, \uparrow_2 | - \langle \uparrow_1, \downarrow_2 |) n \delta_{n,n'} \left(\vec{S}_1 \cdot \vec{S}_2 - \frac{1}{4} + n \right) \frac{1}{\sqrt{2}} (|\downarrow_1, \uparrow_2\rangle - |\uparrow_1, \downarrow_2\rangle) = 2, \quad (2.93)$$

because $n = -1$, $\vec{S}_1 \cdot \vec{S}_2 = 3/4$. Thus operating in the same way for all the matrix elements of Eq. 2.89, and 2.90, one easily can check that the dot Hamiltonian restricted to this new low energy base reads:

$$H_{dot} = K \vec{S}_1 \cdot \vec{S}_2 - \mu B S_{\uparrow}^z + \frac{1}{2\sqrt{2}} \left(V_{so} \left(\vec{S}_- + 2in\vec{T}^- \right) + h.c. \right). \quad (2.94)$$

Appendix 2C

Mapping of the two spin 1/2 model onto the single spin model

The spin orbit Rashba coupling only couples the states $|0, 0\rangle$ and $|1, 1\rangle$ of Eq.s 2.20, therefore is it possible to map the two spin Hamiltonian of Eq.2.27 onto the subspace spanned by a single spin $\tilde{S} = 1/2$ with the following correspondences:

$$\begin{aligned} |\uparrow\rangle &\iff |0, 0\rangle = \frac{1}{\sqrt{2}} (|\uparrow_1, \downarrow_2\rangle - |\downarrow_1, \uparrow_2\rangle), \\ |\downarrow\rangle &\iff |1, -1\rangle = |\downarrow_1, \downarrow_2\rangle, \end{aligned} \quad (2.95)$$

In order to properly map the two spin effective Hamiltonian onto the single spin basis we have to project some important operators from the $4-d$ basis (in the following old basis) of the two spin system to the $2-d$ basis (new basis) of the single spin \tilde{S} .

Defining as $\mathcal{P}' = \sum_s |s\rangle\langle s|$ as the projector on the two state basis, among the operators contained in 2.27 only the following have non zero matrix elements:

$$\begin{aligned}\mathcal{P}' S_+^z \mathcal{P}' &\Rightarrow \tilde{S}^z - \frac{1}{2}, \\ \mathcal{P}' \vec{S}_1 \cdot \vec{S}_2 \mathcal{P}' &\Rightarrow -\tilde{S}^z - \frac{1}{4}, \\ \mathcal{P}' S_-^{\pm} \mathcal{P}' &\Rightarrow \sqrt{2} \tilde{S}^{\pm}, \\ \mathcal{P}' T^{\pm} \mathcal{P}' &\Rightarrow \pm \frac{i}{\sqrt{2}} \tilde{S}^{\pm}.\end{aligned}\quad (2.96)$$

In order to properly understand the mapping, in the following, we sketch the way used to calculate the correspondence between matrix elements in the two different basis that is purely formal. A simple example is the analogy

$$\mathcal{P}' S_+^z \mathcal{P}' \Rightarrow \tilde{S}^z - \frac{1}{2}.$$

First we have to calculate the matrix elements of S_+^z between the states of the old basis $\langle \downarrow_1, \downarrow_2 |$:

$$\langle \downarrow_1, \downarrow_2 | S_+^z | \downarrow_1, \downarrow_2 \rangle = -1, \quad (2.97)$$

$$\frac{1}{\sqrt{2}} (\langle \uparrow_1, \downarrow_2 | - \langle \downarrow_1, \uparrow_2 |) S_+^z \frac{1}{\sqrt{2}} (| \uparrow_1, \downarrow_2 \rangle - | \downarrow_1, \uparrow_2 \rangle) = 0, \quad (2.98)$$

and the off-diagonal elements are zero. The correspondence to the single spin basis is realized by the operator $\tilde{S} - 1/2$, in fact its matrix elements are

$$\langle \downarrow | \tilde{S} - 1/2 | \downarrow \rangle = -1, \quad (2.99)$$

$$\langle \uparrow | \tilde{S} - 1/2 | \uparrow \rangle = 0. \quad (2.100)$$

so the correspondence between matrix elements is reached. Analogously we can proof all the equations 2.96.

By simple mapping each matrix element of Eq.2.27 with the help of equations 2.96 we can map the two spin effective Hamiltonian onto the single spin basis:

$$H_{dot} = -\frac{1}{2} \left(\frac{K}{2} - B \right) + \vec{b} \cdot \vec{S}, \quad (2.101)$$

where $b_z = -(K + B)$ and $b^{+(-)} = b_x + (-)ib_y = 2V_{so}^{(*)}$. Where $|b| = \sqrt{(K + B)^2 + |2V_{so}|^2}$ and the tilting angle θ is defined by $\tan(\theta) = \frac{|2V_{so}|}{-(K+B)}$.

Appendix2D

Adiabatic and exact propagator

In order to find the propagator of the Berry Hamiltonian, we may solve the system of differential equations in the adiabatic basis:

$$i \frac{d}{dt} \begin{pmatrix} u_+ \\ u_- \end{pmatrix} = \begin{pmatrix} r + \omega_o \sin^2 \frac{\vartheta}{2} & \omega_o \sin \frac{\vartheta}{2} \cos \frac{\vartheta}{2} e^{-i\omega_o t} \\ \omega_o \sin \frac{\vartheta}{2} \cos \frac{\vartheta}{2} e^{i\omega_o t} & -r - \omega_o \sin^2 \frac{\vartheta}{2} \end{pmatrix} \begin{pmatrix} u_+ \\ u_- \end{pmatrix}. \quad (2.102)$$

First we neglect the off-diagonal components and evaluate the adiabatic propagator by we solving

$$i \frac{d}{dt} \begin{pmatrix} u_+^A \\ u_-^A \end{pmatrix} = \begin{pmatrix} r + \omega_o \sin^2 \frac{\vartheta}{2} & 0 \\ 0 & -r - \omega_o \sin^2 \frac{\vartheta}{2} \end{pmatrix} \begin{pmatrix} u_+^A \\ u_-^A \end{pmatrix}. \quad (2.103)$$

It easily gives us

$$u_+^A(t) = u_+(0) e^{-irt} e^{-i\omega_o \sin^2 \frac{\vartheta}{2} t}, \quad (2.104)$$

$$u_-^A(t) = u_-(0) e^{irt} e^{i\omega_o \sin^2 \frac{\vartheta}{2} t}. \quad (2.105)$$

After a period $T = 2\pi\omega_o$ the second exponent in the evolution operator is the so called Berry phase:

$$\Gamma_{\pm}(t) = \mp \omega_o t \sin^2 \frac{\vartheta}{2}$$

Now we try to solve the equations for the full propagator $U(t)$, that is we do not neglect off-diagonal component to the Hamiltonian 2.48 that we rewrite here as:

$$H(t) = \begin{pmatrix} r + \omega_o \sin^2 \frac{\vartheta}{2} & \frac{1}{2} \omega_o \sin \vartheta e^{-i\omega_o t} \\ \frac{1}{2} \omega_o \sin \vartheta e^{i\omega_o t} & -r - \omega_o \sin^2 \frac{\vartheta}{2} \end{pmatrix}. \quad (2.106)$$

The solution is trivial. First of all, one may switch to a time-independent coefficient matrix by defining:

$$\begin{pmatrix} y_+ \\ y_- \end{pmatrix} = \begin{pmatrix} e^{-i\frac{\omega_o}{2}t} & 0 \\ 0 & e^{i\frac{\omega_o}{2}t} \end{pmatrix} \begin{pmatrix} u_+ \\ u_- \end{pmatrix}. \quad (2.107)$$

We call the T the matrix transformation of Eq.2.107. So by defining

$$Y = \begin{pmatrix} y_+ \\ y_- \end{pmatrix},$$

$$W = \begin{pmatrix} u_+ \\ u_- \end{pmatrix},$$

we can easily write

$$Y = T W, \quad W = T^{-1} Y. \quad (2.108)$$

The Eq.s 2.102 now read:

$$\begin{aligned} i\frac{dy_+}{dt}(t) &= \left(r - \frac{\omega_o}{2}\cos(\vartheta)\right)y_+(t) + \frac{\omega_o}{2}\sin\vartheta y_-(t), \\ i\frac{dy_-}{dt}(t) &= +\frac{\omega_o}{2}\sin\vartheta y_+(t) + \left(-r + \frac{\omega_o}{2}\cos(\vartheta)\right)y_-(t). \end{aligned} \quad (2.109)$$

Now we define $r' = r - \frac{\omega_o}{2}\cos\vartheta$ and $s = \frac{\omega_o}{2}\sin\vartheta$, so that in matrix form we have:

$$i\frac{d}{dt}\begin{pmatrix} y_+ \\ y_- \end{pmatrix} = \begin{pmatrix} r' & s \\ s & -r' \end{pmatrix} \begin{pmatrix} y_+ \\ y_- \end{pmatrix}, \quad (2.110)$$

in a compact form we can rewrite the last equation as:

$$i\frac{d}{dt}Y = CY, \quad (2.111)$$

and the matrix C is easily identified.

We now decouple the previous system of equation by mean of diagonalizing the matrix C . Its eigenvalues are $\lambda = \pm\epsilon = \pm\sqrt{r'^2 + s^2}$ and the matrix that diagonalizes C is

$$P = \begin{pmatrix} 1 & \frac{r'-\epsilon}{s} \\ \frac{\epsilon-r'}{s} & 1 \end{pmatrix}, \quad (2.112)$$

and its inverse is

$$P^{-1} = \begin{pmatrix} \frac{s^2}{2\epsilon(\epsilon-r')} & \frac{(\epsilon-r')s}{2\epsilon(\epsilon-r')} \\ -\frac{(\epsilon-r')s}{2\epsilon(\epsilon-r')} & \frac{s^2}{2\epsilon(\epsilon-r')} \end{pmatrix}. \quad (2.113)$$

Easily, in fact,

$$P^{-1}CP = \begin{pmatrix} \epsilon & 0 \\ 0 & -\epsilon \end{pmatrix}. \quad (2.114)$$

So Eq.2.111 reads:

$$i\frac{d}{dt}P^{-1}Y = P^{-1}CP P^{-1}Y, \quad (2.115)$$

and by calling $V = P^{-1}Y$, we have

$$i\frac{d}{dt}V = \begin{pmatrix} \epsilon & 0 \\ 0 & -\epsilon \end{pmatrix} V. \quad (2.116)$$

Its formal solution is:

$$V(t) = \begin{pmatrix} e^{-i\epsilon t} & 0 \\ 0 & e^{i\epsilon t} \end{pmatrix} V(0), \quad (2.117)$$

or, in matrix form

$$V(t) = S(t)V(0). \quad (2.118)$$

Now we apply inverse transformations in order to obtain the full Schrödinger propagator, that is the matrix transformation between $(W(t)$ and $W(0)$).

$$W(t) = T^{-1} P S P^{-1}(0) T(0) W(0) ,$$

since P does not depend on time we have $P^{-1}(0) \equiv P^{-1}$. Moreover $T(0) \equiv I_2$ so the full evolution operator is

$$U(t) = T^{-1} P S P^{-1} ; \quad (2.119)$$

by introducing:

$$\begin{aligned} \alpha &= \frac{\omega_o}{2} \cos(\theta) , \\ \beta &= \frac{s}{\epsilon} = \frac{\omega_o}{2\epsilon} \sin(\theta) , \\ \gamma &= \frac{r'}{\epsilon} = \frac{r + \frac{\omega_o}{2} \cos \vartheta}{\epsilon} , \end{aligned}$$

and performing all the matrix products one has:

$$U(t) = \begin{pmatrix} (\cos(\epsilon t) - i\gamma \sin(\epsilon t))e^{i\alpha t} & -i\beta \sin(\epsilon t)e^{i\alpha t} \\ -i\beta \sin(\epsilon t)e^{-i\alpha t} & (\cos(\epsilon t) + i\gamma \sin(\epsilon t))e^{-i\alpha t} \end{pmatrix} . \quad (2.120)$$

Appendix 2E

Path integral for a spinful particle on a ring

We want to calculate the transition amplitude:

$$\langle \varphi_f \mu_f t_f | \varphi_o \mu_o 0 \rangle = \langle \varphi_f \mu_f | e^{-iHt_f} | \varphi_o \mu_o \rangle . \quad (2.121)$$

First we calculate the transition amplitude for a time interval $\epsilon = \lim_{N \rightarrow +\infty} \frac{it_f}{N}$:

$$H_0 = \frac{\hbar^2}{2mR^2} \left(\hat{l} + \frac{\phi}{\phi_0} \right)^2 + \frac{1}{2} \hbar \omega_c \sigma_z .$$

Applying Trotter's formula [29], we obtain:

$$\begin{aligned} M_{1,0} &= \langle \varphi_1 \mu_1 | e^{-\frac{\epsilon}{\hbar}(H_0 + H_{S=0})} | \varphi_o \mu_o \rangle \simeq \langle \varphi_1 \mu_1 | e^{-\frac{\epsilon}{\hbar}H_0} e^{-\frac{\epsilon}{\hbar}H_{so}} | \varphi_o \mu_o \rangle = \\ &= \langle \varphi_1 \mu_1 | e^{-\frac{\epsilon}{\hbar}H_0} \left(\sum_{\mu} \int |p_1 \mu\rangle \langle p_1 \mu| dp_1 \right) e^{-\frac{\epsilon}{\hbar}H_{so}} | \varphi_o \mu_o \rangle . \end{aligned}$$

Where $|p_\varphi\rangle$ are eigenstates of the angular momentum \hat{l} with eigenvalues:

$$\hat{l} |p_1\rangle = \frac{1}{i} \frac{d}{d\varphi} |p_1\rangle = p_1 |p_1\rangle ,$$

this implies the following rule:

$$\langle \varphi_1 \mu_1 | p_1 \mu \rangle = \frac{1}{\sqrt{2\pi}} e^{ip_1 \varphi_1} \delta_{\mu \mu_1} .$$

We stress that in this problem we have no quantization of the momentum p because the covering space \mathbf{U} is unbounded $-\infty < \varphi < +\infty$. By using these relations the transition amplitude becomes:

$$M_{1,0} = \sum_{\mu} \int dp_1 \langle \varphi_1 \mu_1 | e^{-\frac{\epsilon}{\hbar} H_0} | p_1 \mu \rangle \times \\ \langle p_1 \mu | e^{\frac{\epsilon}{\hbar} \frac{\alpha}{2R}} \left[\left(e^{-i\varphi} \left(\hat{l} + \frac{\phi}{\phi_0} \right) + \left(\hat{l} + \frac{\phi}{\phi_0} \right) e^{-i\varphi} \right) \sigma_{++} + \left(e^{i\varphi} \left(\hat{l} + \frac{\phi}{\phi_0} \right) + \left(\hat{l} + \frac{\phi}{\phi_0} \right) e^{i\varphi} \right) \sigma_{--} \right] | \varphi_0 \mu_0 \rangle .$$

In order to calculate the matrix element

$$\langle p_1 \mu | e^{-\frac{\epsilon}{\hbar} H_{so}} | \varphi_0 \mu_0 \rangle ,$$

we have to order in a right way the operators within the Hamiltonian by using the relations:

$$[e^{i\varphi}, \hat{l}] = i e^{i\varphi} [\varphi, \hat{l}] = -e^{i\varphi} , \quad [e^{-i\varphi}, \hat{l}] = -i e^{-i\varphi} [\varphi, \hat{l}] = e^{-i\varphi} ,$$

being $[\varphi, \hat{l}] = i$. So the ordered spin orbit Hamiltonian can be written as:

$$H_{so} = -\frac{\alpha}{2R} \left[\left(e^{-i\varphi} + 2 \left(\hat{l} + \frac{\phi}{\phi_0} \right) e^{-i\varphi} \right) \sigma_{++} + \left(-e^{i\varphi} + 2 \left(\hat{l} + \frac{\phi}{\phi_0} \right) e^{i\varphi} \right) \sigma_{--} \right] .$$

In this form the operators are ordered in a right way (now each operator acts on its own eigenstates and the calculation is straightforward):

$$M_{1,0} = \int dp_1 \langle \mu_1 | \langle \varphi_1 | p_1 \rangle e^{-\frac{\epsilon}{\hbar} \left[\frac{\hbar^2}{2mR^2} \left(p_1 + \frac{\phi}{\phi_0} \right)^2 + \frac{1}{2} \hbar \omega_c \sigma_z \right]} \langle p_1 | \varphi_0 \rangle \\ e^{\frac{\epsilon}{\hbar} \left(\frac{\alpha}{R} \right) \left[\left(p_1 + \frac{1}{2} + \frac{\phi}{\phi_0} \right) e^{-i\varphi_0} \sigma_{++} + \left(p_1 - \frac{1}{2} + \frac{\phi}{\phi_0} \right) e^{i\varphi_0} \sigma_{--} \right]} | \mu_0 \rangle = \\ = \frac{1}{2\pi} \int d\tilde{p}_1 \langle \mu_1 | e^{-i \frac{\phi}{\phi_0} (\varphi_1 - \varphi_0)} e^{-\frac{\epsilon}{\hbar} \left(\frac{\hbar}{2} \omega_c \sigma_z \right)} e^{\frac{\epsilon}{\hbar} \left(\frac{\alpha}{2R} \right) [e^{-i\varphi_0} \sigma_{++} - e^{i\varphi_0} \sigma_{--}]} \times \\ e^{-\frac{\epsilon}{\hbar} \left\{ \frac{\hbar^2}{2mR^2} \tilde{p}_1^2 - \left[\frac{\alpha}{R} [e^{-i\varphi_0} \sigma_{++} + e^{i\varphi_0} \sigma_{--} + \dot{\varphi}_0 \hbar] \right] \tilde{p}_1 \right\}} | \mu_0 \rangle ,$$

where we have introduced $\tilde{p}_1 = p_1 + \frac{\phi}{\phi_0}$, $i \frac{(\varphi_1 - \varphi_0)}{\epsilon} = \dot{\varphi}_0$. Moreover by neglecting terms $o(\epsilon)^2$ it is possible to split the exponents and write the integrals into a simplest form. Now the integral over \tilde{p}_1 is a Gaussian integral like:

$$\int_{-\infty}^{+\infty} d\tilde{p}_1 e^{-a\tilde{p}_1^2 + b\tilde{p}_1} = \sqrt{\frac{\pi}{a}} e^{\frac{b^2}{4a}} ,$$

where the coefficients are, in our case:

$$a = \frac{\epsilon}{2mR^2} , \quad b = \hat{B}_0 = \frac{\epsilon \alpha}{R} (e^{-i\varphi_0} \sigma_{++} + e^{i\varphi_0} \sigma_{--}) + \vec{I} \epsilon \dot{\varphi}_0 ,$$

and

$$\frac{\hat{B}_0^2}{4a} = \frac{\hat{B}_0^2 m R^2}{2\epsilon} = \epsilon \left[\left(\frac{1}{2} m R^2 \dot{\varphi}_0^2 + \frac{\alpha^2 m}{2} \right) \vec{I} + \dot{\varphi}_0 R \alpha m (e^{-i\varphi_0} \sigma_+ + e^{i\varphi_0} \sigma_-) \right].$$

At the end:

$$\begin{aligned} M_{1,0} &= \sqrt{\frac{mR^2}{2\pi\epsilon}} e^{-i\frac{\phi}{\phi_0}(\varphi_1 - \varphi_0)} \langle \mu_1 | e^{-\epsilon(\frac{1}{2}\omega_c \sigma_z)} e^{\epsilon(\frac{\alpha}{2R})[e^{-i\varphi_0} \sigma_+ - e^{i\varphi_0} \sigma_-]} \times \\ &\quad e^{\epsilon \left[\left(\frac{1}{2} m R^2 \dot{\varphi}_0^2 + \frac{\alpha^2 m}{2} \right) \vec{I} + \dot{\varphi}_0 R \alpha m (e^{-i\varphi_0} \sigma_+ + e^{i\varphi_0} \sigma_-) \right]} | \mu_0 \rangle = \\ &= \sqrt{\frac{mR^2}{2\pi\epsilon}} e^{\epsilon \left[-\frac{\phi}{\phi_0} \dot{\varphi}_0 + \frac{mR^2 \dot{\varphi}_0^2}{2} + \frac{\alpha^2 m}{2} \right]} \times \\ &\quad \langle \mu_1 | e^{-\epsilon \left[\frac{1}{2} \omega_c \sigma_z - e^{-i\varphi_0} \sigma_+ \left(\frac{\alpha}{2R} + \dot{\varphi}_0 R \alpha m \right) + e^{i\varphi_0} \sigma_- \left(\frac{\alpha}{2R} - \dot{\varphi}_0 R \alpha m \right) \right]} | \mu_0 \rangle. \end{aligned}$$

Now we can repeat all this machinery for a doubled time slice 2ϵ between the states $(\varphi_2, \mu_2, 2\epsilon)$ and $(\varphi_0, \mu_0, 0)$ and the result is:

$$\begin{aligned} M_{2,0} &= \langle \varphi_2 \mu_2 | e^{2\epsilon(H_0 + H_{so})} | \varphi_0 \mu_0 \rangle = \langle \varphi_2 \mu_2 | e^{\epsilon(H_0 + H_{so})} \left(\sum_{\mu_1} \int d\varphi_1 | \varphi_1 \mu_1 \rangle \langle \varphi_1 \mu_1 | \right) \times \\ &\quad e^{\epsilon(H_0 + H_{so})} | \varphi_0 \mu_0 \rangle = \sum_{\mu_1} \int d\varphi_1 \langle \varphi_2 \mu_2 | e^{\epsilon(H_0 + H_{so})} | \varphi_1 \mu_1 \rangle \langle \varphi_1 \mu_1 | e^{\epsilon(H_0 + H_{so})} | \varphi_0 \mu_0 \rangle = \\ &= \left(\sqrt{\frac{mR^2}{2\pi\epsilon}} \right)^2 \int d\varphi_1 e^{\epsilon \left[-\frac{\phi}{\phi_0}(\dot{\varphi}_0 + \dot{\varphi}_1) + \frac{mR^2(\dot{\varphi}_0^2 + \dot{\varphi}_1^2)}{2} + 2\frac{\alpha^2 m}{2} \right]} \times \\ &\quad \langle \mu_2 | e^{-\epsilon \left[\frac{1}{2} \hbar \omega_c \sigma_z - e^{-i\varphi_1} \sigma_+ \left(\frac{\alpha}{2R} + \dot{\varphi}_1 R \frac{\alpha}{\hbar} m \right) + e^{i\varphi_1} \sigma_- \left(\frac{\alpha}{2R} - \dot{\varphi}_1 R \alpha m \right) \right]} \times \\ &\quad e^{-\epsilon \left[\frac{1}{2} \omega_c \sigma_z - e^{-i\varphi_0} \sigma_+ \left(\frac{\alpha}{2R} + \dot{\varphi}_0 R \alpha m \right) + e^{i\varphi_0} \sigma_- \left(\frac{\alpha}{2R} - \dot{\varphi}_0 R \alpha m \right) \right]} | \mu_0 \rangle. \end{aligned}$$

We define \hat{C}_i the matrix:

$$\hat{C}_i = \left[-\frac{1}{2} \hbar \omega_c \sigma_z + e^{-i\varphi_i} \alpha \sigma_+ \left(\dot{\varphi}_i R m + \frac{1}{2R} \right) + e^{i\varphi_i} \alpha \sigma_- \left(\dot{\varphi}_i R m - \frac{1}{2R} \right) \right]. \quad (2.122)$$

In \hat{C}_i the contribution $\dot{\varphi}_i R \frac{\alpha}{\hbar} m$ is clearly due to the Rashba coupling, by contrast $\frac{\alpha}{2R}$ comes from commutation operations, therefore it is an explicit quantum correction: it represents a quantum fluctuation of the order \hbar/R around the classical momentum $m\dot{\varphi}_i R$. Starting from $M_{1,0}$ and $M_{2,0}$ it is possible to generalize to finite times the path integral procedure in order to obtain the transition amplitude between (φ_f, μ_f, t_f) and $(\varphi_0, \mu_0, 0)$:

$$\begin{aligned} \langle \varphi_f \mu_f t_f | \varphi_0 \mu_0 0 \rangle &= \lim_{N \rightarrow +\infty} M_{N,0} = \lim_{N \rightarrow +\infty} \left(\sqrt{\frac{mR^2}{2\pi\epsilon}} \right)^N e^{it_f \frac{\alpha^2 m}{2}} \times \\ &\quad \int d\varphi_1 \dots d\varphi_{N-1} e^{\epsilon \sum_{i=1}^N \left(\frac{m}{2} R^2 \dot{\varphi}_{i-1}^2 - \frac{\phi}{\phi_0} \dot{\varphi}_{i-1} \right)} \langle \mu_f | \prod_{i=1}^N e^{\epsilon \hat{C}_i} | \mu_0 \rangle, \quad (2.123) \end{aligned}$$

or in a more compact form by using the following correspondence:

$$\lim_{N \rightarrow +\infty} \left(\sqrt{\frac{mR^2}{2\pi\epsilon\hbar}} \right)^N \int d\varphi_1 \dots d\varphi_{N-1} = \int_{\varphi_0}^{\varphi_f} \mathcal{D}[\varphi(t)],$$

the transition amplitude appears as:

$$\langle \varphi_f \mu_f t_f | \varphi_0 \mu_0 0 \rangle \equiv e^{it_f \frac{\alpha^2 m}{2}} \int_{\varphi_0}^{\varphi_f} \mathcal{D}[\varphi(t)] e^{i \int_0^{t_f} \left(\frac{m}{2} R^2 \dot{\varphi}^2(t) - \frac{\phi}{\phi_0} \dot{\varphi}(t) \right)} \langle \mu_f | \hat{T} e^{i \int_0^{t_f} C[\varphi(t)]} | \mu_0 \rangle, \quad (2.124)$$

where \hat{T} indicates the chronologically ordered product. The first phase factor in Eq. (2.124) originates from the Rashba coupling and the term

$$\int_0^{t_f} \left(\frac{m}{2} R^2 \dot{\varphi}^2(t) - \hbar \frac{\phi}{\phi_0} \dot{\varphi}(t) \right) dt = \int_0^{t_f} \mathcal{L}(\dot{\varphi}) dt,$$

is the action of a quantum particle moving on a ring in the presence of a magnetic field. Now it is easy to recognize the effective Lagrangian $\mathcal{L}(\dot{\varphi})$ inclusive of the spin effects contained in \hat{C} .

Bibliography

- [1] D. P. DiVincenzo, *Science* **270**, 255 (1995).
- [2] Y. Nakamura, Y. A. Pashkin and J. S. Tsai, *Nature* **398**, 786 (1999).
- [3] J. E. Mooij, T. P. Orlando, L. Levitov, L. Tian, C. H. van der Wal and S. Lloyd *Science* **285**, 1036 (1999).
- [4] M. Bayer, P. Hawrylak, K. Hinzer, S. Fafard, M. Korkusinski, Z. R. Wasilewski, O. Stern and A. Forchel, *Science* **291**, 451 (2001).
- [5] E. Farhi, J. Goldstone, S. Gutmann, J. Lapan, A. Lundgreen and D. Preda, *Science* **292**, 472 (2001); J. Pachos, P. Zanardi and M. Rasetti, *Phys. Rev. A* **61**, 010305(R) (2000).
- [6] M. V. Berry, *Proc. R. Soc. London, A* **392**, 45 (1984).
- [7] G. Gaitan and S. R. Shenoy, *Phys. Rev. Lett.* **76**, 4404 (1996).
- [8] G. Falci, R. Fazio, G. M. Palma, J. Siewert, V. Vedral, *Nature* **407**, 355 (2000).
- [9] M. A. Kastner, *Ann. Phys.* **9**, 885 (2000); S. Sasaki, S. De Franceschi, J. M. Elzerman, W. G. van der Wiel, M. Eto, S. Tarucha, L. P. Kouwenhoven *Nature* **405**, 764 (2000).

- [10] B. Jouault, G. Santoro and A. Tagliacozzo, Phys. Rev. B **61**, 10242 (2000); L. P. Kouwenhoven, T. H. Oosterkamp, M. W. S. Danoesastro, M. Eto, D. G. Austing, T. Honda and S. Tarucha, Science **278**, 1788 (1997).
- [11] P. Lucignano, B. Jouault and A. Tagliacozzo Phys. Rev. B **69**, 045314 (2004).
- [12] P. Lucignano, B. Jouault, A. Tagliacozzo and B. L. Altshuler, submitted (2004).
- [13] D. Giuliano, P. Sodano and A. Tagliacozzo Phys. Rev. B **67**, 155317(2003).
- [14] J. Schliemann, D. Loss and A. H. MacDonald, Phys. Rev. B **63**, 085311 (2001).
- [15] Y. Aharonov, J. Anandan, Phys. Rev. Lett. **58**, 1593 (1987).
- [16] A. Messiah, Quantum Mechanics vol.2 North Holland, Amsterdam (1962).
- [17] I. J. R. Aitchinson, Phys. Scr. **23**, 12 (1988).
- [18] M. Pustilnik and L. I. Glazman, Phys. Rev. B **64**, 045328 (2001), M. Pustilnik and L. I. Glazman, Phys. Rev. Lett. **85**, 2993 (2000).
- [19] M. Eto and Y. Nazarov, Phys. Rev. Lett. **85**, 1306 (2000).
- [20] M. Pustilnik, Y. Avishai and K. Kikoin Phys. Rev. Lett. **84**, 1756 (2000).
- [21] D. Giuliano, P. Lucignano, A. Tagliacozzo, "Spin manipulation in quantum dots by mean of electric field and voltage gates" in print in Materials Science.
- [22] R. Landauer, IBM J. Res. Dev. **1** 223 (1957).
- [23] M. Buttiker, IBM J. Res. Dev. **32** 317 (1988).
- [24] E. Capozza, D. Giuliano, P. Lucignano, A. Tagliacozzo *Model hamiltonian and adiabatic evolution*, unpublished notes.
- [25] D. Frustaglia, K. Richter, Phys. Rev. B **69** 235310 (2004).
- [26] G. Morandi, E. Menossi Eur. J. Phys. **5** 49-58 (1984).
- [27] D. Bercioux private communication.
- [28] Y. Ahronov, D. Bohm, Phys. Rev. **115** 485 (1959).

- [29] R. P. Feynmann, *Quantum Mechanics and Path Integral*, Mc Graw-Hill, New York 1965.

You can know the name of a bird in all the languages of the world, but when you're finished, you'll know absolutely nothing whatever about the bird... So let's look at the bird and see what it's doing, that's what counts.

Richard Feynman (1918-1988)

3

Fast optical control of an out of equilibrium Josephson junction

Abstract

By irradiating with a single ultrafast laser pulse a superconducting electrode of a Josephson junction it is possible to drive the quasiparticles (qp's) distribution strongly out of equilibrium. The behavior of the Josephson device can, thus, be modified on a fast time scale, shorter than the qp's relaxation time. This could be very useful, in that it allows fast control of Josephson charge qubits and, in general, of all Josephson devices. If the energy released to the top layer contact $S1$ of the junction is of the order of $\sim \mu J$, the coherence is not degraded, because the perturbation is very fast. Within the framework of the quasiclassical Keldysh Green's function theory, we find that the order parameter of $S1$ decreases. We study the perturbed dynamics of the junction, when the current bias is close to the critical current, by integrating numerically its classical equation of motion. The optical ultrafast pulse can produce switchings of the junction from the Josephson state to the voltage state. The switches can be controlled by tuning the laser light intensity and the pulse duration of the Josephson junction^a.

^aA large part of this chapter is taken from Ref. [1]

3.1 Introduction

The characteristic frequency in the dynamics of a Josephson junction (JJ) is the so-called Josephson plasma frequency ω_{pJ} (e.g. $10 \div 100 GHz$). Coupling of a JJ to a microwave field leads to the well known lock-in conditions, which show up as Shapiro steps in the I/V characteristic. On the other hand, photo-response to radiation in a superconductor induces heat relaxation (bolometric effect [2]) and non equilibrium generation of quasiparticles (qp's) [3, 4]. Both phenomena are extensively studied since they are relevant for the fabrication of fast and sensitive detectors. The models used are phenomenological [5–9], mainly involving different temperatures associated

to separate distributions of electrons and phonons out of equilibrium.

Recently, laser light with pulses of femtosecond duration $\tau_c \in (10^{-14} s, 10^{-13} s)$

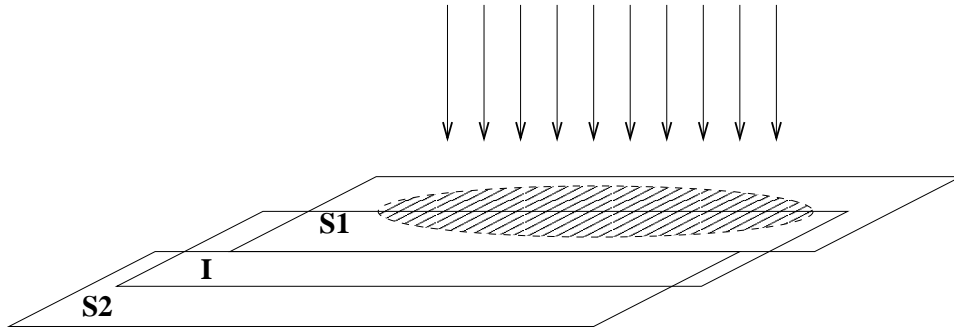


Figure 3.1: Sketch of the Josephson junction exposed to a laser radiation pulse.

has become available, as a source to test the photo-response of a JJ [8]. Ultrafast pulses can be extremely useful, in that they allow studying an unexplored regime in non equilibrium superconductivity. Indeed, photon absorption, by creating electron-hole (e-h) pairs at very high energies, drives the quasi-particle (qp) energy distribution out of equilibrium during the time τ_c . The qp non-equilibrium distribution depends on the energy relaxation time parameter τ_E , defined as the time by which a ‘hot’ electron is thermalized by repeated scatterings with other electrons or phonons. The process involves generation of many qp’s during energy degradation, until the system relaxes back to the equilibrium distribution function $n_o(\omega)$. This time scale is determined by the electron-electron interaction time τ_{e-e} and the electron-phonon interaction time τ_{e-ph} , which are strongly material dependent [10], ranging from $4 \cdot 10^{-7} s$ for *Al* to $1.510^{-10} s$ for *Nb*. In this chapter we analyze the possibility that, keeping temperature quite low, ultrashort laser radiation induces direct switches out of the Josephson conduction state at zero voltage, due to coherent reduction of the critical current J_c .

There are many reasons for the switching from the zero to the resistive state in a Josephson junction. Among these, thermal escape [11], quantum tunneling [12], latching logic circuits [13] and pulsed assisted escape [14]. A clear cut discrimination between different mechanisms can be difficult to achieve. In our case quantum escape is ruled out because the temperature is not expected to be low enough. Also, we assume that there is no external circuit to induce switching and re-set of the zero voltage state as in latching logic elements.

Pulsed assisted escape is a generic term for a large class of phenomena including in principle bolometric heating of the junction which is re-set in relatively slow times [3]. Production of quasiparticles generated by *X*-ray radiation has been studied up to recently [15, 16]. A cascade follows, which

increases the number of excitations and lowers their energy down to the typical phonon energy ω_D in a duration time, which is of the order of the nanoseconds. Subsequently, qp's decay by heating the sample. However, the power of the laser can be reduced enough and both the substrate and the geometry can be chosen such that the energy released by the radiation on the junction can be small. On the other hand, appropriate experimental conditions can make the time interval between two pulses long enough, so that the bolometric response is negligible.

Generally speaking, junctions are more sensitive to pulses especially when their harmonic content is close to ω_{pJ} , but this is not our case. In fact the laser carrier frequency ($\Omega \sim 100THz$) is quite high compared to ω_{pJ} and we consider the case $\Omega \gg \tau_c^{-1} > \omega_{pJ} > \tau_E^{-1}$, what implies that little relaxation takes place during the duration of the pulse. τ_c should also be shorter than the pair-breaking time $\hbar/\Delta_o \sim 1 \div 5ps$. Here Δ_o is the unperturbed gap parameter. Our approach assumes that, on a time scale intermediate between the pulse duration and the relaxation time $\sim \tau_E$, the order parameter of the irradiated superconductor is sensitive to the non-equilibrium qp distribution, which modulates it coherently till it switches out of the zero voltage state.

To analyze the dynamics of the order parameter and the way how the latter affects the Josephson current, we adopt a non-equilibrium formalism based on quasiclassical Green's functions [17, 18]. The quasiclassical approach has been mostly used in the past in connection with the proximity effect [18], as well as with non-equilibrium due to other space inhomogeneity conditions [19]. As far as we know, in [1] it is the first time that an extension of a time dependent out of equilibrium quasiclassical Green's function theory is applied to a coherent response after an ultrafast laser irradiation.

The quasiclassical approximation to the Gorkov equations, is obtained by averaging over the period of the optical frequency Ω , which is a fast time scale [20]. Our equations include the physics of the cascade process, which occurs when one focuses on the kinetics of the qp diffusion. A kinetic equation approach to the steady state non equilibrium qp distribution, including phonon scattering has been developed in Ref. [23], for electromagnetic irradiation, mostly in the microwave range. The cascade regime is extensively discussed in Ref. [16], however it will not be specifically addressed here.

Instead, if the switching of the irradiated superconductor due to the ultrafast pulse takes place prior to the occurrence of qp relaxation, an approximate solution of the dynamical equations can be derived, which describes an instantaneous response of the order parameter.

We take a low T_c JJ with an *s*-wave order parameter as the reference case (e.g. a high quality *Nb* or *Al* junction) and $T \ll T_c$. The optical penetration depth of the laser light λ_δ in the topmost superconductor exposed to radiation *S1* is assumed to be shorter than its thickness, so that any modification induced by the radiation field only involves *S1* itself [3] (see.

Fig.(3.1)). In a small size JJ the spatial variation of the order parameter along the lateral dimension of $S1$ is not taken into account, except when the qp diffusion process cannot be ignored.

We consider just one pulse of given duration τ_c which releases the energy \mathcal{E} per pulse, by exciting $e - h$ pairs and by creating a non equilibrium distribution of qp's. A related dimensionless quantity q , as defined in Eq. (3.12), parametrizes the strength of the perturbation due to the radiation. The perturbation is assumed to be small so that only the lowest order in the expansion in q is retained. This allows us to derive a temporary reduction of the order parameter Δ induced by the pulse, as shown in Fig.(3.3). We do not give a detailed description for the relaxation of the non-thermal qp distribution in the irradiated superconductor. The self-energy terms corresponding to this process require further analysis. According to the Eliashberg formulation [10] these terms affect the quasiparticle amplitude $Z(\omega)$ introducing changes in the phonon distribution and retardation in the response. Nevertheless, we expect that these self-energy terms become effective only on a longer time scale after the laser pulse. Our equations pinpoint a non retarded evolution of the order parameter prior to relaxation, which implies a reduction of the critical current. This shows that the coherent modulation of the gap parameter can produce switchings of the junction out of the Josephson state.

The switchings are studied numerically by solving the classical equation of motion of a current biased JJ with current J close to the critical current J_c , during the excitation process. After the switching the dissipation is not treated self-consistently: a standard dissipation, typical of thermal equilibrium, is assumed in the JJ dynamics, by adding a conductance term in the numerical simulation. We stress that the assumed model for dissipation determines the actual qp branch of the I-V characteristics, but does not affect substantially the switching probability. The switching from the Josephson state to the voltage state in the parameter space $(q, \tau_c, J/J_c)$ is reported in Fig.3.6. Interestingly, we find that for fixed value of q and J/J_c there is an optimum pulse duration to achieve the strongest sensitivity of the junction to the switching process. We show that this is due to the way how the non equilibrium qp's distribution affects the pairing in $S1$.

3.2 Characteristic time scales

As explained in the introduction, there are many characteristic times that regulates the dynamics of an out of equilibrium superconductor. In this section we focus with more detail on the different relaxation-interaction mechanisms and on their characteristic time scales.

The most important phenomena regulating the non-equilibrium photo-response of a Josephson junction are certainly the pair breaking and the related pair

recombination. All the other observed phenomena, such as the quantum photo-fluxonic effect, the Josephson effect between inter-grain weak links, and the subsequent time and space modulation of the order parameter has to be intended as a consequence of the pairs and qp's dynamics in the non equilibrium regime.

The mechanisms involving pair breaking and pair recombination are mainly regulated by the electron-electron and the electron-phonon interaction. Let us start discussing the $e - ph$ interaction. There are two main contributions: the first one is due to the interaction of the qp's of a broken pair with longitudinal phonons(lp), the second one with the transverse phonons(tp): in general, because of Matheisen law

$$\frac{1}{\tau_{e-ph}} = \frac{1}{\tau_{e-lph}} + \frac{1}{\tau_{e-tph}},$$

and in the case of a normal metal one should have

$$\frac{1}{\tau_{e-ph}^n} = \frac{\pi^4 \beta_l T^4}{5} p_F l \left(\frac{\beta}{(p_F u_l)^3} + \frac{3\beta_t}{2(p_F u_t)^2} \right), \quad (3.1)$$

where p_F is the Fermi momentum, l is the mean free path, u_l (u_t) are the longitudinal (transverse) phonon velocities, $\beta_{l(t)} = \frac{2}{3} \varepsilon_F \frac{\nu(0)}{2\rho u_{l(t)}^2}$ is the $e - ph$ interaction kinetic constant, and $\nu(0)$ the density of electronic states at the Fermi level. If $T \sim T_c$ the τ_{e-ph} of a superconductor is of the order of the one of a metallic sample (3.1). By contrast we are very interested in the very low temperatures ($T \ll \Delta$) regime where: [7]

$$\frac{1}{\tau_{e-ph}^s} = \frac{2}{5} \left(\frac{\beta_l}{(p_F u_l)^3} + \frac{3\beta_t}{2(p_F u_t)^3} \right) (p_F l) \Delta^3 (2\pi \Delta T)^{1/2} e^{-\Delta/T}. \quad (3.2)$$

In the low T regime the $e - e$ interaction time takes the form:

$$\frac{1}{\tau_{e-e}^s} = \frac{1}{\tau_{e-e}^n} \frac{\Delta}{\pi T} e^{-2\Delta/T} \quad (3.3)$$

If we introduce the vanishing dimensionless parameter

$$x = \frac{1}{2\Delta} \left(\frac{\pi T \Delta}{2} \right)^{1/2} e^{-\Delta/T}$$

one can show that the $e - ph$ contribution to the pair recombination is of the order of $1/\tau_{e-ph}^s \propto x$ while the contribution due to the $e - e$ interaction of higher order $1/\tau_{e-e}^s \propto x^2$. As a consequence the main recombination mechanism that regulates the 'fastest' part of the superconducting photo-response is the electron phonon interaction: so the main time scale is the $\sim \tau_{e-ph}$. Another important time is the phonon escape time in the substrate

$$\tau_{es} = \frac{4d}{K_{fs} u} \quad (3.4)$$

where d is the transverse dimension of the sample, K_{fs} is the phonon transmission coefficient at the interface between the sample and the substrate and u is the sound velocity in the sample. This is mainly responsible for thermal effects as the temperature relaxation in the sample (bolometric effect). The non equilibrium response is usually in competition with the bolometric response but the last one has longer time scales: this is the reason why usually the photo-response of a superconducting sample in the thermal regime is a biexponential curve: the first part of the signal is fast, on the τ_{e-ph} time scale, then the second one is slower and develops on a time scale τ_{es} . In the case of a JJ, correspondingly to (or a bit before of) the peaks of

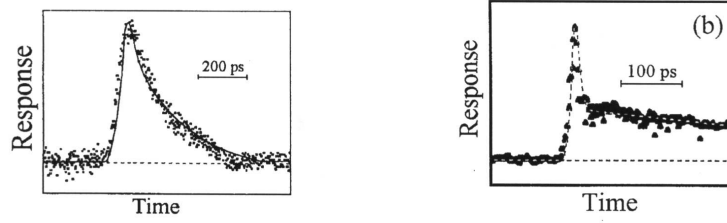


Figure 3.2: Biexponential response for low T_c [left panel] and high T_c samples.

the curves in Fig.s 3.2 the junction can switch in the voltage state: we are mainly interested on the possibility of inducing controlled switchings of the junction so, in the following, we shall focus on the microscopic mechanisms that develop on time scale of the order of (or shorter than) the electron phonon interaction time τ_{e-ph} . Generally speaking we define this regime as *non equilibrium regime*.

3.3 The non-equilibrium qp distribution

3.3.1 Non-equilibrium electron-hole pair excitations induced by optical irradiation

The optical frequencies ($\Omega \sim 100THz$) building the wavepacket of the laser pulse excite $e - h$ pairs at high energies. As explained in the introduction the non-equilibrium arising from the alteration of the qp distribution has a relaxation time τ_E which is long compared to the optical period: $\Omega\tau_E \gg 1$. In addition to this, the duration of the pulse $\tau_c \sim \omega_c^{-1}$ is even shorter than the pair breaking time, so that we expect that, in our case, dissipative phenomena do not affect the coherence of the superconductor on the time scale τ_c .

Qp's are generated as if the metal were normal, because superconductivity doesn't play any role in their excitation at large energies. They propagate according to something very similar to the free particle time-ordered Green's

function g_o (from now on we put $\hbar = 1$):

$$g_o^T(k; t-t') \equiv -i\langle T[c_k(t)c_k^\dagger(t')] \rangle = -ie^{-i\xi(t-t')} [(1-n_k)\theta(t-t') - n_k\theta(-t+t')]. \quad (3.5)$$

Here ξ is the qp energy with momentum k and is measured from the chemical potential μ . n_k is the qp distribution function. We assume that $e-h$ symmetry is conserved in the excitation process, so that μ is not altered with respect to its equilibrium value.

The equation of motion for the Green's function \tilde{g} in the presence of the radiation field is:

$$\left(i\frac{\partial}{\partial t} - \frac{1}{2m}[\vec{\nabla}_r - \frac{e}{c}\vec{A}(\vec{r}, \vec{R}, t)]^2 + \mu \right) \tilde{g}(\vec{r}, \vec{R}, t, t') = \delta(r)\delta(t-t'), \quad (3.6)$$

\vec{r} is the relative space coordinate, while \vec{R} is the center of mass coordinate. The vector potential is a wave-packet centered at frequency Ω according to:

$$\vec{A}(\vec{r}, \vec{R}, t) = \sum_{\pm} \sum_{\vec{p}} \vec{a}_{\pm}(\vec{p}, \vec{R}, t) e^{\mp i(\vec{p}\cdot\vec{r} - \Omega t)}. \quad (3.7)$$

Here \vec{a}_{\pm} are slowly varying 'envelope' functions of \vec{R} on the size of the irradiated spot and on the time scale Ω^{-1} . We look for solutions of Eq.(3.6) in the form:

$$\tilde{g}(\vec{r}, \vec{R}; t, t') = g(\vec{r}, \vec{R}; t, t') + \sum_{\pm} \sum_{\vec{p}} g^{\pm}(\vec{p}, \vec{R}, t, t') e^{\mp i(\vec{p}\cdot\vec{r} - \Omega t)}, \quad (3.8)$$

where g and g^{\pm} are slowly varying functions of \vec{R} and t on the same scales. A similar expansion can be done w.r.to the variable t' . Following Eq. (3.8), a decomposition of Eq.(3.6) into harmonics arises [20, 21]. We define the zero order harmonic equation as the one that does not contain exponentials $e^{\pm i\Omega t}$. By averaging over a period Ω^{-1} we neglect harmonics of order two, or higher. This amounts to include one photon excitation processes only, with released energy \mathcal{E} . Some extra details can be found in Appendix 3C:

$$\left(i\frac{\partial}{\partial t} + \frac{1}{2m}\nabla_r^2 + \frac{e^2}{mc^2} \sum_{\vec{p}, \vec{p}'} \vec{a}_+(\vec{p}', \vec{R}, t)\vec{a}_-(\vec{p}'', \vec{R}, t) e^{i(\vec{p}' - \vec{p}'')\cdot\vec{r}} + \mu \right) g(\vec{r}, \vec{R}, t, t') = \delta(r)\delta(t-t'). \quad (3.9)$$

Fourier transforming w.r.to \vec{r} ($\vec{r} \rightarrow \vec{p} \rightarrow \xi$) we have:

$$\left(i\frac{\partial}{\partial t} - \left(\frac{p^2}{2m} - \mu \right) \right) g(\vec{p}, \vec{R}, t, t') + \frac{e^2}{mc^2} \sum_{\vec{p}', \vec{p}'} \vec{a}_+(\vec{p}', \vec{R}, t)\vec{a}_-(\vec{p}'', \vec{R}, t) g(\vec{p}' - \vec{p}'', \vec{R}, t, t') = \delta(t-t'). \quad (3.10)$$

The radiation field generates and annihilates high energy $e-h$ pairs. Hence we assume that the forcing term conserves the total momentum, $\vec{p}' + \vec{p}'' \sim 0$, but $\vec{p}' - \vec{p}''$ transfers an energy 2ξ to the electrons. Therefore we take the coupling term in the Hamiltonian as:

$$\frac{e^2}{mc^2} \vec{a}_+(\vec{p}', \vec{R}, t) \vec{a}_-(\vec{p}'', \vec{R}, t) \rightarrow q \frac{\omega_c}{\sqrt{\pi}} e^{-\frac{1}{2}\omega_c^2 t^2} \delta(2\xi + \xi') \delta(\vec{p}' + \vec{p}''). \quad (3.11)$$

A Gaussian shaped time dependence has been chosen for the pulse with half-width ω_c^{-1} , while the space dependence has been neglected for simplicity. In Eq. (3.11) the dimensionless quantity appears:

$$q \sim \frac{e^2}{c} \frac{\omega_D}{\Omega} \frac{\mathcal{E}}{m\Omega^2 R_o^2}, \quad (3.12)$$

Where R_o is the laser spot (see Eq.3.21). Here the number of excited $e-h$ pairs is $\sim \Omega/\omega_D$, with ω_D the Debye energy. Experiments [3, 8] show that the energy released by the pulse can be very low, so that we shall always expand in q . In fact, while in the case of an rf radiation $q \sim 1$, in the case of a femtosecond laser pulse $q \sim 0.01 \div 0.1$, corresponding to a fraction of μJ released per pulse on the superconducting surface of $\sim 100 \mu m^2$.

The zero order harmonic equation, Eq. (3.10), becomes :

$$(i\partial_t - \xi) g(\xi; t, t') + q \frac{\omega_c}{\sqrt{\pi}} e^{-\frac{1}{2}\omega_c^2 t^2} g(-\xi; t, t') = \delta(t - t'). \quad (3.13)$$

To derive the non-equilibrium correction to the qp distribution function, the kinetic equation 3.63 (see appendix 3B) should be solved. In place of this we proceed in this chapter in an heuristic way. Our approach lacks mathematical rigor, but singles out directly the role of the laser induced $e-h$ excitations at frequencies $(\Omega - \omega_c, \Omega + \omega_c)$. Our result is valid in the limit of large ξ 's and zero temperature, before relaxation takes place.

We solve Eq(3.13) for the retarded Green's function for $t > 0$ and $-t' \sim 0^+$ by truncating the Dyson equation to lowest order in q :

$$\begin{aligned} g^R(\xi; t, t') &= g_o^R(\xi; t - t') - q \frac{\omega_c}{\sqrt{\pi}} \int dt'' g_o^R(\xi; t, t'') e^{-\frac{1}{2}\omega_c^2 t''^2} g_o^R(-\xi; t'' - t') \\ &= g_o^R(\xi; t - t') + iq \frac{\omega_c}{\sqrt{\pi}} \int_{-\infty}^{+\infty} \frac{d\omega}{2\pi} \frac{e^{-i\omega t}}{\omega - \xi + i0^+} \int_{0^+}^{+\infty} dt e^{i(\omega - \xi)t} e^{-\frac{1}{2}\omega_c^2 t^2} \end{aligned} \quad (3.14)$$

where $g_o^R(\omega) = \{\omega - \xi + i0^+\}^{-1}$ is the Fourier transform of the retarded Green's function. The time integral can be expressed in terms of the function $w[z] \equiv e^{-z^2} \text{erfc}(-iz)$. If we now approximate Eq. (3.14) by evaluating $w[z]$ only at the pole and use the the integral representation of the step function:

$$\theta(t) = \frac{e^{izt}}{2\pi i} \int_{-\infty}^{+\infty} d\omega \frac{e^{-i\omega t}}{\omega - z} \quad \text{for } \Im mz < 0, \quad (3.15)$$

the correction $\delta g^R(\xi, t)$ to g^R for $\xi \gg 0$, which includes the non equilibrium qp's distribution, is:

$$\delta g^R(\xi, t, 0^-) = -\frac{q}{\sqrt{2}} e^{-i(\xi-i0^+)t} w \left[-2\xi/(\sqrt{2}\omega_c) \right] \theta(t), \quad (3.16)$$

From Eq.(3.16) we obtain the time ordered Green's function for $t > 0$, $t' = 0^-$ and $\xi > 0$:

$$g(\xi, t > 0, 0^-) = (-i)e^{-i(\xi-i0^+)t} \theta(t) \left(1 - \frac{q}{\sqrt{2}} \rho \left[2\xi/(\sqrt{2}\omega_c) \right] \right), \quad (3.17)$$

with

$$\rho[x] \equiv e^{-x^2} \frac{2}{\sqrt{\pi}} \int_0^x ds e^{s^2}. \quad (3.18)$$

$\rho[x]$ increases linearly with x and it decreases slowly, as $1/x$, at large arguments. In Eq. (3.17) we have neglected $\Re e[w]$ because $|\xi| \gg 0$.

Eq. (3.17) is to be compared with the free propagating time ordered Green's function of Eq.(3.5) for the same time arguments. Comparison yields the amount by which the distribution function is driven out of the equilibrium:

$$\delta n(\xi) \approx \frac{q}{\sqrt{2}} \rho \left[2\xi/(\sqrt{2}\omega_c) \right] \quad \text{for } |\xi| \gg \Delta_o. \quad (3.19)$$

Note that the expression of Eq. (3.19) changes sign according to $\text{sign} \{\xi\}$. This stems from the assumed $e-h$ symmetry. In turn this implies that no charge imbalance occurs.

Eq. (3.19) can be considered as the non equilibrium distribution for qp's starting at the time of the pulse $t \sim 0^+$.

In the absence of relaxation, a change in the available qp density of states follows. Because $(g^R(\xi, \omega))^* = g^A(\xi, \omega)$ if ω is real, the correction to the density of state $\delta\nu(\xi)$ is:

$$\delta\nu(\xi) = -\frac{1}{\pi} (\delta g^R - \delta g^A) (\xi, 0^+) \approx \frac{q}{\pi\sqrt{2}} \rho \left[2\xi/(\sqrt{2}\omega_c) \right] \quad \text{for } \xi > 0. \quad (3.20)$$

The first stages of the relaxation process involve the inelastic diffusion of qp's in the medium which is qualitatively discussed in the next section.

3.3.2 Inelastic diffusion of the qp's at initial times

Let us discuss shortly what was neglected in the derivation of the change in the equilibrium qp distribution $\delta n(\xi)$ given by Eq.(3.19).

The single particle Green's function $g(p, R, t, t')$ is assumed to be a slowly varying function of $(t+t')/2 = \bar{t}$ and a fast varying function of $t-t'$. Fourier transforming w.r.to the latter variable (see Appendix 3C) there is an ω

dependence even in the stationary case (i.e. with no \bar{t} dependence). This ω dependence is determined by the frequency dependent Eliashberg $e - ph$ coupling $\alpha^2 F(\omega)$ and is contained in the $e - ph$ self-energy $M_{e-ph}(\omega)$ [22]. Accordingly, the complex qp renormalization parameter $Z_n(\omega)$ is defined by $[1 - Z_n(\omega)]\omega = M_{e-ph}(\omega)$. In our derivation we have not included the self-energy, so that we are implicitly taking $Z_n(\omega) \rightarrow 1$, what applies for large $\omega (\sim \Omega)$, prior to relaxation.

Moreover, because the system is in the superconducting state, we should have dealt with the corresponding superconducting parameter $Z_s(\omega)$. The latter is derived together with the complex gap parameter $\Delta(\omega, \bar{t})$ with $\Delta(\Delta_o, \bar{t} = 0^-) = \Delta_o$ from the coupled Eliashberg equations (we drop the overline on t in the following).

The procedure of averaging over the fast time scale Ω^{-1} singles out two frequency components of $\Delta(\omega, t)$ and $Z_s(\omega, t)$: $\omega = \Delta_o$ and $\omega = \Omega$ as a consequence a retardation arises from frequencies up to $10\omega_D$ is neglected. Ω is so large that Z_s and Z_n do not differ sizeably. In fact, their real parts differ by a quantity of the order of $(\omega_D \Delta_o / \Omega^2)^2 \ln(\omega_D / \Delta_o)$. $\Delta(\Omega, t)$ itself is expected to be so small that it can be neglected altogether. Indeed, in connection with Eq. 3.53 of Appendix 3C we do not discuss the self-energy terms. Of course this approximation breaks down on the time scale of the $e - ph$ relaxation.

Let us now discuss the t dependence. The equation of motion for the qp distribution function $n(\vec{R}, t)$ is derived in Appendix 3B, where we take $n_T = 0$, because we neglect charge imbalance corrections.

In averaging over a few optical periods the kinetic equation for δn_L , the electric field \vec{E} averages to zero. The qp relaxation is governed by the collision integral $I[n(\vec{R}, t); t]$ which describes the inelastic processes. In Ref. [16] the cascade of the $e - h$ excitations due to inelastic scattering is studied in detail. Two stages occur. In the first stage e-e interactions multiply the number of excited qp's in the energy range from Ω to ω_D which is taken as the cutoff energy of the pairing interaction. This happens in a time interval short w.r.to the pulse duration ($\sim 10^{-14}s$). In the second stage a much slower relaxation process takes place, by which the energy of the qp's reaches Δ . This process involves electron-phonon scattering on a time scale $\hbar\omega_D^2/\Delta^3 \sim 10^2 ns$ which is much larger than any time scale in our problem. Here we shall leave this stage aside. In the time interval we are concerned with, we have little relaxation and the energies involved are $\omega \gg \Delta$.

According to Eq. (3.61) the distribution function prior to relaxation deviates from the equilibrium value by the quantity $\delta n_L = -2\delta n(\xi)$ given by Eq. (3.19). There is no explicit dependence on ω in our correction, because retardation is neglected. Still qp's diffuse in space inside the junction over a characteristic distance $R_o \sim \sqrt{D\tau_{e-e}}$, where D is the diffusion coefficient.

Hence

$$\delta n_L(\xi, \vec{R}, t) = -2 \frac{R_o^2}{R_o^2 + Dt} \delta n(\xi) e^{\left\{ -\frac{R^2}{R_o^2 + \frac{D}{T}} \right\}} . \quad (3.21)$$

For relatively large times $\tau_{e-ph} \gg t \gg R_o^2/D$ we shall ignore the spatial dependence by putting $R = 0$. This is the first step of a perturbative analysis of the non equilibrium distribution functions.

3.4 Changes of the superconductive properties on the time scale ω_c^{-1}

3.4.1 The correction to the gap parameter

In this Subsection we derive the Keldysh Green's function in the presence both of a time dependent gap $\Delta(t)$ and of a non-equilibrium qp distribution as given by Eq. (3.21). We assume weak coupling superconductivity and we neglect here the frequency dependence of the $e - ph$ coupling parameter λ . This follows by neglecting the retardation effects mentioned in Sec. 3.3.2 on time scales much faster than the $e - ph$ relaxation time. From the Keldysh Green's function \hat{g}^K (where the hat denotes matrix representation in the Nambu space, see Appendix 3C) we recalculate the gap self-consistently, according to the formula:

$$\Delta(t) = -\frac{\nu(0)\lambda}{4} \int_{-\infty}^{\infty} \langle f^K(\vec{p}/|\vec{p}|, \omega, t) \rangle_{\vec{v}_F} d\omega . \quad (3.22)$$

The average over the direction of the momenta on the Fermi surface is indicated. The Keldysh Green's function in thermal equilibrium is:

$$\hat{g}_o^K = \tanh \frac{\beta\omega}{2} (\hat{g}^R - \hat{g}^A) . \quad (3.23)$$

Out of equilibrium we use the definition:

$$\hat{g}^K = \hat{g}^R \hat{h} - \hat{h} \hat{g}^A . \quad (3.24)$$

However, \hat{h} defined in Appendix 3B is here diagonal, because we assume that no charge imbalance arises. Hence, up to first order in q ,

$$\delta \hat{g}^K \approx n_L^0 (\hat{g}_{ad}^R - \hat{g}_{ad}^A) + \delta n_L (\hat{g}_o^R - \hat{g}_o^A) . \quad (3.25)$$

Here $n_L^0 = \tanh(\beta\omega/2)$ is the equilibrium distribution and $\hat{g}_{ad}^R - \hat{g}_{ad}^A$ is introduced in Appendix 3C (see Eq.3.65) and is discussed in the following.

We now first derive the contribution coming from the second term of Eq. (3.25). We start from the outset using Eq. (3.21) and performing the quasiclassical approximation. The latter involves an energy integration:

$$\delta n_L \cdot (\hat{g}_o^R - \hat{g}_o^A) \equiv \frac{i}{\pi} \int_{-\infty}^{+\infty} d\xi \delta n_L(\xi, t) \cdot (\hat{g}_o^R(\xi, \omega, t) - \hat{g}_o^A(\xi, \omega, t)) . \quad (3.26)$$

Using the equilibrium BCS functional forms, the Green's functions appearing on the diagonal of $\hat{g}^{A/R}$ are [25]:

$$g^R(\xi, \omega) = \frac{u_\xi^2}{\omega - E_\xi + i0^+} + \frac{v_\xi^2}{\omega + E_\xi + i0^+}, \quad (3.27)$$

$$g^A(\xi, \omega) = \frac{u_\xi^2}{\omega - E_\xi - i0^+} + \frac{v_\xi^2}{\omega + E_\xi - i0^+}. \quad (3.28)$$

The equilibrium values for u_ξ and v_ξ are:

$$u_\xi^0 = \left(\frac{1}{2} \left(1 + \frac{\xi}{E} \right) \right)^{\frac{1}{2}}, \quad v_\xi^0 = \left(\frac{1}{2} \left(1 - \frac{\xi}{E} \right) \right)^{\frac{1}{2}}, \quad (3.29)$$

with $E = \sqrt{\xi^2 + |\Delta_o|^2}$. From now on we shall drop the subscript in the equilibrium gap parameter (i.e. $\Delta \equiv \Delta_o$ if no time dependence is indicated explicitly). Because the factor $\delta n_L(\xi, t)$ appearing in Eq.(3.26), as given by Eq. (3.21) is odd w.r. to ξ only the second term in u^2 and v^2 survives, when the integral in Eq. (3.26) is performed. Let us consider the case $\omega > \Delta$ only and specialize Eq. (3.26) to its diagonal part. According to Eq. (3.21) we have:

$$\begin{aligned} \Re \{ \delta n_L \cdot g_o^R \} = \Re \left\{ -\frac{\sqrt{2}i}{\pi} q(t) \int_{-\infty}^{+\infty} d\xi \frac{\xi}{2E} \rho \left[2\xi / (\sqrt{2}\omega_c) \right] \left(\frac{1}{\omega - E + i0^+} + \right. \right. \\ \left. \left. - \frac{1}{\omega + E + i0^+} \right) \right\} = -q(t) 2\sqrt{2} \rho \left[2(\omega^2 - |\Delta|^2)^{\frac{1}{2}} / (\sqrt{2}\omega_c) \right]. \quad (3.30) \end{aligned}$$

Here we have defined the function $q(t)$:

$$q(t) = q \frac{\pi R_o^2}{R_o^2 + Dt}. \quad (3.31)$$

Doing similarly for g^A and subtracting, the imaginary part cancels:

$$\delta n_L \cdot (g_o^R - g_o^A) = -q(t) 4\sqrt{2} \rho \left[2(\omega^2 - |\Delta|^2)^{\frac{1}{2}} / (\sqrt{2}\omega_c) \right], \quad \text{for } \omega > \Delta. \quad (3.32)$$

Here the largest contribution of the non-equilibrium excitations arises from $\omega \sim \omega_c$. On the other hand ω_c can be larger or smaller than ω_D .

Now we evaluate the correction due to $\hat{g}_{ad}^R - \hat{g}_{ad}^A$. In Appendix 3C we show that an *adiabatic solution* of the motion equation of $g^{R,A}$ is possible, in the sense that the functional dependence on ω is the same as the equilibrium one, but the gap parameter changes slowly with time (see Eq. (3.65)):

$$\hat{g}_{ad}^{R(A)} = +(-) \frac{\hat{M}}{\sqrt{(\omega \pm i0^+)^2 - |\Delta(t)|^2}} \quad (3.33)$$

with

$$\hat{M} = \begin{pmatrix} \omega & \Delta(t) \\ -\Delta(t)^* & -\omega \end{pmatrix}. \quad (3.34)$$

This functional form for the R/A functions is obtained if the $e-h$ symmetry is maintained and if one neglects the diffusion in space-time which will be mainly important at intermediate times [16].

This adiabatic approximation in the advanced and retarded Green's functions allows us to write the Keldysh propagator in the form:

$$g^K = g_{ad}^K - q(t)4\sqrt{2}\rho \left[2(\omega^2 - |\Delta|^2)^{\frac{1}{2}}/(\sqrt{2}\omega_c) \right]. \quad (3.35)$$

To calculate f^K we resort to the analogous of Eq.(3.64) which is valid for \hat{g}^K : $f^K = g^K \Delta/\omega$. Hence we have:

$$f^K = f_{ad}^K - q(t)4\sqrt{2}\frac{\Delta}{\omega}\rho \left[2(\omega^2 - |\Delta|^2)^{\frac{1}{2}}/(\sqrt{2}\omega_c) \right] \quad \text{for } \omega \gg \Delta. \quad (3.36)$$

Now we insert Eq. (3.36) into Eq. (3.22) and consider the linear correction to the gap of the irradiated contact according to :

$$\Delta(t) = \Delta + \delta\Delta(t).$$

Here $\delta\Delta(t)$ is the correction to the unperturbed gap parameter Δ due to the radiation. In the limit of zero temperature, up to first order in $q(t)$ and Δ/ω_D , $\delta\Delta(t)$ is given by:

$$\frac{\delta\Delta(t)}{\Delta} = -\frac{q(t)4\sqrt{2}}{\ln(2\omega_D/\Delta) - 2 + \mathcal{O}(\Delta^2/\omega_D^2)} \int_{\Delta}^{\omega_D} \frac{d\omega}{\omega} \rho \left[2(\omega^2 - |\Delta|^2)^{\frac{1}{2}}/(\sqrt{2}\omega_c) \right]. \quad (3.37)$$

It is interesting to note that the correction arising from the adiabatic dynamics has the role of renormalizing the coupling $q(t)$ via the prefactor $-[\ln(2\omega_D/\Delta) - 2]^{-1}$. This prefactor is negative because $\ln(2\omega_D/\Delta) > 2$. Therefore Eq. (3.37) shows that the gap of the irradiated superconductor is decreased due to the non equilibrium distribution of the qp excitations.

Eq. (3.37) has the same structure as Eq. (14) of Ref. [23]. There is a striking difference however. The inverse square root singularity at the gap threshold, which shows up in Eq.(14) of Ref. [23] does not appear in Eq. (3.37).

The inverse square root singularity originates from the unperturbed density of states at the excitation threshold and is usually present in non-stationary superconductivity [24]. It is responsible for retardation and oscillating tails. In our case, the gap threshold plays a little role, because we do not have extensive pair-breaking and q.p. generation at energies $\sim \Delta$. Hence, just a tail $\sim 1/\omega$ survives in the integrand.

In Fig.(3.3) the variation of the gap immediately after the pulse ($t \sim 0$), is plotted vs the inverse of the pulse duration ω_c in units of Δ , for different

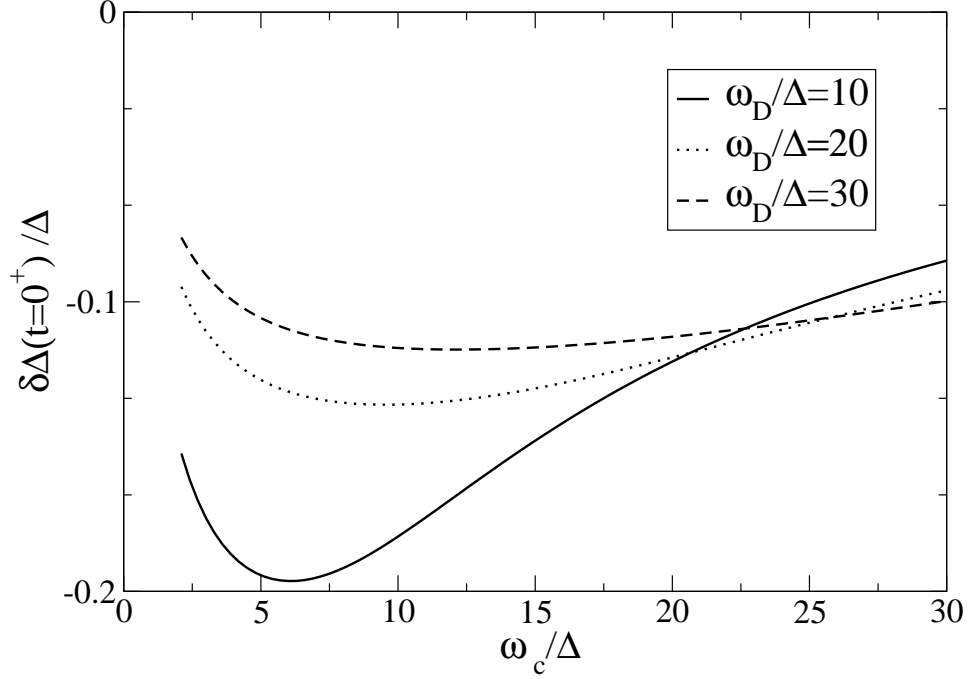


Figure 3.3: Variation of the gap immediately after the pulse vs the inverse of duration of the pulse $\tau_c^{-1} = \omega_c$ in units of Δ . Our approximations break down for very low ratios ω_c/Δ (long pulses). On the other hand, large ω_c/Δ represent very short pulses: this situation is unrealistic with the available optical devices.

values of ω_D . Our approximations are not valid when the pulse becomes too long (very low values of ω_c/Δ). For longer pulses the integrand in Eq. (3.37) has a narrow peak lined up at the gap threshold. In this case the inverse square root singularity in the density of states at the gap threshold is important and the adiabatic approximation Eq.(3.35) breaks down.

For shorter pulses the peak becomes broader and is centered at larger ω 's. If the integration range is small, the result is quite sensitive to the location of the peak (see full line in Fig. (3.3)): most remarkably, a minimum appears in the curve when the pulse is rather long ($\omega_c/\omega_D < 5$). By contrast, the gap correction is rather flat w.r.to changes of ω_c when ω_D/Δ is larger (broken and dotted line in Fig.3.3).

3.4.2 Correction to the Josephson current

In this subsection we derive the correction to the Josephson current arising from the two terms of the anomalous propagator $f(R, t, t')$ given by Eq. (3.36). Eq.s(3.35, 3.36) show that the non equilibrium Keldysh Green functions of the irradiated superconductor can be separated into two terms. The

first one is what we call the 'adiabatic' contribution, while the second one is strongly dependent on the non equilibrium qp's distribution function and is first order in $q(t)$.

Within the linear response theory in the tunneling matrix element $|T_o|^2$, the pair current at zero voltage is:

$$J(\vec{R} = 0, t) = 2e|T_o|^2 \int_{-\infty}^{\infty} dt' e^{2ieV(t-t')} \left(f_1^{>\dagger}(0, t, t') f_2^A(0, t', t) + f_2^{R\dagger}(0, t, t') f_1^<(0, t', t) \right), \quad (3.38)$$

where $|T_o|^2$ is assumed to be independent of energy, for simplicity. The current of Eq. (3.38) is evaluated at the junction site, defined by $\vec{R} = 0$ and the irradiated superconducting layer $S1$ is labeled by 1 here, while the superconductor unexposed to radiation $S2$ is labeled by 2. The perturbed Josephson current has an adiabatic term $J^{ad}(t)$ obtained by inserting the first term of Eq. (3.36) into Eq. (3.38), plus a correction $\delta J(t)$ arising from the second term of Eq. (3.36). Using the definitions $f^K = f^> + f^<$ and $f^R - f^A = f^> - f^<$ and expanding to lowest order in $q(t)$ the adiabatic critical current is:

$$J^{ad} = J_c^{ad}(t) \sin(\varphi), \quad J_c^{ad}(t) = \frac{\pi\hbar\Delta}{2eR_N} \left(1 + \frac{\delta\Delta(t)}{2\Delta} \right), \quad (3.39)$$

where R_N is the normal resistance, Δ is the unperturbed gap parameter of both contacts (assuming $\Delta_1 = \Delta e^{i\varphi}$ and $\Delta_2 = \Delta$ in the absence of laser perturbation), and $\delta\Delta(t)/\Delta$ is given by Eq. (3.37). Denoting by δf^K the second term of Eq. (3.36) the correction $\delta J(t)$ is:

$$\delta J(t) = e|T_o|^2 \int_{-\infty}^{\infty} d\omega \left((\delta f^K(\omega + ieV))_1^\dagger f_2^A(\omega - ieV) + (f^R(\omega + ieV))_2^\dagger (\delta f^K(\omega - ieV))_1 \right). \quad (3.40)$$

At zero temperature and $V = 0$, this gives:

$$\delta J(t) = \frac{\pi\hbar}{eR_N} \int_{-\infty}^{\infty} d\omega \frac{|\Delta|^2 q(t)}{\omega} \rho \left[2(\omega^2 - |\Delta|^2)^{\frac{1}{2}} / (\sqrt{2}\omega_c) \right] \left(\frac{e^{-i\varphi}}{\sqrt{(\omega + i0^+)^2 - |\Delta|^2}} + \frac{e^{i\varphi}}{\sqrt{(\omega - i0^+)^2 - |\Delta|^2}} \right). \quad (3.41)$$

which is zero for parity. This conclusion holds because we assume that no charge imbalance occurs. If $V \neq 0$ the contributions to the integral evaluated in the complex plane are finite.

$\delta J(t)$ is a $\cos\varphi$ -like correction. In the unperturbed Josephson effect a ' $\cos\varphi$ ' term only arises when $V > 2\Delta$ [2]. By contrast, our calculation shows that a $\cos\varphi$ term can arise in the Josephson current with a small nonzero voltage in the presence of an ultrafast laser pulse.

3.5 Classical dynamics of the irradiated junction

In this section we integrate the classical equation of motion of the irradiated junction numerically. Here we discuss the possibility that the laser pulse induces switches of the junction from the zero voltage state, to the resistive state. The characteristics of the Josephson junction for a finite voltage, is obtained within the RCSJ (resistively and capacitively shunted junction) model [2]. The phase of the superconductor S2 is taken as the reference phase.

In the absence of the pulse, the junction is biased by a current constant in time J_b . As discussed in the previous Section, the pulse activates the superconductor S1 by varying its gap dynamically in time.

Consequently, a voltage V arises at the junction, related to the dynamics of the phase difference $\varphi(t)$. The latter solves the differential equation:

$$\ddot{\varphi} + Q_0^{-1}\dot{\varphi} + \frac{J_c^{ad}(t)}{J_c^o} \sin \varphi(t) = \gamma, \quad (3.42)$$

where $\gamma = J_b/J_c^o$ and $J_c^o = (\pi\hbar\Delta)/(2eR_N)$ is Josephson critical current of the unperturbed junction. The time-dependent driving term is deduced from Eq. (3.39). We assume $\omega_{pJ0} > \tau_E^{-1}$ ($\tau_E^{-1}(Nb) \sim 7GHz$), where ω_{pJ0} is the plasma frequency at zero bias. This condition is satisfied for high quality Nb junctions, where ω_{pJ0} is in the range $40GHz \div 120GHz$ [26], but it holds also if we take into account the dependence of the plasma frequency on γ : $\omega_{pJ} = \omega_{pJ0}(1 - \gamma^2)^{1/4}$. At $\gamma = 0.98$ the term $(1 - \gamma^2)^{1/4} = 0.44$: this still gives a large plasma frequency for the given range. In any case the plasma frequency changes marginally when the energy is degraded into heat if q is small. Under this conditions the relaxation process occurs long after the switch to resistive state.

In Eq. (3.42), $Q_0 = \omega_{pJ0}R(\varphi)C$ is the quality factor, where $R(\varphi)$ is the junction intrinsic resistance, which is in general a non-linear function of the phase. The dissipative $Q_0^{-1}\dot{\varphi}$ term includes thermal incoherent pair breaking effects at equilibrium. In the simulation we use both a constant junction resistance R and a patchwork model given by [27]:

$$Q^{-1}(\dot{\varphi}) = Q_0^{-1} \frac{\omega_{pJ}}{\Delta} \frac{(\frac{\dot{\varphi}\omega_{pJ}}{\Delta})^N}{1 + (\frac{\dot{\varphi}\omega_{pJ}}{\Delta})^N} \quad (3.43)$$

with $N = 16$ and $Q_0^{-1} = 0.636$, which corresponds to a normal resistance above the gap $R_N = (\omega_{pJ}\varphi_0)/(cJ_c^0)$. In general we ignore the direct dependence of $R(\varphi)$ on the phase. By the way, Q should also depend on the energy which is released by each single laser pulse due to the incoherent pair breaking processes. However, under the hypothesis that this energy is very low we assume that the quality factor, due to the optically induced normal resistance of the sample, is constant within the considered energy range.

Actually, in the presence of the pulse, also the current contribution of Eq. (3.41) should be plugged into the l.h.s. of Eq. (3.42). This current term depends on the voltage $V = \dot{\varphi}$. However, in view of the fact that in this work we are only concerned with the switching of the junction out of the zero voltage state, we do not derive the full dynamics of the phase self-consistently.

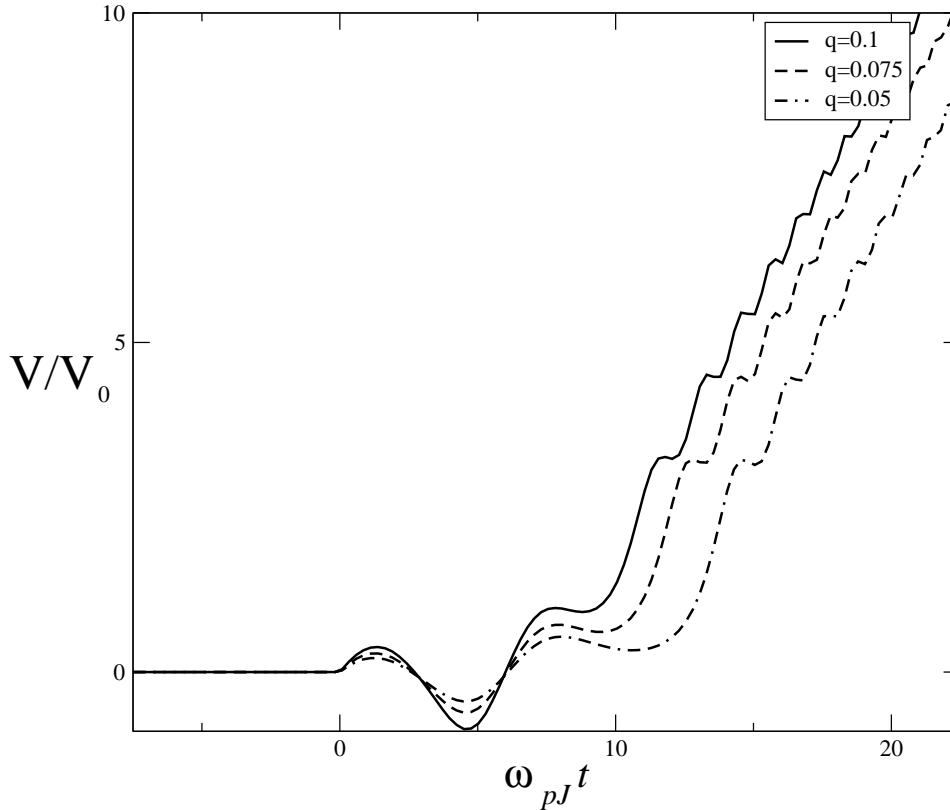


Figure 3.4: Voltage behavior in time for different energy released on the sample and the quality factor $Q = 100$. The voltage is normalized to $V_0 = \omega_{pJ}\varphi_0/c$.

In Fig. (3.4) we show the voltage just after the pulse for different values of the released energy. The time evolution of the voltage is sketched for some successfully induced switches. The junction starts in the zero voltage state. At $\omega_{pJ}t = 0^+$ it is irradiated by the laser pulse. There are few oscillations at frequency ω_{pJ} before the switching occurs, followed by an overall increase of the oscillating voltage. The larger is q the faster is the switch. If no switch is induced the junction remains in the zero voltage state: the phase and the voltage are weakly perturbed by the radiation and show decaying plasma oscillations around their equilibrium values.

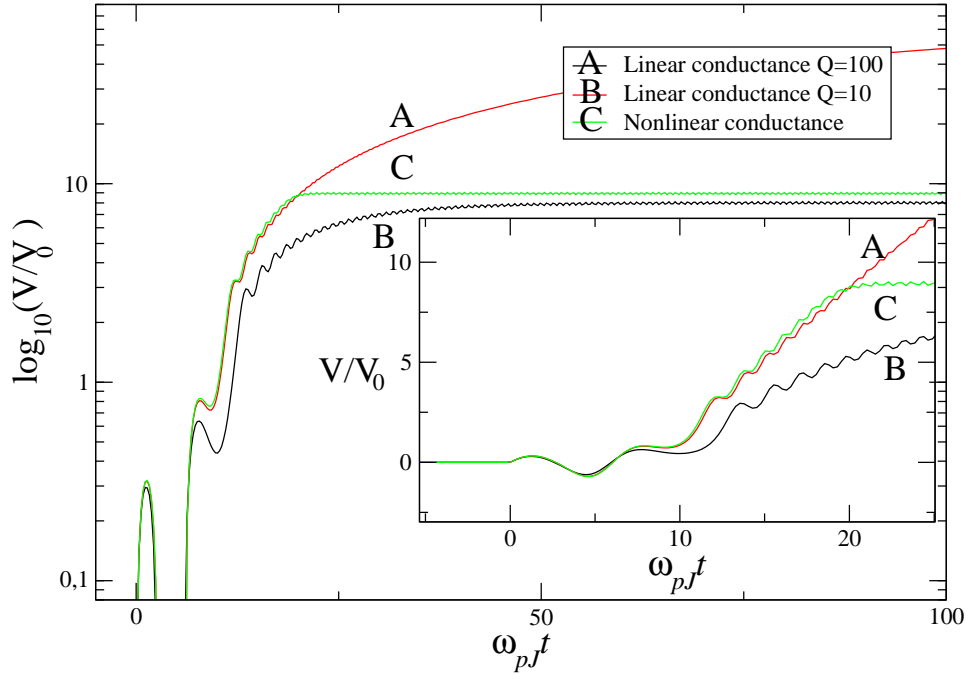


Figure 3.5: Voltage behavior in time with different quality factors Q in the linear conductance model (A,B) and the non-linear conductance model as given by Eq. (3.43) (C). The voltage is normalized to $V_0 = \omega_p J \varphi_0 / c$.

In Fig.(3.5) we show the approach to the gap voltage for different Q values and two different conductance models. Except for the asymptotic trend, the curves for $Q = 10$ (B) and $Q = 100$ (A) show a similar behavior. The non-linear conductance gives rise to a more pronounced shoulder in the curve after the first increase of the voltage. The first phase oscillation at frequency $\omega_p J$ are largely independent of the dissipation model used.

The switching of the junction out of the zero voltage state depends on the bias current J_b , on the released energy per pulse q , and on the pulse duration. In Fig.(3.6) we sketch the switching front in the parameter space a) $(\omega_c/\Delta, q)$ at fixed γ and b) (γ, q) at fixed ω_c/Δ , for $Q = 100$ and $\omega_D/\Delta = 10$. For each point $(q, \omega_c/\Delta, \gamma)$ we calculate $J_c^{ad}(t)$ from Eq.s(3.39, 3.37). Next we plug the result into the equation of motion Eq. (3.42). Numerical simulation of the dynamics shows whether the junction is stable in the zero voltage state, or it switches to a running state. The points of the curve mark the frontier between the two behaviors. The full curve is just a guide for the eye. The non-monotonicity of $\delta\Delta(t)/\Delta$ with the pulse duration, appearing in Fig.(3.3) forces a similar behavior in Fig.(3.6a). This means that the pulse duration can be appropriately chosen, in order to optimize the junction switching with the laser field. Indeed, if ω_c/Δ is of the order of $5 \div 15$ a very small

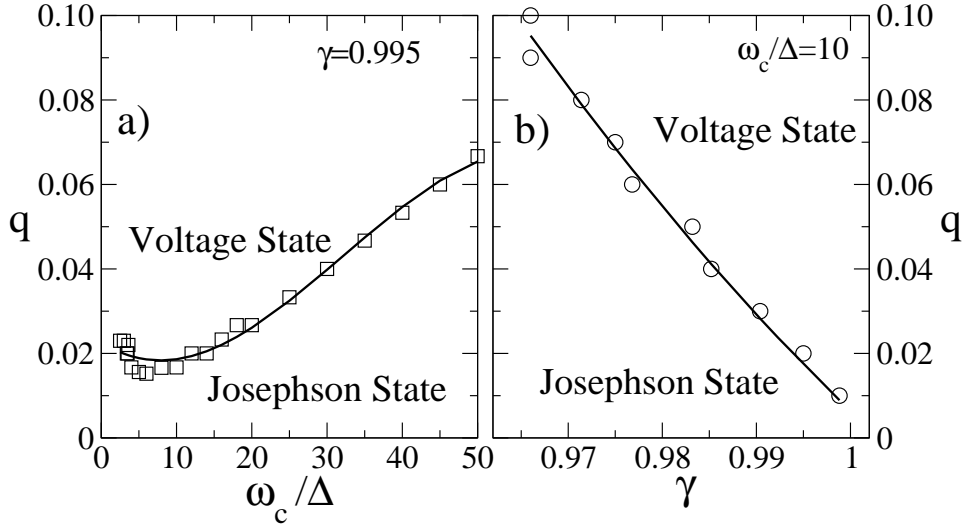


Figure 3.6: Switching front in the parameter space a) $(\omega_c/\Delta, q)$ at fixed current bias $\gamma = J_b/J_c^o$ and b) (γ, q) at fixed ω_c/Δ , for $Q = 100$ and $\omega_D/\Delta = 10$. The full curves have been added as a guide for the eye: they mark the border between the zero voltage (Josephson) state and the voltage state. q is the coupling strength due to the laser pulse.

released energy is required for the switching of the junction, because the order parameter is much depressed by the laser pulse in that range. Out of this range the shorter is the pulse the larger is the energy required. By contrast a slightly larger released energy is also required for longer pulses ($\omega_c/\Delta < 5$). This is because longer pulses imply a more extended change in the qp distribution up to higher energies. As a consequence the maximum of the function ρ of Eq. 3.37 contributes less to the correction of the gap parameter. Nevertheless caution should be used in considering our results for longer pulses because of the neglected relaxation effects.

3.6 Discussion

The effect of an ultrafast laser pulse on the superconducting coherence at a Josephson Junction allows studying an unexplored regime in non equilibrium superconductivity. Non-equilibrium in superconductivity is usually addressed in the context of one of the possible applications of Josephson junctions, that is radiation/particle detectors. Highly energetic radiation produces pair breaking and quasiparticles which, in turn, excite a large number of them, in a cascade process. Usually the setup is optimized such that the qp's can be collected and contribute to the current across the junction with a sharp signal. Losses are due to degradation of the released energy into

heat during the relaxation process. To achieve optimum performance, the Josephson current is usually suppressed by applying a magnetic field. This picture has been discussed quantitatively by examining the quasiclassical kinetic equation for the non equilibrium qp distribution function [16].

In this work we have concentrated on a quite different time scale: the one fixed by the duration of an ultrafast laser pulse. While the relaxation process mentioned above takes place on a time scale of $0.1 \div 100$ ns, we have considered a laser perturbation lasting at most hundreds of femtoseconds. This type of tool can be quite valuable for future applications, because fast pulses in flux and gate voltages are extremely important when processing information in superconducting quantum computing devices (qubits) [28]. Indeed, finite rise and fall times of pulses may result in a significant error in dynamical computation schemes [29]. The carrier frequency of the laser is ~ 100 THz and the optical radiation is expected to produce many $e-h$ pair excitations as it would occur in a normal metal. In our case, qp's do not have enough time to relax down to the typical phonon frequencies ($\sim \omega_D$) and to heat the sample before the stimulated switching occurs. We do not wish to collect qp's either, what requires a suitable geometry of the junction.

Instead, we have addressed the question how the critical current for Josephson conduction J_c can be coherently affected by a laser induced small perturbation with an unrelaxed non-equilibrium distribution of qp's, that is before the dissipative response sets in.

Using the quasiclassical approach to non-equilibrium Keldysh Green's functions, we have shown that, if the temperature is very low, the order parameter of the irradiated superconductor can respond adiabatically to a weak perturbing signal. A non equilibrium distribution of qp's is generated and consequently J_c is temporarily reduced (see Eq. (3.39) and Fig(3.3)). This reduction can drive switches of the junction out of the zero voltage state. In our approach the retardation effects which arise from the frequency dependence of the $e-ph$ coupling $\alpha^2 F(\omega)$ and from the actual features of $e-ph$ relaxation processes have been neglected. They come into play on a time scale longer than the duration of the laser pulse, $\omega_c^{-1} \sim \tau_c$. Indeed in the equation of motion for the Keldysh Green's function reported in Appendix 3B and 3C the role of the frequency dependent self-energy terms has not been discussed.

The parameter which is related to the energy released by the radiation and describes the strength of the perturbation is q . In our case, the switches can be induced by pulses with $q \sim 0.05$, with relatively low values of $\omega_c/\Delta \sim 10$, by polarizing the junction very close to the critical current.

In experiments on laser induced non-equilibrium effects in superconductors [3] or Josephson junctions [4], the released energy is of few μJ , which corresponds to values of q between 0.25 and 0.67 for the given laser spot dimension. In our case for $q = 0.05$ the switching occurs at 98% of the critical current. Therefore, a coherent effect of the laser on the superconducting

condensate is sufficiently large to be observed in sensitive experiments monitoring the escape rate [11,12]. These experiments can appreciate very small variations of the critical current, if temperature is kept low and the released energy is sufficiently small, so that sizeable heating effects do not occur.

We have also found a ‘ $\cos \varphi$ ’ contribution to the Josephson conduction due to the presence of the excited qp’s (see Eq. (3.41)). This term, which will be examined in detail elsewhere, vanishes at zero V, T , provided excitations do not generate charge imbalance. A similar term, proportional to the voltage V , can be derived also in the BCS theory of Josephson conduction [2] but it is identically zero as long as $V \leq 2\Delta/e$, because of the absence of qp’s at zero temperature. This is not the case here, due to the presence of a non-equilibrium qp distribution.

Our derivation of Eq.s(3.37,3.39,3.41) assumes that no charge imbalance is created by the perturbation. This is because the radiation excites $e - h$ pairs and the pulse duration is short enough, so that pair breaking is very limited. The absence of charge imbalance is a crucial approximation in our solution scheme. This assumption allows us to keep the unperturbed functional form of the quasiclassical Green’s functions and to insert a time dependent gap parameter $\Delta(t)$ in their expressions. $\Delta(t)$ follows the perturbation adiabatically and is determined by the non equilibrium $e - h$ pair distribution produced by the pulse. Charge imbalance corrections should be reconsidered, but they are usually expected to have a minor effect on the dynamics of the junction.

To complete the picture, we have simulated the classical dynamics of the junction switching to the resistive state. This picture is only valid over few periods $2\pi/\omega_{pJ}$ on time duration less than the electron-phonon relaxation time.

Precursor oscillations can be seen in Fig. (3.4) at the Josephson plasma frequency ω_{pJ} . Most remarkably the duration of the pulse can be optimized in order to induce controlled coherent switching at the minimum possible released energy \mathcal{E} .

Appendix 3A

Quasiclassical time dependent Green's function approach

In normal metals the classical kinetic equation is applicable when the electron mean free path is large with respect to the wavelength of the electrons. In superconductors in addition to the excitation wavelength there is another important parameter: the size of a pair or the correlation length. Therefore the standard kinetic equation is applicable only in the cases the mean free path and the range in which the order parameter changes, greatly exceeds the correlation length. Using these argument Larkin and Ovchinnikov [30] had obtained the quasiclassical equations in the non stationary case as a generalization of the stationary case [31]. In these appendixes we reproduce Larkin and Ovchinnikov argument in a different way in order to simplify the time averages and all the difficulties related to the ultrafast laser signal we intend to study.

The quasiclassical Green's function solve the Eilenberger form of the Gorkov equations which can be expressed by the following commutator [18]:

$$\left[\left(\check{G}_0^{-1} - \check{\Sigma} - \check{\Delta} \right), \check{G} \right]_{\otimes} = 0 . \quad (3.44)$$

The matrix Green's function \check{G} in the Keldysh space is:

$$\check{G} = \begin{pmatrix} \hat{G}^R & \hat{G}^K \\ \hat{0} & \hat{G}^A \end{pmatrix} , \quad (3.45)$$

where, in turn, $\hat{G}^R, \hat{G}^A, \hat{G}^K$ are the retarded, advanced and Keldysh Green functions in the Nambu space:

$$\hat{G}^{(A,R,K)} = \begin{pmatrix} g^{(A,R,K)} & f^{(A,R,K)} \\ -f^{(A,R,K)\dagger} & -g^{(A,R,K)\dagger} \end{pmatrix} . \quad (3.46)$$

Here f is the anomalous propagator and its Keldysh component defines the gap:

$$\Delta = \frac{\nu(0)\lambda}{4} \int_{-\infty}^{+\infty} d\omega \langle f^K \rangle_{\vec{v}_F} . \quad (3.47)$$

The average $\langle \rangle_{\vec{v}_F}$ denotes angular averaging over the Fermi surface. The gap matrix $\check{\Delta}$ is defined as:

$$\check{\Delta} \equiv \begin{pmatrix} \hat{\Delta} & 0 \\ 0 & \hat{\Delta} \end{pmatrix} , \quad \hat{\Delta} = \begin{pmatrix} 0 & -\Delta \\ \Delta^* & 0 \end{pmatrix} . \quad (3.48)$$

The self-energy $\check{\Sigma}$ includes elastic and inelastic scattering with impurities and gives rise to relaxation processes. The commutator is evaluated w.r. to

the \otimes operation, which implies integration over the intermediate variables according to:

$$\check{G}_0^{-1} \otimes \check{G}_0 \equiv \int d2 \check{G}_0^{-1}(1, 2) \check{G}(2, 1'), \quad (3.49)$$

where $1 \equiv (\vec{r}_1, t_1)$. The differential operator $\check{G}_0^{-1}(1, 2)$ is

$$\check{G}_0^{-1}(1, 2) = \left[i\check{\sigma}_3 \partial_{t_1} - \frac{1}{2m} \left(\vec{\nabla}_{\vec{r}_1} - i\frac{e}{c} \check{\sigma}_3 \vec{A}(1) \right)^2 + (e\phi(1) - \mu) \check{I} \right] \delta(1 - 2). \quad (3.50)$$

Here

$$\check{\sigma}_i \equiv \begin{pmatrix} \hat{\sigma}_i & 0 \\ 0 & \hat{\sigma}_i \end{pmatrix}, \quad \check{I} \equiv \begin{pmatrix} \hat{I} & 0 \\ 0 & \hat{I} \end{pmatrix}, \quad (3.51)$$

where $\hat{\sigma}_i (i = 1, 2, 3)$ are the usual Pauli matrices and \hat{I} the 2×2 unit matrix. The vector potential $\vec{A}(1)$ describes the laser radiation field of frequency Ω :

$$\vec{A}(1) = \sum_{\pm} \sum_{\vec{p}} \vec{a}_{\pm}(\vec{p}, t) e^{\mp i(\vec{p} \cdot \vec{r}_1 - \Omega t)}, \quad (3.52)$$

where \vec{a}_{\pm} can be slowly varying 'envelope' functions of space, on the light spot size R_o and on time, on the scale Ω^{-1} . These are the reference space and time scales in the following. In the frame of the quasiclassical approximation, the original Green's functions $G(1, 2) \equiv G(\vec{r}, t, \vec{r}', t')$ are assumed to be slowly varying function of the coordinate $\vec{R} = (\vec{r} + \vec{r}')/2$ while they oscillate fast as functions of $\vec{r} - \vec{r}'$ on the scale of the Fermi wavelength λ_F . It is customary to rewrite also the time dependence in terms of the new variables $\bar{t} = (t + t')/2$ and $t - t'$ and to Fourier transform *w.r.to* $\vec{r} - \vec{r}'$ and $t - t'$, thus obtaining $G(\vec{p}, \omega, \vec{R}, \bar{t})$.

The motion equation for the Keldysh component of Eq.(3.44) reads:

$$\left[\hat{G}_0^{-1} - \Re e(\hat{\Sigma}) - \hat{\Delta}, \hat{G}^K \right]_{\otimes} = \left[\hat{\Sigma}^K, \Re e(\hat{G}) \right]_{\otimes} + \frac{i}{2} \left\{ \hat{\Sigma}^K, \hat{A} \right\}_{\otimes} - \frac{i}{2} \left\{ \hat{\Gamma}, \hat{G}^K \right\}_{\otimes}, \quad (3.53)$$

where we have defined a quantity proportional to the density of states $\hat{A} = i(\hat{G}^R - \hat{G}^A)$ (not to be confused with the vector potential), and written down the imaginary and the real part of the self-energy, $\hat{\Gamma} = i(\hat{\Sigma}^R - \hat{\Sigma}^A)$ and $\Re e \hat{\Sigma} = \frac{1}{2}(\hat{\Sigma}^R + \hat{\Sigma}^A)$, respectively, as well as the real part of the retarded/advanced Green's function $\Re e \hat{G} = \frac{1}{2}(\hat{G}^R + \hat{G}^A)$ ($\{, \}$ denotes the anticommutator). The next step is the gradient expansion of the \otimes product (we drop the overline on t in the following):

$$\hat{C} \otimes \hat{B} = \exp 1/2(\partial_t^C \partial_{\omega}^B - \partial_{\omega}^C \partial_t^B) \exp 1/2(\partial_p^C \partial_R^B - \partial_R^C \partial_p^B) \hat{C} \hat{B}, \quad (3.54)$$

(here ∂_p^C stands for the gradient w.r.to the impulse operating on \hat{C}), followed by the averaging of the result for $|\vec{p}|$ close to p_F , that is over the energies

$p^2/2m - \mu \equiv \xi$ while the direction of \vec{p} , \hat{p} , is untouched:

$$\hat{g}(\hat{p}, \omega, \vec{R}, t) = \frac{i}{\pi} \int d\xi \hat{G}(\vec{p}, \omega, \vec{R}, t) . \quad (3.55)$$

This is justified, because λ_F is much shorter both of the superconducting correlation length and of the spatial range of the laser spot ($e-h$ symmetry is assumed). Eventually \hat{g} depends on \hat{p}, ω, R, t . The average of Eq.(3.53) over all directions in the Fermi surface, can be done if no external bias is applied and anisotropies of the diffusion and relaxation process are not expected. In the presence of radiation with optical frequency it is customary to average out the fast oscillating components with frequency Ω [32]. Following Eq.(3.7), we expand the Green's functions similarly:

$$\hat{g}(\omega, R, t) = \underline{\hat{g}}(\omega, R, t) + \sum_{\pm} \hat{\chi}^{\pm}(\omega, R, t) e^{\pm i\Omega t} . \quad (3.56)$$

Here $\underline{\hat{g}}(\omega, R, t)$ is assumed to be the slowly varying part on the scale of the pulse duration τ_c , while $\hat{\chi}^{\pm}$ are fast varying ones. All these functions are slowly varying functions of space as well, on the light spot size scale. A decomposition of Eq. (3.53) into harmonics arises. We are interested in the zero order harmonic equation, which shows a slow dynamics that can be followed coherently by the irradiated superconductor. Leaving the self-energy terms in Eq. (3.53) for the moment aside and dropping the superscript (K) , we obtain

$$[\tau_3 a_+, \hat{\chi}^-] + [\tau_3 a_-, \hat{\chi}^+] + [(\omega \hat{\tau}_3 - \hat{\Delta}), \underline{\hat{g}}] - \frac{1}{2} \{ \hat{\tau}_3, \partial_t \underline{\hat{g}} \} + \frac{1}{2} \{ \partial_t \hat{\Delta}, \partial_\omega \underline{\hat{g}} \} - \frac{e^2}{2mc^2} \partial_t A^2 \partial_\omega \underline{\hat{g}} = \dots, \quad (3.57)$$

where the ellipsis refers to the missing self energy terms. The first order harmonic equations are:

$$\pm i \{ \tau_3, \hat{\chi}^{\pm} \} + \frac{e}{2mc\Omega} [a_{\pm}, \underline{\hat{g}}] = 0 , \quad (3.58)$$

they show that the first two terms in Eq. (3.57) are $\mathcal{O}(\Omega^{-1})$ smaller than the others and can be neglected to lowest order. Hence the effective equations for the Green functions are

$$[(\omega \hat{\tau}_3 - \hat{\Delta}), \underline{\hat{g}}] - \frac{1}{2} \{ \hat{\tau}_3, \partial_t \underline{\hat{g}} \} + \frac{1}{2} \{ \partial_t \hat{\Delta}, \partial_\omega \underline{\hat{g}} \} - \frac{e^2}{2mc^2} \partial_t A^2 \partial_\omega \underline{\hat{g}} = \dots , \quad (3.59)$$

The last three terms in Eq. (3.59) include the time dependent non equilibrium dynamics that is absent in the case of a time independent approach. Retarded, advanced and Keldysh Green's function, they all satisfy analogous equations.

Appendix 3B

Kinetic equation for $n(\omega, r, t)$

One can linearize Eq. (3.59) for Keldysh Green's function by posing $\hat{g}^K = \hat{g}^R \hat{h} - \hat{h} \hat{g}^A$. This yields the kinetic equation for the distribution function $n(\omega, R, t)$ [23]. We neglect any variation in space and concentrate on the t dependence here. The distribution matrix \hat{h} is defined starting from the n_L and n_T functions according to:

$$\hat{h} = n_L \hat{1} + n_T \hat{\sigma}_3, \quad (3.60)$$

or

$$\hat{h} = \begin{pmatrix} n_L(E) + n_T(E) & 0 \\ 0 & n_L(E) - n_T(E) \end{pmatrix} \equiv \begin{pmatrix} 1 - 2n(E) & 0 \\ 0 & 2n(-E) - 1 \end{pmatrix}. \quad (3.61)$$

The second equality defines the relation with the qp distribution function $n(E)$. We always assume $e-h$ symmetry, so that $n(E) + n(-E) = 1$ and $n_T = 0$. In the equilibrium case one has $n_o(E) = \frac{1}{e^{E/T} + 1}$, so that:

$$n_{L(T)}^o = \frac{1}{2} \left[\tanh\left(\frac{E}{2T}\right) + (-) \tanh\left(\frac{E}{2T}\right) \right]. \quad (3.62)$$

Substituting Eq. (3.24) in Eq. (3.59), we get the kinetic equation for the distribution matrix \hat{h} . In particular, in case there is no charge imbalance, the equation for the longitudinal component n_L is [16]:

$$\begin{aligned} \partial_t n_L \text{Tr}((\hat{g}^R \hat{\tau}_3 - \hat{\tau}_3 \hat{g}^A)) + \partial_\omega n_L \text{Tr}(\partial_t \hat{\Delta}(\hat{g}^R - \hat{g}^A)) + \\ - \frac{e^2}{2mc^2} \partial_t A^2 \text{Tr}(\partial_\omega n_L (\hat{g}^R - \hat{g}^A)) = -4I[n_L(\omega)], \end{aligned} \quad (3.63)$$

where $I[n_L(\omega)]$ is a collision integral which regulates the relaxation of the qp distribution toward equilibrium. Eq. (3.63) is fully discussed in Ref. [16].

Appendix 3C

Equation of motion of G^R

We now write down the equations Eq. (3.59) explicitly for the retarded Green's functions. We label the matrix components by (i, j) ($i, j = 1, 2$) and drop the superscript R everywhere. The matrix elements of Eq. (3.57) in the

Nambu space become :

$$\begin{aligned}
(1, 1) &\rightarrow \partial_t g - \Delta f^\dagger + \Delta^* f + \partial_t \Delta \partial_\omega f^\dagger + \partial_t \Delta^* \partial_\omega f + \frac{e^2}{2mc^2} \partial_t A^2 \partial_\omega g = \dots \\
(2, 2) &\rightarrow \partial_t g^\dagger + \Delta f^\dagger - \Delta^* f + \partial_t \Delta \partial_\omega f^\dagger + \partial_t \Delta^* \partial_\omega f - \frac{e^2}{2mc^2} \partial_t A^2 \partial_\omega g^\dagger = \dots \\
(1, 2) &\rightarrow 2\omega f - \Delta g^\dagger - g \Delta + \partial_t \Delta \partial_\omega g^\dagger - \partial_\omega g \partial_t \Delta + \frac{e^2}{2mc^2} \partial_t A^2 \partial_\omega f = \dots \\
(2, 1) &\rightarrow +2\omega f^\dagger - \Delta^* g - g^\dagger \Delta^* + \partial_t \Delta^* \partial_\omega g - \partial_\omega g^\dagger \partial_t \Delta^* - \frac{e^2}{2mc^2} \partial_t A^2 \partial_\omega f^\dagger = \dots
\end{aligned}$$

The equilibrium result suggests that

$$f = \frac{\Delta(t)}{\omega} g \quad (3.64)$$

solves Eq.(1,2) except for terms $\propto \partial_t A^2$ which describe the relaxation at later times. Let us assume that this relation holds also in the non-equilibrium case. Then the formal solution, follows adiabatically the t -dependence of the gap parameter Δ by keeping an equilibrium-like shape:

$$g_{ad} = \frac{\omega}{\sqrt{\omega^2 - |\Delta|^2(t)}}, \quad f_{ad} = \frac{\Delta(t)}{\sqrt{\omega^2 - |\Delta|^2(t)}} \quad (3.65)$$

This approximate solution is quite appealing, because it satisfies the equilibrium condition for Δ at $t \rightarrow \infty$. However it neglects diffusion in space-time which will be mainly important at later times w.r. to the pulse duration.

Bibliography

- [1] P. Lucignano, G. Rotoli, E. Santamato, A. Tagliacozzo, Phys. Rev. B **70**, 024520, 2004.
- [2] A. Barone and G. Paternó, *Physics and applications of Josephson effect*, Wiley New York, 1982.
- [3] L. R. Testardi, Phys. Rev. B **4**, 2189, 1971.
- [4] W. H. Parker and W. D. Williams, Phys. Rev. Lett. **29**, 924, 1972.
- [5] C. S. Owen and D. J. Scalapino, Phys. Rev. Lett. **28**, 1559, 1972.
- [6] R. A. Vardanyan and B. I. Ivlev, Sov. Phys. JEPT **38**, 1156, 1974.
- [7] A. V. Sergeev, M. Yu. Reizer, J. Mod. Phys. B **6** 635 (1996), M. Yu. Reizer, Phys. Rev. B **39** 1602 (1989), A. V. Sergeev, M. Yu. Reizer, Zh. Eks. Teor. Fiz. **90** 1096 (1986) [Sov. Phys. JETP **63** 616 (1986)]

- [8] M. Lindgren, M. Currie, C. Williams, T. Y. Hsiang, P. M. Fauchet, R. Sobolewski, S. H. Moffat, R. A. Hughes, J. S. Preston, and F. A. Hegmann *Appl. Phys. Lett.* **74** 853 (1999)
- [9] A. D. Semenov, R. S. Nebosis, Yu. Gousev, M. A. Heusinger, K. F. Renk, *Phys. Rev. B* **52** 581 (1995).
- [10] S. B. Kaplan, C. C. Chi, D. N. Langenberg, J. J. Chuang, S. Jafarey, D. J. Scalapino, *Phys. Rev. B* **14**, 4854, 1976.
- [11] M. H. Devoret, J. M. Martinis, D. Esteve and J. Clarke, *Phys. Rev. Lett.* **53**, 1260, 1984.
- [12] M. H. Devoret, J. M. Martinis and J. Clarke, *Phys. Rev. Lett.* **55**, 1908, 1985.
- [13] A. Moopenn, E. R. Arambula, M. J. Lewis, H. W. Chan, *IEEE Trans. Appl. Supercond.* **3**, 2698, 1993,
- [14] G. P. Pepe, G. Peluso, M. Valentino, A. Barone, L. Parlato, E. Esposito, C. Granata, M. Russo, C. De Leo and G. Rotoli *Appl. Phys. Lett.* **79**, 2770, 2001.
- [15] *Superconductive Particle Detectors*, edited by A. Barone (World, Singapore, 1988); A. Barone, *Nucl. Phys. B* **44** 645 (1995).
- [16] Yu. N. Ovchinnikov and V. Z. Kresin *Eur. Phys. J. B* **32**, 297, (2003), Yu. N. Ovchinnikov and V. Z. Kresin, *Phys. Rev. B* **58**, 12416, (1998).
- [17] A. I. Larkin and Yu. N. Ovchinnikov *Zh. Eksp. Teor. Fiz* **55**, 2262 (1968) [*Sov. Phys. JETP* **28**, 1200, 1969]; J. Rammer, H. Smith, *Rev. Mod. Phys.*, **58**, 323, (1986).
- [18] W. Belzig, F. K. Wilhelm, C. Bruder, G. Schoen, E. D. Zaikin *Superlattices and Microstructures* **25**, 1251 (1999).
- [19] M. H. S. Amin, *Phys. Rev. B* **68** , 054505, (2003).
- [20] P. Lucignano, F. J. W. Hekking and A. Tagliacozzo, in “Quantum computing and Quantum bits in mesoscopic systems”, A. J. Leggett, B. Ruggiero, P. Sivestrini ed.s, Kluwer Academic, Plenum Publishers N.Y. (2004).
- [21] P. Lucignano Laurea Thesis “Interazione di radiazione laser ultraveloce con dispositivi a superconduttore” (2001), unpublished
- [22] G. Grimvall ‘The electron phonon interaction in metals’, North Holland Publ. Co. Amsterdam 1981.

- [23] J. J. Chang and D. J. Scalapino, Phys. Rev. B **15** , 2651, (1977).
- [24] L. P. Gorkov and G. M. Eliashberg, Soviet Physics, JEPT27, 328 (1968).
- [25] A. A. Abrikosov, L. P. Gor'kov, I. E. Dzyaloshinski, *Methods of quantum field theory in statistical physics* Dover;
- [26] A. Wallraff, A. Franz, A. V. Ustinov, V. V. Kurin, I. A. Shereshevsky and N. K. Vdovicheva, Physica B **284-288**, 575, 2000.
- [27] K. K. Likharev, *Dynamics of Josephson junctions and circuits*, Gordon and Breach Science Publishers, 1986.
- [28] Yu. Makhlin, G. Schön, and A. Shnirman, Rev. Mod. Phys. **73**, 357 (2001).
- [29] M. S. Choi, R. Fazio, J. Siewert, and C. Bruder, Europhys. Lett. **53**, 251 (2001).
- [30] A. I. Larkin and Yu. N. Ovchinnikov, 'Vortex motion in Superconductors' in Nonequilibrium Superconductivity, Edited by D. N. Langenberg and A. I. Larkin, Elsevier Science Publishers B. V., 1986;
A. I. Larkin and Yu. N. Ovchinnikov, J. Low Temp. Phys. **10**, 407 (1973);
A. I. Larkin and Yu. N. Ovchinnikov, Zh. Eksp. Teor. Fiz. **68**, 1915 (1975) [Sov. Phys. JETP, **41**, 960 (1976)];
A. I. Larkin and Yu. N. Ovchinnikov, Zh. Eksp. Teor. Fiz. **73**, 299 (1977) [Sov. Phys. JETP, **46**, 155 (1977)].
- [31] A. I. Larkin and Yu. N. Ovchinnikov, Zh. Eksp. Teor. Fiz. **55**, 2262 (1968) [Sov.Phys.JETP, **28**, 1200 (1969)].
- [32] see Kapitza method with classical oscillators in L. D. Landau, E. M. Lifshits, Mechanics, Pergamon Press (1960).